Summer 8-9-2017

Study of Static and Dynamic Properties of Magnetic Nanostructures

Shankar Khanal
skhanal2@uno.edu

Study of Static and Dynamic Properties of Magnetic Nanostructures

A Dissertation

Submitted to the Graduate Faculty of the
University of New Orleans
in partial fulfillment of the requirements
for the degree of

Doctor of Philosophy
In
Engineering and Applied Science
Physics

By
Shankar Khanal

B.Sc. Tribhuwan University, 2006
M.Sc. University of New Orleans, 2014

August, 2017

Acknowledgements

My great gratitude goes to Prof. Leonard Spinu for providing me an opportunity to join his research group. His consistent support regarding academic as well as personal aspects was truly significant.

I am thankful to committee members Dr. Leszek Malkinski, Dr. Weilie Zhou, Dr. John Wiley and Dr. Damon Smith for their support. Theirs comments and suggestions were substantial to put everything in context.

Thank you Dr. J M Vargas, Dr. C. Garcia, Dr. C. A. Ross, Dr. R. A. Gallardo for providing the exchange bias samples and working together as collaborators.

I would like to appreciate the help received from Poncho and Jennifer with all administrative paperwork during my tenure at AMRI. I would like to thank Harry J. Rees for helping to solve technical problems with instruments.

I am thankful to our present and past group members: Daniel, Pemba, Jose, Artur, Abhishek, Andrei, Pratik, Asif, Denny, Nicolas and Ali. I also like to thank Taha, Satish, Rahmat, Zheng, Shuke and all graduate as well as undergraduate students in AMRI.

It would be impossible to complete sample fabrication and characterization process without having access to MINT center University of Alabama, Tulane University (CIF microscopy lab), Louisiana State University (shared instrumentation facility). I would like to thank the people who helped me on these institutions.

It would be hard to imagine to complete my PhD without funding support from NSF award ECCS1101798, LASiGMA award No EPS-10003897 and NSF grant No. ECCS – 1546650.

Finally, I would like to acknowledge my thankfulness to all my family members and Love to my wife Tirtha and daughter Selene.

Table of Contents

Abstract

Magnetic materials are one of the most interesting and promising class of materials for technological applications [1]. Among them, patterned ferromagnetic systems have an important role especially in the prospect of high density data storage [2], domain wall logic devices [3] and magnetic memory [4, 5]. Coupled systems of ferromagnetic and antiferromagnetic materials have been implemented to design sensors such as giant magnetoresistance (GMR) [6-8] and tunnel magnetoresistance (TMR) [9, 10]. Ferromagnetic nanoparticles have been used for the drug targeting, cancer therapy, Magnetic Resonance Imaging (MRI) and many more applications [11, 12]. In addition, more recently, significant attention has been paid to the exploration of the dynamic properties of magnetic materials in the GHz range and use them for technological applications such as microwave filters, signal processing, phase shifter, nonreciprocal microwave devices, spin wave guide, high frequency memory, logic elements [13-19]

Boundary conditions, interactions between individual entities, and lateral confinement of magnetic charges generate diverse magnetic properties especially at nanoscale length [20, 21]. The variation of magnetic properties are quite different when the size of the magnetic structure is smaller or comparable with the magnetic characteristic length such as mean free path of electron, width of domain wall and even the spin diffusion length [22-24].

In this study, we have considered different magnetic systems with at least one dimension in the nanometer scale, i.e. *magnetic nanostructures*. Firstly, the multilayers of coupled ferromagnetic and antiferromagnetic system have been considered to evaluate the exchange bias anisotropy. $[FeNi/IrMn]_n$ multilayer systems with different thicknesses of ferromagnetic layer and exchange bias strength were studied. Their static and dynamic properties were revealed through Vibrating Sample Magnetometry (VSM) measurements and ferromagnetic resonance (FMR) techniques respectively. Angular variation of

first order reversal curve (AFORC) and ferromagnetic resonance (AFMR) were performed to learn the intrinsic exchange bias distribution. Secondly, patterned periodic magnetic structures, i.e. magnonic crystals, were synthesized to understand the magnetization dynamics in confined geometry. Surface modulated thin films with different periodicity, dumbbell-shaped structures with variable size and three dimensional magnonic crystals have been studied using both static and dynamic measurement techniques. Micromagnetic simulations were performed to understand and explain the experimental results.

Keywords: *magnetic nanostructures, ferromagnetic resonance, exchange bias, coplanar waveguide, magnetization dynamic, micromagnetic simulation, magnonic crystals.*

Introduction

The most fascinating aspect of magnetic materials is that their properties are strongly dependent on the physical shape, size, the distance between them as well as their symmetry [25, 26]. Thin films, patterned structures, free nanoparticles and now three dimensional magnetic structures have attracted incredible attention in scientific community. Control of magnetization with external magnetic field, temperature, spin current and pressure make magnetic systems more interesting regarding both fundamental as well as technological application [27]. Development in cloud computing to improve data storage has been pushed to a different level because of the better understanding of magnetism at nanoscale [28]. Understanding domain, domain walls, and their dynamics are always fascinating as sensors to read and write data [29]. In dynamic aspect, spin wave dynamics have been emerging in confined magnetic nanostructures with the possibility of tuning them in wide range of frequency, so called magnonics [30-32]. Magnonics for future data storage and logic has been already realized [31]. Magnonic crystal, which has alternative properties within the system, can be achieved without complicated compositional changes.

In addition, magnetic multilayer systems are the most promising asset in many technological perspectives [33-35]. Among them, exchange bias, which exists at the interface between ferromagnetic and antiferromagnetic layers, has been already implemented as a sensor to read and write data in magnetic memory. The superparamagnetic effects, especially occurring for nanometer scale magnetic materials, can be controlled by considering the coupling of antiferromagnetic material with magnetic nanostructure [36].

In this thesis, different aspects of magnetism have been revealed. Coupling scheme between ferromagnetic and anti-ferromagnetic in thin films has been studied in detail. Different magnetic

structures have been fabricated and characterized with different techniques. The outline of the thesis will be presented in the following.

Chapter 1 presents on overview of magnetism concepts that will be used in the subsequent chapters. The different scientific terms and energy terms involved in magnetic materials will be discussed. The magnetic switching in the static regime will be described using the Stoner-Wohlfarth model. The existence of magnetic domain in ferromagnetic materials, domain walls and their dynamics will be presented. Magnetization switching in the dynamic regime will be explained using the Landau- Lifshitz-Gilbert (LLG) equation. Ferromagnetic resonance phenomenon that will used to characterize the dynamic properties of studied magnetic nanostructures will be presented. Theory of spin wave dynamics in magnetic thin film is also discussed.

Chapter 2 describes Sample Fabrication and Characterization Techniques. Fabrication techniques such as photolithography, electron beam lithography, focused ion beam, sputtering, and liftoff have been discussed. Design of micrometer size coplanar waveguide (CPW) and fabrication of magnetic structures exactly on the top has been achieved. Static and dynamic characterizations have been performed using different characterization techniques. For example, the static case, Vibrating Sample Magnetometer (VSM), First Order Reversal Curve (FORC), Magneto-optical Kerr Effect (MOKE) and magnetic force microscopy (MFM) have been reviewed. In dynamic regime, the X-band ferromagnetic resonance at 9.8 GHz and broad band vector network analyzer ferromagnetic resonance (VNA-FMR) technique have been presented.

Chapter 3 is about the Exchange bias in (FeNi/IrMn)n multilayer films evaluated by static and dynamic techniques. We studied the coupled ferromagnetic and anti-ferromagnetic system by varying the thickness of ferromagnetic layer. The static and dynamic properties of these coupled systems have been used to evaluate the exchange bias anisotropy. The angular dependent measurements of static

properties have been performed using angular FORC (AFORC) technique. The angular dependent dynamic properties have been studied using angular FMR. Finally, results from both techniques have been compared.

In chapter 4, static and dynamic properties surface modulated structures were studied. This chapter presents the study of several configuration of one dimensional magnonic crystals. Surface modulated structures were fabricated using a combination of different techniques. The periodicity of modulated region was varied to understand their effect on the statics and dynamic properties. Angular variation of Major Hysteresis Loops was measured to study the static properties. The angular dependence FMR was used to reveal the field and frequency dependent dynamic properties. The experimental results have been explained and verified using micromagnetic simulation.

Static and dynamic study of shape modulated structures as well as conclusion and prospective of future work have been presented in chapter 5. The hybrid structures (dumbbell) of wire and dot have been considered to evaluate the static and dynamic properties. The size of the dots has been varied to understand static and dynamic magnetization. The switching of magnetization in confined and restricted geometry has been studied in static case. In terms of dynamics, excitation and propagation of spin waves in confined geometry has been discussed.

Chapter 1: Overview of Magnetism

1.1 Introduction

In this chapter, it will be presented the fundamental concepts and scientific terms which will facilitate to understand the following chapters.

Microscopically, magnetism originates from the motion of electrons around nucleus. There are two types of motion of an electron. The first is that electron revolves around the nucleus and generates orbital angular momentum. Similarly, the second is the electron spins around its own axis and generates spin angular momentum. Finally, the total angular momentum is the sum of these two momenta. However, classically, magnetic moment (μ), which is considered as fundamental unit of magnetism, can be explained by comparing angular momentum of electron with the current in a loop. For example, if current (I) is flowing in a circular wire and area enclosed by the wire is A, the magnetic moment associated with that moving electron can be expressed as

$$\mu = \mathrm{I}.\mathrm{A} \tag{1.1}$$

Where, A is the area enclosed by circle.

Magnetic moment can now be expressed in terms of angular momentum (L = m v r) by simply substituting value of current (I=e/t) and A in equation 1.1.

$$\mu = \left(\frac{\mathrm{e}}{2\mathrm{m}}\right)\mathrm{L} \tag{1.2}$$

Substituting $\gamma = \mathrm{e}/2\mathrm{m}$, magnetic moment finally can be written as;

$$\mu = -\gamma\,\mathrm{L} \tag{1.3}$$

where, γ is gyromagnetic ratio.

For time dependent magnetic moment, it is expressed as,

$$\frac{d\boldsymbol{\mu}}{dt} = \gamma \frac{d\mathbf{L}}{dt} = \gamma\tau \tag{1.4}$$

In presence of external magnetic field (H), the equation of motion for the magnetic moment is

$$\frac{d\boldsymbol{\mu}}{dt} = \gamma\, \boldsymbol{\mu} \times \mathbf{H} \tag{1.5}$$

Finally, total energy of magnetic moment on external magnetic field can be expressed as

$$E = -\mu 0 \boldsymbol{\mu}.\mathbf{H} \tag{1.6}$$

1.2 Magnetic interaction and energies:

A unique property of magnetic materials is that they interact with other magnetic materials, especially ferromagnetic materials. Magnetic moments in ferromagnetic materials align in certain orientation even in the absence of external field and have spontaneous magnetization. The interaction can be between neighboring magnetic moments or with external magnetic field. In addition, interaction may be classical or quantum in origin. The main interactions, especially in ferromagnetic materials, are dipole and exchange interactions. In the following section, they will be described in brief.

1.3 Exchange interaction

Exchange interaction, which is quantum in origin, initiates as a result of quantum mechanical interaction between electrons. It is important to mention that depending on the orientation of a spin with respect to the neighboring one, the materials are classified as ferromagnetic, anti-ferromagnetic and ferromagnetic. Let us consider the exchange interaction between two electrons with spin S_1 and S_2 . The Hamiltonian because of exchange interaction for two electrons system is written as,

$$\boldsymbol{H}_{ex} = -2J_{12}\boldsymbol{S}_1.\boldsymbol{S}_2 \tag{1.7}$$

With,

$$J_{12} = \iint \Psi 1\,(r_1)\Psi 2\,(r_2) H_{ex}\, \Psi 1\,(r_2)\Psi 2\,(r_1)\; d^3 r_1 d^3 r_2 \tag{1.8}$$

It is important to mention that although the exchange interaction is very strong, it decays exponentially with space. However, this interaction is strong enough to keep neighboring spin align together. Finally, Positive value of J corresponds to the parallel alignment of spin and results ferromagnetic ordering. Negative value of J causes the antiparallel orientation of spins and leads anti-ferromagnetism.

1.4 Dipole interaction

Let us consider two magnetic dipoles μ_1 and μ_2 which are separated by distance r. The dipolar interaction energy, from electromagnetism, can be expressed as [37]

$$\text{Edipole} = \mu_0/4\pi r^3[\boldsymbol{\mu_1}.\boldsymbol{\mu_2} - \frac{3}{r^3}(\boldsymbol{\mu_1}.\mathbf{r})(\boldsymbol{\mu_2}.\mathbf{r})] \tag{1.9}$$

Where, μ_0 is permeability of free space. From above equation it can be clearly observed that dipolar energy depends on the third order of the distance between dipoles. Since the dipolar interaction exists at long range, it has significant contribution on demagnetization field as well as for long wavelength spin waves.

1.5 Magnetic Anisotropy:

Magnetic materials are anisotropic, i.e., their static and dynamic properties are strongly dependent on the direction of the applied field. In terms of origin, some anisotropies are intrinsic in nature, such as magneto-crystalline, and some are extrinsic, for example shape anisotropy. Tuning magnetic properties by manipulating these anisotropies is critical in fundamental as well as technological applications. Most important contributions to the magnetic anisotropy are discussed in the following sections.

1.5.1 Magneto-crystalline anisotropy:

Magneto-crystalline anisotropy is induced due to spin-orbit interaction in magnetic materials[38]. Spin-spin coupling assists to keep spins either parallel or anti-parallel and it simply depends on the angle between them. Hence, it does not necessarily depend on the crystal axis, and spin-spin interaction does not help to induce magneto-crystalline anisotropy[38]. In contrast, the coupling of orbit with lattice is strong. This strong quenching of orbital magnetic moment with the lattice needs a much stronger field to breakdown coupling and results magneto-crystalline anisotropy.

Generally, the direction of easy axis is the direction of spontaneous magnetization in the demagnetized state. External work is needed to rotate the magnetization from easy axis to any other orientations. Depending on the type of crystals, there would be cubic or hexagonal magneto-crystalline anisotropy.

For cubic crystal, if magnetization (Ms) orients with cosine angle α1, α2 and α3 with crystal axis a, b, and c respectively, the cubic anisotropy can be expressed as [38],

$$E = K0 + K1(\alpha1^2\,\alpha2^2 + \alpha2^2\alpha3^2 + \alpha3^2\alpha1^2) + K2(\alpha1^2\,\alpha2^{\,2}\alpha3^2) + \ldots\ldots\ldots \quad (1.10)$$

Where, K0, K1 and K2 are anisotropy constants, and they depend on temperature as well as type of material.

In case of hexagonal materials, for example cobalt, the basal plane is equally magnetically hard. Thus, anisotropy energy depends on the angle between Ms and c axis of the crystal. For example, if θ is the angle between Ms and c axis, the anisotropy energy can be expressed as

$$E = K0 + K1\sin^2\theta + K2\sin^4\theta + \cdots \quad (1.11)$$

Where, constant K1 and K2 are both positive constants.

The hexagonal crystal structure of cobalt and the magnetization vs field at different crystalline axes are presented in figure 1.1. When the angle θ is zero, there will be minimum energy thus the c-axis is the easy axis of magnetization. The dependence of magnetization with the magnetic field for two different axis of crystal for cobalt is presented in figure 1.1 [b].

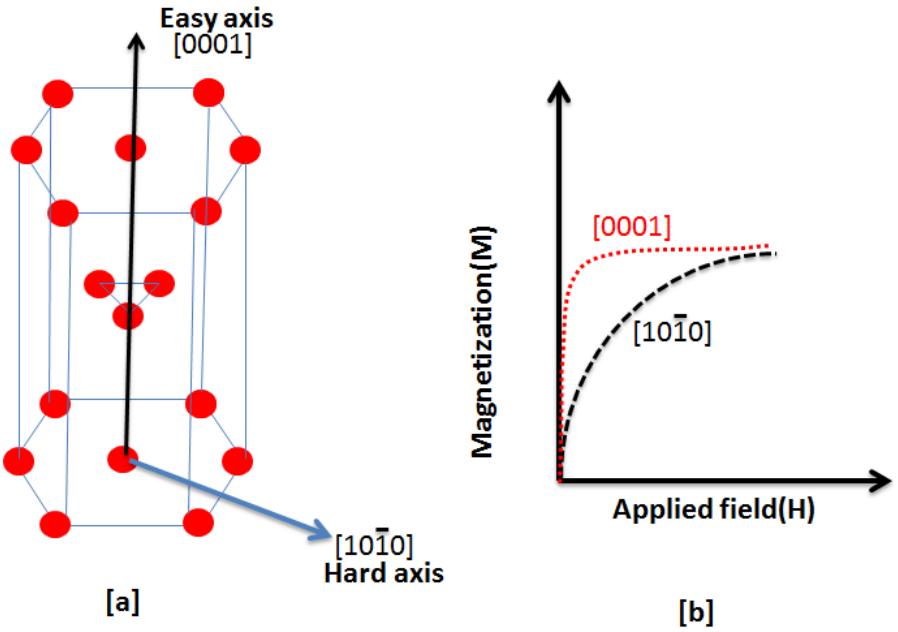

Figure 1.1: [a] Unit cell of Cobalt with easy and hard axis.[b] M vs H for two different axis of crystal.

1.5.2. Shape anisotropy:

The orientation of spontaneous magnetization in ferromagnetic materials also depends on its own shape. For example, spherical shape samples are isotropic. In contrast, if the sample is not spherical, it is easy to magnetize in one orientation than other. If we consider a long wire, it is easy to magnetize along the length of wire rather than perpendicular to it. The demagnetization field opposes the external applied field and reduce effective field. Generally, shape anisotropy is expressed in terms of magneto-static energy when the applied field is zero. The magneto-static energy can be expressed as [38]

$$E_{ms} = \frac{1}{8\pi}\int H_d^2 \, dv \tag{1.12}$$

The magneto-static energy in vector form is written as

$$E = -\frac{1}{2}\,\mathbf{H_d}\,.\,\mathbf{M} \tag{1.13}$$

The negative sign is for the opposite direction of $\mathbf{H_d}$ with **M**.

Now let us consider a prolate spheroid to calculate the magneto-static energy. The semi-minor and major axis are represented by a and c respectively in figure 1.2.

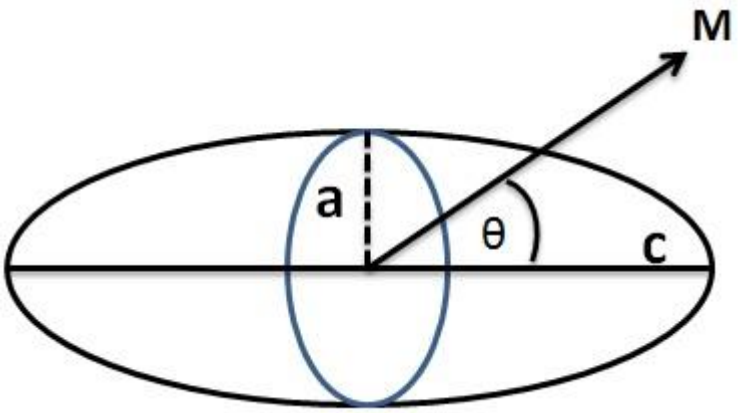

Figure 1.2: Prolate ellipsoid

If we consider the component of magnetization along the c-axis, the magneto-static energy can be expressed as,

$$E_{ms} = \frac{1}{2}\,[(M\cos\theta)^2 N_c + (M\sin\theta)^2 N_a \tag{1.14}$$

Na and Nc are the demagnetization factors along the a and c-axis. Substituting the cosθ with sinθ, equation 1.18 becomes,

$$E_{ms} = \frac{1}{2}\,M^2 N_c + \frac{1}{2}\,(Na - Nc)M^2\,(\sin\theta)^2 \tag{1.15}$$

The shape anisotropy, which is also angle dependence, is expressed in equation 1.15.

1.5.3 Magnetostriction and stress anisotropy:

When external magnetic field is applied to ferromagnetic materials, the dimension of these materials changes during magnetization process. The resulting strain is called magnetostriction (λ) [39]. In case of one dimensional structure, it can be expressed as[40],

$$\lambda = dl/l \tag{1.16}$$

Where, dl is the change on length (l).

1.6 Stoner Wohlfarth model

Stoner Wohlfarth model explains the magnetization reversal curve for single domain specimen with uniaxial anisotropy[41]. The uniaxial anisotropy might be because of shape anisotropy or magneto-crystalline anisotropy or both. Let us consider the ellipsoidal shaped single domain specimen as in figure 1.3 below.

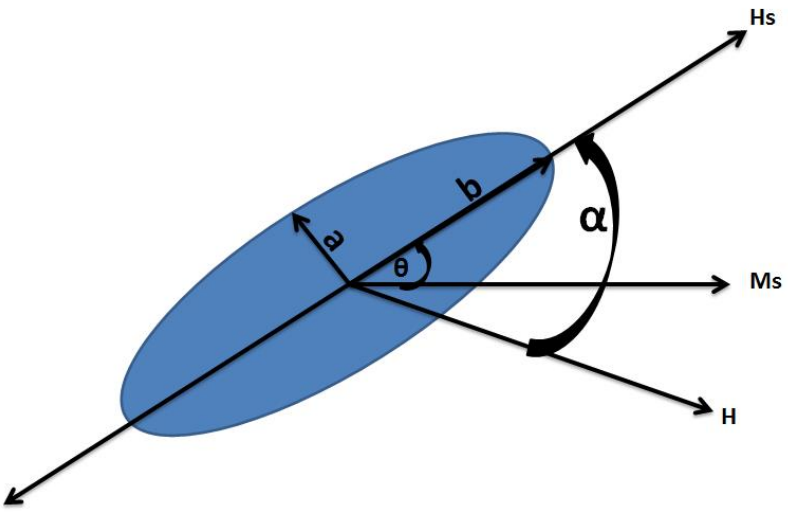

Figure 1.3: Systematic of orientation of easy axis as well as applied magnetic field for ellipsoidal particle.

If θ is the angle between the magnetization (Ms) and easy axis, anisotropy energy can be expressed as[40]

$$E_{an} = K \sin^2\theta$$

The misalignment of easy axis and magnetization induce torque and it is written as,

$$\tau_{an} = -\frac{dE_{an}}{d\theta}$$

$$= -2K \sin\theta \cos\theta$$

If external field is applied (H) as shown in figure1.4, torque produce due the external field is

$$\boldsymbol{\tau}_H = \mu 0\ \mathbf{Ms}\times\mathbf{H}$$

$$= \mu 0\ HMs \sin\varphi$$

Where, φ is angle between magnetization and field direction.

At equilibrium condition, sum of torques due to and external field and anisotropy is zero i.e.

$$\tau_H + \tau_{an} = 0$$

$$\mu 0\ HMs \sin(\alpha - \theta) - 2\ K \sin\theta\ \cos\ \theta\ = 0$$

If Hk is the field strength to rotate the magnetization from easy axis, which is 90 degree with applied field to the field direction, then the anisotropy field can be expressed as

$$Hk = 2K/\mu 0Ms \tag{1.17}$$

If the applied field is perpendicular to the anisotropy field it creates reversible changes of magnetization as in figure 1.4(b)

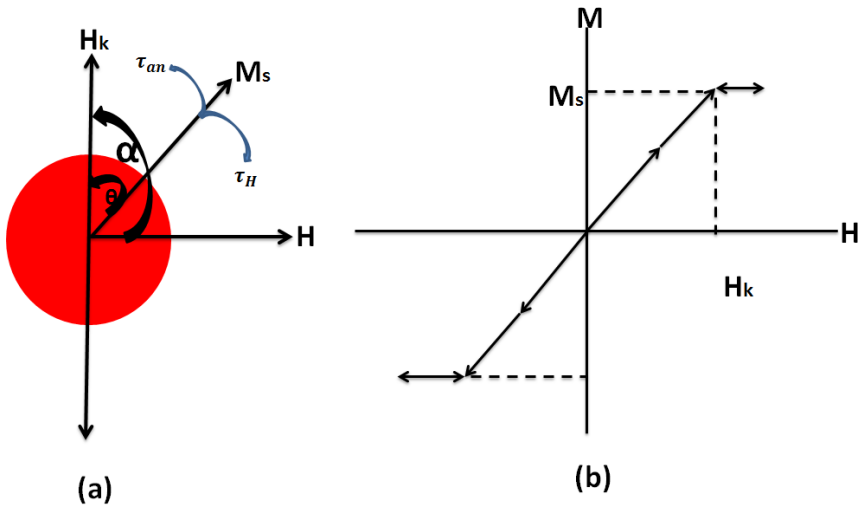

Figure 1.4: (a) Magnetic field perpendicular to easy axis with anisotropy field Hk (b) MHL curve for situation (a)

However, for magnetic field and anisotropy field are parallel, the magnetization switching is irreversible if applied field is less then 2K/μ0Ms as in figure 1.5

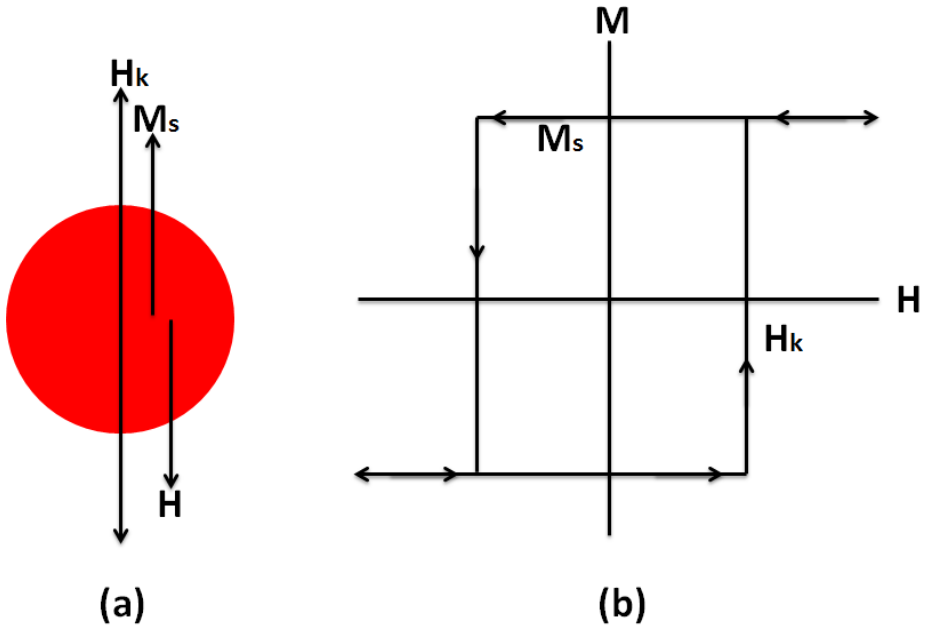

Figure 1.5: (a) magnetic field parallel to easy axis with anisotropy field Hk (b) MHL for case corresponds to (a)

For the applied magnetic field at arbitrary direction with the anisotropy axis, both the reversible and irreversible components of magnetization contribute on MHL. MHL for a spherical single domain particle when the external magnetic field is at 45^0 with the anisotropy field is presented figure 1.6.

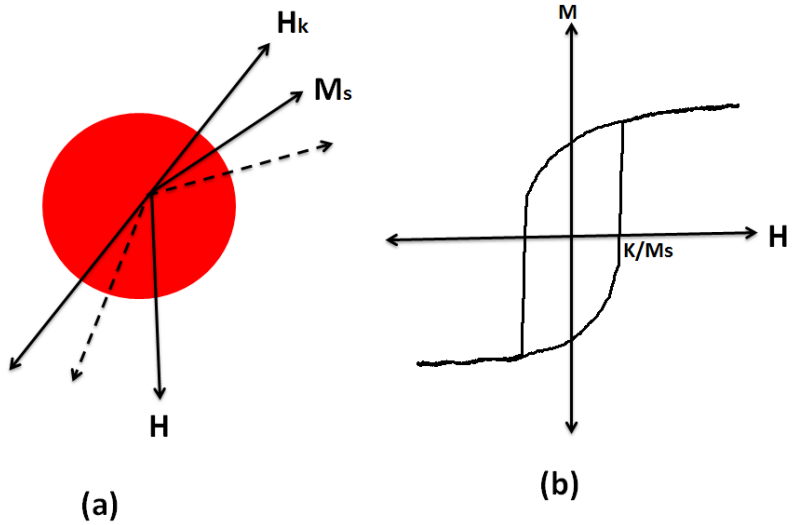

Figure1.6: (a) single domain particle with field Hk and magnetic field (H) at arbitrary orientation with the easy axis (b) corresponding MHL for case (a)

Despite the wide application of Stoner – Wohlfarth model, there are limitations to apply this model in many practical aspects. The reasons for that are this model does not consider the effect of interaction between the particles, temperature dependence magnetization and multi-domain magnetic systems.

1.7 Magnetic domain

Magnetic moments, in ferromagnetic materials, are aligned parallel within small volume is called magnetic domain. The orientation of the magnetic moments in a domain will be different from the neighboring one. The boundary wall between two domains is called domain wall. Depending on the nature of orientation of spins in domains walls, domain wall are classified in different categories.

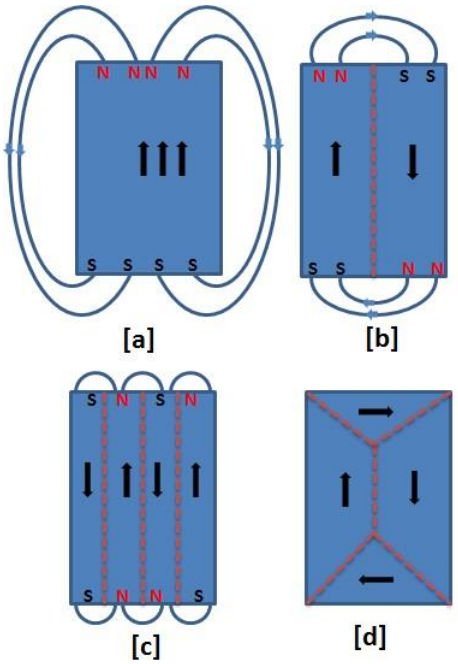

Figure1.7: systematic of formation of domains in ferromagnetic materials

Generally Bloch wall presents on the bulk materials and Neel wall on the thin samples. In addition, there is very interesting phenomena for the formation of domain wall especially in ferromagnetic materials. The systematic of the domains formation will be discussed here considering a bar magnet as in figure 1.7.

When external magnetic field is applied along a bar magnet as in figure 1.7[a], the magnet is saturated and the magnetic surface charges appear at the edge of the magnet. There will be a demagnetization field associate with these surface charges which essentially reduce the effective magnetic field of sample. Energy associate with these surface charges is called magneto-static energy. One way to reduce magneto-static energy is to divide the single domain magnet in multi-domain as in figure1.7 [b] and [c]. When magnetic moment within a bar magnet oriented in opposite direction, the distance between the positive and negative charge decrease and consequently the spatial extend of the demagnetization field also decrease. However, one thing we need to keep in mind is that this process does not go infinitely. The reason is that there will be a domain wall between two domains and the energy is required to create and maintain domain wall. When the magneto-static energy is equal with the energy required to maintain domain wall, the equilibrium will be reached and splitting of domain stops.

1.8 Domain wall

As discuss earlier, the domain wall is an interface between the two domains where spontaneous magnetization are at different orientations. The change of magnetization in the interface between two domains is not abrupt. As presented in figure 1.9, the orientation of the magnetic moment might be 180^0 (Bloch wall) or 90^0 (Neel wall) or any other depending on the geometry as well as composition of specimen. In the following, we will calculate the domain wall width for Bloch type domain wall which is depicted in figure 1.8.

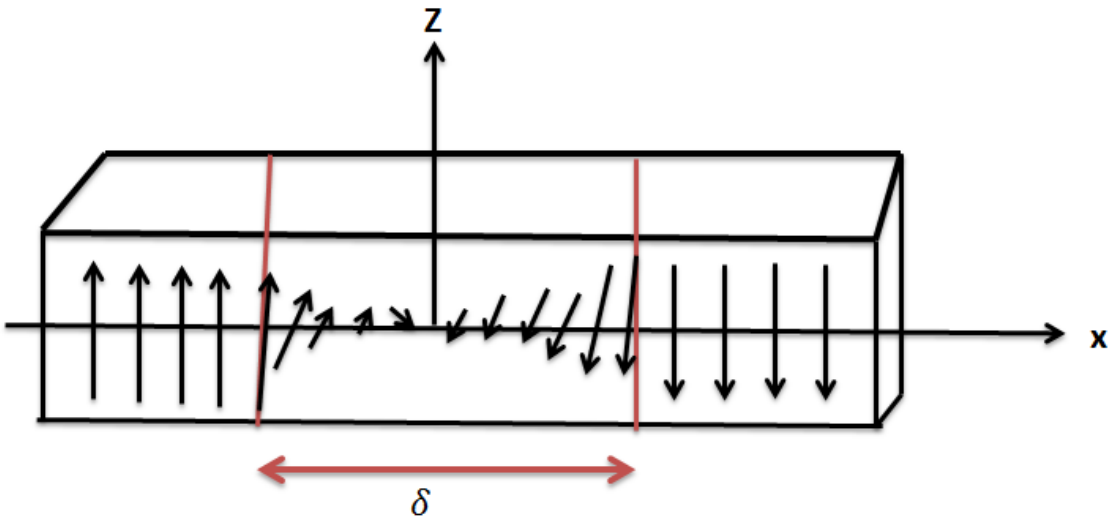

Figure 1.8: Systematic of domain wall for Bloch type domains

Let us consider two closest spins S_1 and S_2, the exchange energy between them can be expressed as [40]

$$E_{ex} = -2\,J_{12}\,S_1 . S_2 = -2JS^2\cos\theta$$

This means that the exchange energy depend on the angle between two spins. For example, if the angle between two spin is π, there will be maximum exchange energy. Let us consider a wall with N lattice spacing so angle between two neighboring lattices is

$$\theta = \frac{\pi}{N}$$

The exchange energy difference, when first spin at zero degree orientation and second with small theta, is

$$\Delta E_{ex} = E_{ex} - E_{ex}^{\theta=0}$$

$$= -2JS^2\,cos\theta + 2J\,S^2$$

$$\approx 2JS^2[1 - 1 + \theta^2]$$

$$\approx 2JS^2\frac{\pi^2}{N^2}$$

Total energy for N spin is expressed as,

$$E_{ex}^{total} = NJS^2\frac{\pi^2}{N^2} = JS^2\frac{\pi^2}{N}$$

If a is the lattice constant, the exchange energy per unit area is

$$\sigma^{ex} = JS^2\frac{\pi^2}{Na^2} \tag{1.15}$$

Thus if N→∞, $\sigma^{ex} \rightarrow 0$, it means wide domain wall is preferred for minimum energy, which means the spin will be randomly oriented. However in case of ferromagnetic materials, this does not occur because the magnetic anisotropy energy increases when the spins are randomly oriented. Thus, width of the domain wall is determined by the balance between the exchange and magnetic anisotropy energies. To calculate the anisotropy energy, let θ is the angle between the easy axis and the magnetic dipole, the magnetic anisotropy could be expressed as[40],

$$E_{ani} \approx K_u \sin^2\theta$$

If there are N lattice along the wall, the total energy is

$$E_{ani}^{total} = \sum_{i=1}^{N} K_u \sin^2\theta_i$$

$$\approx \frac{1}{d\theta} K_u \int_0^{\pi} \sin^2\theta \, d\theta$$

$$= \frac{NK_u}{2}$$

Since total anisotropy constant is per unit volume, the anisotropy energy density per unit area is

$$\sigma_{ani} = \frac{NK_u a}{2}$$

The total energy associate with Bloch domain wall per unit area can be expressed as

$$\sigma = \sigma^{ex} + \sigma_{ani}$$

$$= JS^2 \frac{\pi^2}{Na^2} + \frac{NK_u}{2}$$

The number of lattice spacing can be derived by minimizing the energy density of wall

$$\frac{d\sigma}{dN} = -\frac{JS^2\pi^2}{N^2a^2} + \frac{K_u a}{2} = 0$$

$$\Rightarrow N = \pi S \sqrt{\frac{2J}{K_u a^3}}$$

Substituting this value in above equation, the domain wall width can be expressed as,

$$\sigma^{ex} = JS^2 \frac{\pi^2}{Na^2} \qquad (1.16)$$

The equation (1.16) clearly suggests that the width of the domain wall depends on the exchange integral and anisotropy constant. The domain wall width increases when the exchange integral increases and decrease when the anisotropy constant increase. The competition between these two energies determines the width of the domain wall.

1.9 Magnetization dynamics

So far we have discussed static magnetic properties of magnetic specimens. In the following, we will be discussing about the dynamics of magnetic moments especially in presence of external magnetic field. For this, let us consider external magnetic field is applied in ferromagnetic material which forces the magnetic moments to align along the field direction and precess. We have already discussed the torque on the magnetic moment (μ) due to the external field. Again, it can be expressed as

$$\boldsymbol{\tau} = \mu_0 \boldsymbol{\mu} \times \mathbf{H}$$

Where μ_0 represents the magnetic permeability in free space. The torque causes the precession of magnetic moments with frequency ω_L called Larmor frequency. Mathematically it can be expressed as

$$\omega_L = \mu_0 \gamma H$$

Where, γ is gyromagnetic ratio.

The time dependence of the magnetization in presence of external magnetic field can be written as[42]

$$\frac{d\mathbf{M}}{dt} = -\gamma\, \mathbf{M} \times \mathbf{H} \tag{1.17}$$

This is the Landau- Lifshitz equation. This equation explains the magnetization dynamic for the system with uniform magnetization. To realize this dynamic motion practically, if we consider one end of magnetization fastened and other kept free, it moves on the surface of sphere and this kind of motion is called precession motion. For the case of cylindrical symmetry, magnetization moves in circle and more complicated on others configuration.

In reality, the precession of spin dose not last forever. If external magnetic field is turned off, damping of the oscillation of magnetization amplitude takes place due to the dissipation of the energy. The energy generally transforms to other form such as heat energy. Thus, precession of spins finally stops. To

consider this effect, Gilbert introduced an extra term to equation of motion of magnetization (equation (1.27)). Now the complete equation of motion for the magnetization can be written as[42],

$$\frac{d\mathbf{M}}{dt} = -\gamma\, \mathbf{M}\times\mathbf{H} + \frac{\alpha}{Ms}(\mathbf{M}s\times\frac{d\mathbf{M}s}{dt}) \tag{1.18}$$

This equation is Landau-Lifshitz-Gilbert (LLG) equation where α is Gilbert damping parameter. The systematic of precession and damping of magnetization is presented in figure 1.9. First term in equation (1.28) contributes for precession and the second term for the damping of magnetization.

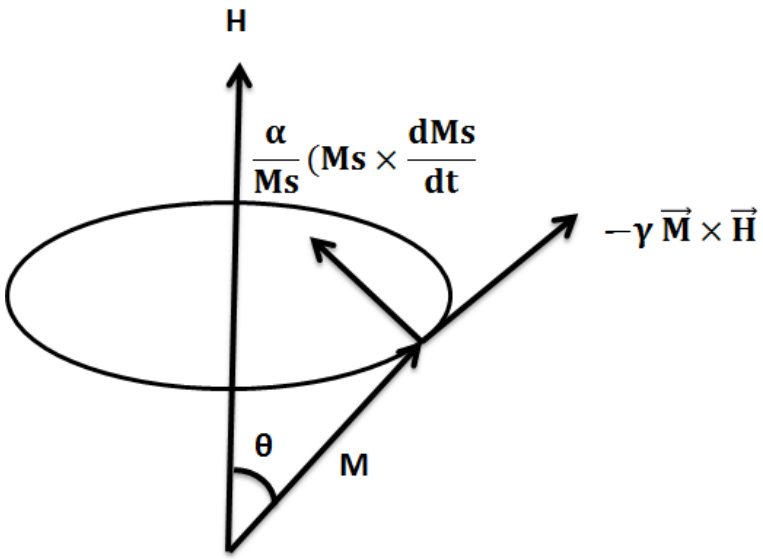

Figure 1.9: Precessional motion of spin in external magnetic field

1.10 Ferromagnetic resonance and high frequency susceptibility

Ferromagnetic resonance (FMR) is a firmly established experimental technique to determine not only susceptibility at high frequency but also for anisotropies in magnetic materials [43]. There are two established approach to do FMR experiment. The first approach is that the microwave with fixed frequency excites the sample and the external magnetic field is swept to get FMR spectra. In second, the

microwave frequency is swept at constant external magnetic field. The most important aspect of FMR technique is that it allows investigating the ground states of ferromagnetic specimen without perturbation[44]. The low energy excitation of microwave field allows for it.

The spin dynamic, which occurs at nanosecond time scale, is extremely difficult to observe. For that reason, it is easy to explain dynamic of spin in frequency domain. In the following, we will be discussing about how FMR technique can be implemented to get information about magnetic susceptibility at high frequency.

Let us consider an infinitely large ferromagnetic specimen and external magnetic field ($\mathbf{H} = \mathrm{H}_0.\boldsymbol{e_z}$) is applied along the Z- direction. If the sample is excited with the time dependent microwave field in x-y plane, i.e.$\mathrm{h_{rf}}(t) = \left(\mathrm{h_x}, \mathrm{h_y}, 0\right).e^{-i\omega t}$, time varying magnetization along the Z-direction the can be expressed as$\mathbf{M} = \mathrm{M}_s\,\mathbf{e_z} + \mathbf{m}\,e^{-i\omega t}$. If the microwave field and dynamic components of magnetization are small, we can neglect the product of these two terms which leads the LLG equation as [44]

$$\frac{\mathrm{d}\mathbf{m}}{\mathrm{dt}} = \gamma(\mathbf{H}_0 \times \mathbf{m}_{\mathrm{rf}} + \mathbf{h_{rf}} \times \mathbf{M}_{\mathrm{S}}) + \frac{\alpha}{\mathrm{M_s}}\mathbf{M} \times \frac{\mathrm{d}\mathbf{m}_{\mathrm{rf}}}{\mathrm{dt}}$$

$$\approx \gamma\,\mathbf{e_z} \times (B_0\mathbf{m}_{rf} - \mu_0 M_s \mathbf{h}_{rf}) + \alpha\vec{e}_z \times \dot{\mathbf{m}}_{rf}$$

If we consider the ac components of magnetization and magnetic field, the above equation can be expressed as,

$$-\mathrm{i}\omega\mathrm{m_x} + (\gamma\mathrm{B}_0 - \mathrm{i}\omega\alpha)\mathrm{m_y} = \gamma\mathrm{M_s}\mu_0\mathrm{h_y}$$

$$-\mathrm{i}\omega\mathrm{m_y} - (\gamma\mathrm{B}_0 - \mathrm{i}\omega\alpha)\mathrm{m_x} = -\gamma\mathrm{M_s}\mu_0\mathrm{h_x}$$

$$-\mathrm{i}\omega\mathrm{m_z} = 0$$

The solution of the above equations can be expressed in terms of polder's susceptibility tensor which relates the dynamic magnetization with RF magnetic field [44].

$$\mathbf{m}_{rf} = \chi \mathbf{h}_{rf} = \begin{pmatrix} \chi_L & -i\chi_T & 0 \\ i\chi_T & \chi_L & 0 \\ 0 & 0 & 0 \end{pmatrix} \begin{pmatrix} h_x \\ h_y \\ h_z \end{pmatrix}$$

Where $\chi_L = \frac{(\omega_0 - i\omega\alpha)\,\omega_M}{(\omega_0 - i\omega\alpha)^2}$ and $\chi_T = \frac{\omega\omega_M}{(\omega_0 - i\omega\alpha)^2 - \omega^2}$ are longitudinal and transverse susceptibility respectively.

And $\omega_0 = \gamma B_0$ and $\omega_M = \gamma \mu_0 M_S$

From above equation it is clearly observed that when α≠0, the susceptibility will not be zero and it gives non- zero complex susceptibility. In this case, the microwave power will be absorbed by the sample and mathematically the average power absorbed within sample is

$$P = \frac{\mu_0}{2}\, \omega\, \chi_L''(h_{rf}^{\chi})^2 V \tag{1.19}$$

Here V is the volume of specimen and the magnetization is restricted only on X-direction.

1.11 Spin wave

LLG equation describes the magnetization dynamic of homogenously magnetized specimen using macro-spin approximation. However, in reality, it is extremely hard to realize a specimen with uniform magnetization because of the thermal fluctuation as well as edge effects on ferromagnetic specimens. For example, at absolute zero temperature, magnetic moments of ferromagnetic materials are perfectly aligned but when the temperature reach at Curie temperature the magnetization is completely vanish. Bloch introduced the temperature dependence of the magnetic moment by stating that the low temperature dependence excitation of magnetic moment creates wave called spin wave[45]. In fact, the spin can be generated by means of any perturbation on the system. For example, it can be pulse,

electromagnetic wave or even heat [46]. Heller and Kramers explained the spin wave in terms of the precessing spins[47]. In ground state, there will be the interaction between the nearby spin which give rise to the parallel arrangement of them. However, if the external perturbation is applied on the system, the spins will start to precess with slightly different phase with the neighboring spin and there will be phase difference which ultimately results the wave like behavior. As shown in figure 1.10 [a], where all spin precess in phase with infinite wavelength which means that the wave vector (k) is zero. In figure

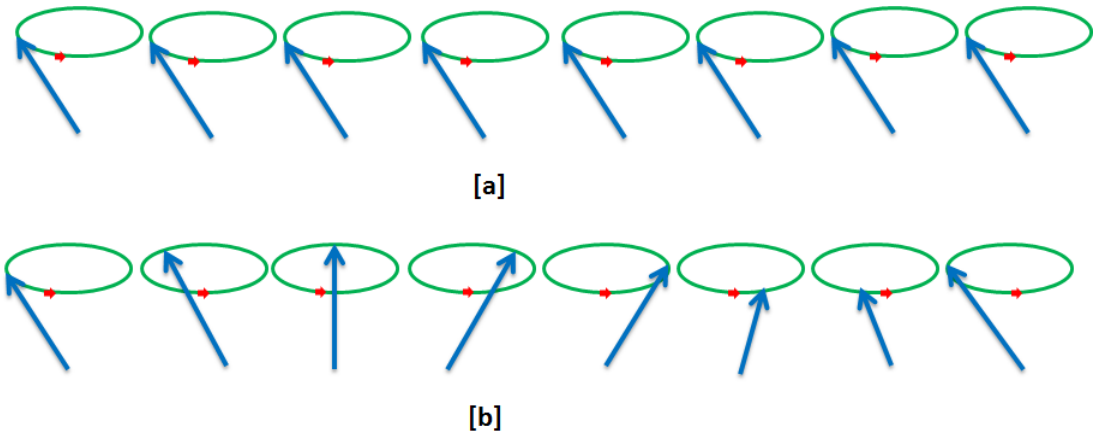

Figure 1.10: (a) Oscillation of spin in phase (b) out of phase

1.10[b], spins prcecess out of phase with certain wave vector and behave as wave called spin wave.

The wavelengths of the excited spin wave are determined by two factors. For long wavelength, there will be dipolar dominated interaction and for short wave length there will be the exchange dominated interaction between spins [48, 49].In addition, there are three main types of spin waves especially in thin films samples. For a given structure, they are classified by propagation direction of the spin wave with respect to the external applied field. In the following, we will be discussing about these three types of modes.

Forward volume magneto-static spin wave (FVMSW): FVMSW is excited when the sample is magnetized in the perpendicular direction with respect to the direction of propagation of spin wave. Dispersion relation for this configuration can be expressed as [50]

$$f_{FVMSW} = f_H \sqrt{\left(f_H + f_M\left(1 - \frac{1 - \exp(-kdo)}{kdo}\right)\right)} \quad (1.20)$$

Where $f_M=4\pi\gamma M_0$ and $f_H=\gamma H_0$. M_0 and do are saturation magnetization and thickness of film respectively.

Similarly, when the sample is magnetized in plane, there exists two types of spin wave and they are named as backward volume magnetostatic waves (BVMSW) and magnetostatic surface spin waves (MSSW).

For BVMSW, the propagation of spin wave occurs along the magnetization direction and the dispersion relation can be expressed as [50]

$$f_{BVMSW} = f_H \sqrt{\left(f_H + f_M \frac{1 - \exp(-kdo)}{kdo}\right)} \quad (1.21)$$

Finally, MSSW generally localized on one surface of thin films. The amplitude of precession is exponential in nature with the minimum on one surface and maximum on next one. The dispersion relation for MSSW wave could be expressed as [50]

$$f_{BVMSW} = f_H \sqrt{\left(f_H + f_M \frac{1 - \exp(-kdo)}{kdo}\right)} \quad (1.22)$$

The systematic of the direction of propagation of spin wave and magnetization for all configurations is presented in figure 1.11.

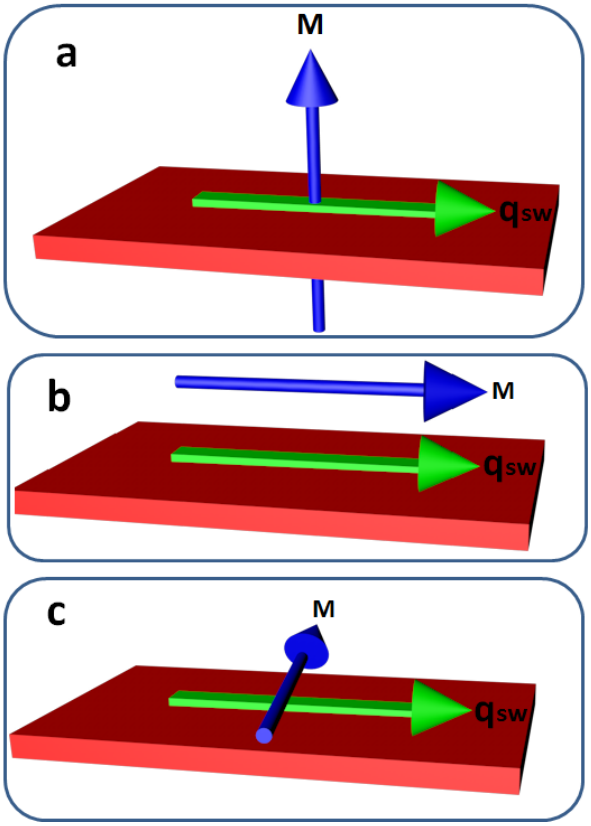

Figure 1.11: [a] FVMSW [b] BVMSW [C] MSSW modes on thin film

Chapter 2: Sample fabrication and characterization techniques

In this chapter, various sample fabrication and characterization techniques will be discussed. In terms of fabrication techniques; different state of the art techniques have been used. For example, photolithography, electrons beam lithography, sputtering, lift-off and focus ion beam (FIB). In terms of characterization methods, several advanced scientific instruments such as Vibrating Sample Magnetometer (VSM), Magneto Optical Kerr Effect (MOKE), Atomic force microscopy (AFM), Magnetic force microscopy (MFM) and broadband ferromagnetic resonance (FMR) techniques have been implemented. In the following sections, all techniques that had been implemented will be discussed briefly.

2.1Sample fabrication techniques

2.1.1Design of coplanar waveguide (CPW)

The high frequency characterization of almost all samples was carried out using the VNA-FMR technique. The first step in experimental procedure was to design ideally loss-less CPW. Two types of CPWs have been fabricated to study the magnetic systems.

The first type of CPW was fabricated to study the thin films samples which were bigger in size and had strong magnetic signals. Before fabrication of CPW, the CST MWS STUDIO software was used to determine the shape, size and dimension of CPW and to achieve characteristic impedance of 50 Ohm. It has been a well-established technique to use dielectric material and conductor to fabricate lossless transmission lines. Slab of Rogers with gold on both sides were used to fabricate the CPW. Vias from top to bottom were created to get uniform electric and magnetic field on the signal line of CPW. The typical structure of CPW which was used in this study is presented in figure 2.1. The red arrow at the ends represents the ports and circle on the both side of signal line are vias.

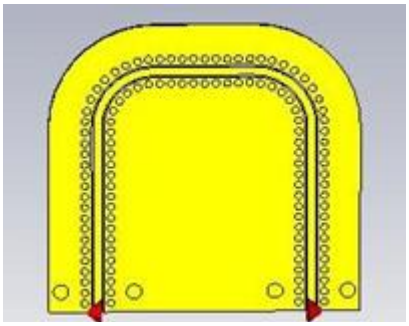

Figure 2.4: CPW with ports at ends.

Scattering parameters (S-Parameters) are the most important parameters to consider for characterization of microwave devices. In the process of characterization of magnetic samples, we tracked these parameters as a function of magnetic field and microwave frequency. In the following, we will be discussing about S-parameters and express them mathematically.

The uses of current and voltage concept on a circuit, where hundreds of components (such as resistor, capacitor and inductor) are involved, are rather complicate [51]. The concept of S-parameter allows us to get complicated information in a simple way like as a black box. For microwave devices, it is important to consider that the ports at the end of the circuit's components are connected with each other. Transmission and reflection of microwave signal takes place when signal go through the different ports. Generally the amplitude of these signal are considered to express S-parameter mathematically. In addition, since S-parameters are complex in nature, which allows us to get information about also the phase of the signal along the circuit. For N port system, there are N^2 S-parameters and we will express them mathematically in the following.

For simplicity, let us consider a two port device. a1 and b1 are the amplitude of incident wave and reflected wave at port 1 and 2 respectively and a2, b2 are for port 2 as in figure2.2. If the ports are

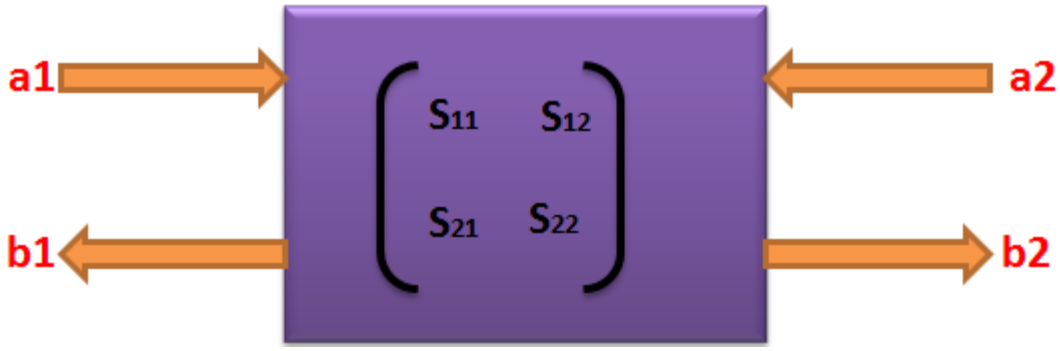

Figure 2.5: 2 port devise with S-parameters

terminated with the characteristic impedance, the S-parameters are defined as[51],

$$S_{11} = \frac{b1}{a1}$$

$$S_{12} = \frac{b1}{a2}$$

$$S_{21} = \frac{b2}{a1}$$

$$S_{22} = \frac{b2}{a2}$$

We can also express the relation between amplitude of signal and S- parameters in matrix form,

$$\begin{pmatrix} b1 \\ b2 \end{pmatrix} = \begin{pmatrix} S_{11} & S_{12} \\ S_{21} & S_{22} \end{pmatrix} \begin{pmatrix} a1 \\ a2 \end{pmatrix}$$

For lossless transmission lines, it is most important to have characteristic impedance on each port of components of a device. The simulated normalized impedance of CPW is presented in figure 2.3. The microwave frequency was swept from o to 25 GHz and impedance was tracked. Ideally CPW with

characterized impedance was achieved and pink line represents the variation of impedance with

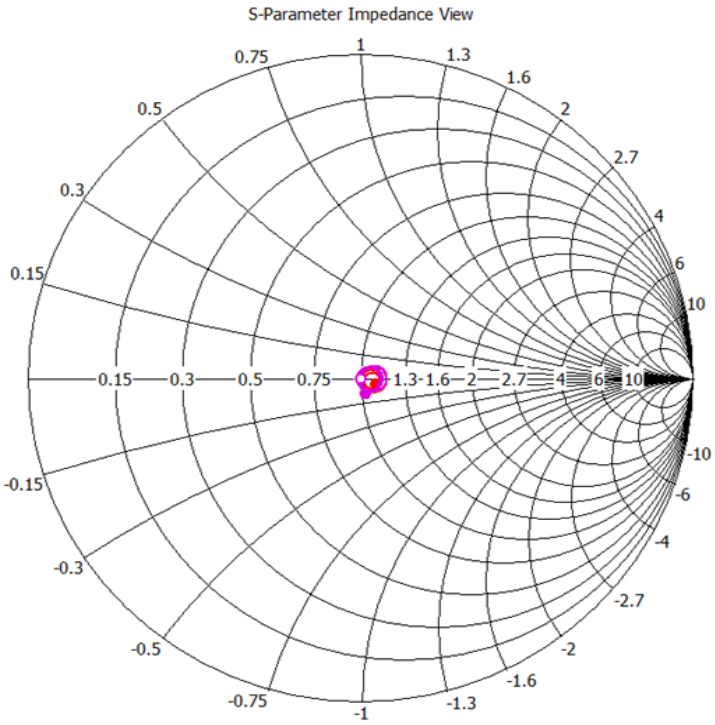

Figure2. 6: Smith chart with normalized impedance

frequency. The CPW with ideal impedance of 50 Ohm was fabricated.

Now we will be discussing about the second type of CPWs that were fabricated and used to study the magnetization dynamic of magnetic nanostructure. CPW, which is bigger in size, has lower sensitivity for smaller amount of sample because the radiation loss is proportional to the volume of CPW[52]. To overcome this challenge, it is important to fabricate smaller CPW in size. Creating nanostructure directly on the top of signal line does not only increase sensitivity but it also reduce the fabrication cost of sample especially using electron beam lithography.

Before fabrication of CPW, the shape, size, structure and materials for CPW was designed using CST microwave studio. The standard photolithography, sputtering and lift-off process was used to fabricate CPWs. The systematic of this process is presented in figure 2.4. In figure 2.4 [a], the process of

fabrication of CPW is depicted systematically which involves multiple steps. Similarly in figure 4 [b], the typical SEM image of final product of CPW is depicted. In brief, the following procedure was used to

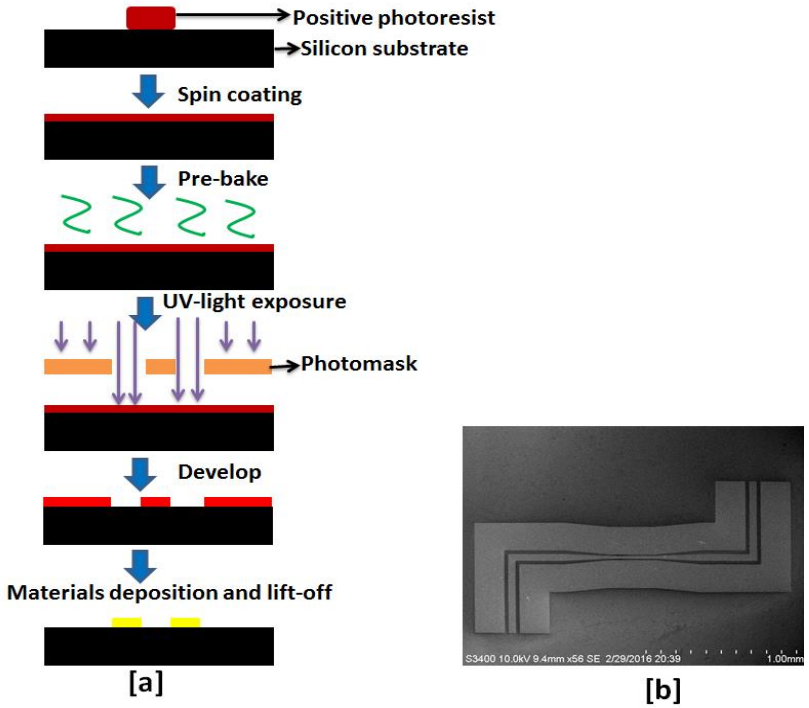

Figure2. 7: [a] systematic to fabricate CPW [b] SEM image of CPW

fabricate CPW. The positive photoresist was coated on clean silicon substrate using spin coating technique. Then, it was baked on a hot plate at temperature 110^0 C for 1 minute. After that the substrate was covered with the photomask and exposed with the UV light for 2 minutes. Then it was developed with the developer. Cr (5 nm)/Cu (150 nm)/Pt (10nm) were deposited with the help of sputtering technique. Finally lift-off technique was used to achieve CPW with characteristic impedance of 50 Ohm and the final product is depicted on [b] figure 2.4.

2.1.2Electron beam lithography (EBL):

EBL is a state-of- art technique to fabricate especially nanostructures materials[53]. This technique offer high resolution to produce nanostructures compare to photo-lithography process. Short wavelength of electron beam overcomes the diffraction effects which especially exist with UV light and ultimately allows creating structures which is impossible by using photolithography technique. Although the process that EBL technique works is similar to the photolithography process, the fundamental difference is that coherent electron beam is used to write pattern in EBL technique whereas UV light is used for the photolithography process. The resolution up to few nanometers has been achieved using e-beam lithography technique.

In the following, we will be discussing about the electron beam lithography process in detail. Firstly, since we were preparing sample on the top of signal line of CPW, the first step was to fabricate CPW. Substrate, with CPW on it, was coated with 950 Poly-methyl-Methacrylate (PMMA) positive resist. Spin coater at speed of 4000 rpm was used to distribute resist layer homogenously all over the substrate. The sample was then baked for 80 second at temperature of 130^0 C. The pattern which we would like to fabricate was designed using AutoCAD software and loaded to the NPGS software. Working distance of 9mm was used on the writing process. The electron beam current of 20 pico-amperes was used to achieve high resolution patterns. When the writing process completed, resist was developed by using solution of Methyl-isobutyl-ketone (MIBK) and isopropyl alcohol in 3:1 ratio for 60 second. Finally, deposition and liftoff process was used to fabricate sample with desired shape and size on the top of signal line of CPW.

2.3Focus ion beam (FIB):

FIB is an advance technique that has been widely used in semiconductor industry, biology and materials science [54-57]. Although the FIB looks similar in physical outlook with SEM, the way it works is

different. In a FIB system, beam of focused ions are used instead of an electron beam as in SEM. The Quanta 3D DualBeam FEG, which was combined with FIB, was used to fabricate samples. Focused Ga ion beam was used to etch surface of thin film and to fabricate the periodic pattern structure in the form of grooves[58]. The samples with high resolution were achieved. During etching process, beam current 1.5 pico-ampere was used. The etching time was kept constant to achieve ideally the constant etched thickness for all samples. A sample fabricated by etching the material from the surface of Permalloy's thin film to produce one dimensional groove and SEM image is presented in figure2.5.

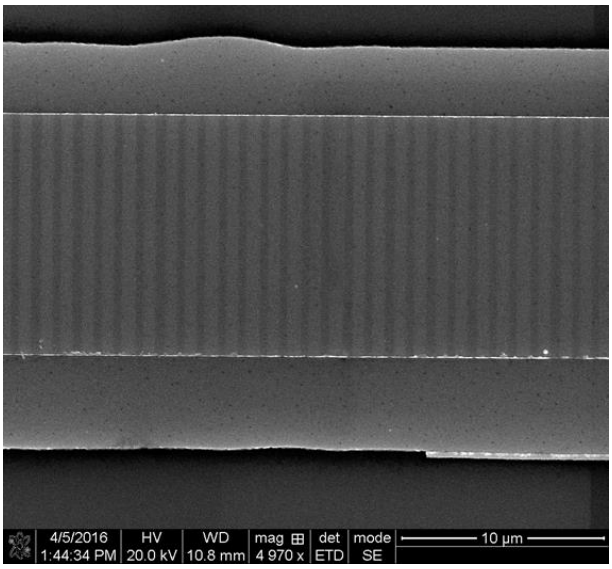

Figure2. 8: SEM image of surface modulated structure using FIB.

2.2 Characterization techniques

2.2.1 Static characterizations techniques

Generally magnetic materials are characterized by two techniques which are static and dynamic. These techniques are classified by taking account the time scale to probe magnetic properties. Static characterization technique is used to probe the magnetic properties on long time scale. In contrast, for the dynamic, the time scale that the properties of samples are probed is generally short. It might be in nanosecond or even at femtosecond range. Static technique generally provides information about the

type of materials, for example, whether it is diamagnetic, paramagnetic or ferromagnetic material. In addition, information about the domain, magnetic hysteresis loop, susceptibility can also be achieved using it. Similarly, in dynamic characterization technique, it is possible to get information about different type of anisotropies in magnetic system. In addition, spin dynamic in time domain as well as in frequency domain can be realized. In the following, we will be discussing about experimental techniques that were used to characterize samples.

2.3.1Vibration sample magnetometer (VSM)

VSM is generally used to get information about the magnetic moment as a function of applied external field. Basically it works based on the Faraday's law of electromagnetic induction. Experimentally, the sample is mounted on the sample holder and inserted in between the electromagnets. The systematic sketch of VSM is presented in figure 2.6.

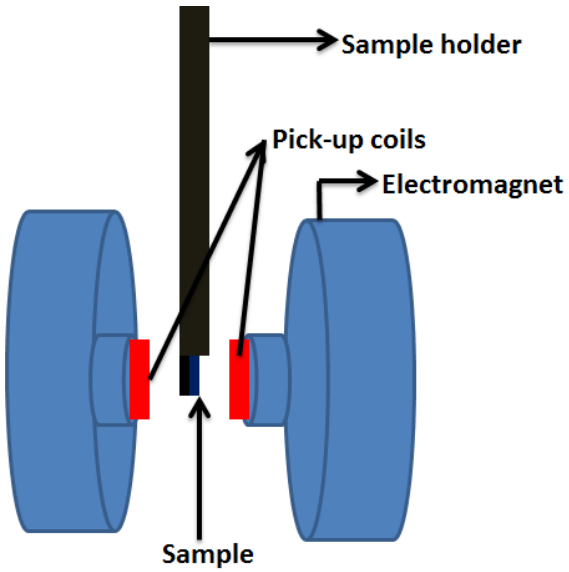

Figure2. 9: Systematic of VSM

When external magnetic field is applied using electromagnets as in figure 6, it induces the magnetic moment within sample. The sample vibrates in sinusoidal motion which changes the magnetic flux.

Changes on flux induce a voltage and it is proportional to the magnetic moment of the samples. The AC voltage is detected by the pick-up coil. Finally the magnetic moment is achieved as a function of applied field [59]. This technique allows getting information about coercively, remanence, saturation magnetization and anisotropy of samples. In addition, the temperature dependence magnetic properties can be measured both in low and high temperature range.

To get more information about the switching field distribution and coercively distribution, First Order Reversal Curve (FORC) technique can be used using VSM [60]. FORC is a robust experimental technique to get critical information about interaction and coercivity distribution of magnetic materials which is not possible with the regular MHL [60-62]. The standard MHL loop can be used to get information about the saturation magnetization, remanence field, coercivity of the composite magnetic materials. However, the switching behavior such as the reversal and irreversible components of magnetization can be achieved with the FORC technique.

This technique has been used in scientific community for different purposes. For example, in geological samples, FORC technique can be used to get information about composition as well as grain size distribution of magnetic materials[63]. In data storage application, it is possible to get information about the exchange bias as well as switching field distribution of magnetic media[64]. In addition, FORC diagram can be used to get the different kind of interaction in magnetic materials such as magnetostatic, dipolar as well as exchange[65, 66]

2.3.2 Magneto-Optic Kerr Effect (MOKE) spectroscopy

The concept of MOKE was introduced by Micheal faraday in 1845. He found that when polarized light passes especially through dielectric medium, the plane of polarization of light is changed in presence of external magnetic field. In 1877, Kerr observed similar phenomenon when polarized light was reflected from the magnetic sample. This principal was used to probe the magnetic properties using MOKE

spectroscopy. Walker later also discovered that the internsity of reflection of the polarized light also changes in presence of mangetic field. These phenomena is very important to read and write data on magnetic memory. For example, when light reflected from magnetic sample with different domain orientaion, the polarity of the reflected light also different. The change in polarity can be used as 1 or 0 in data read and write process.

Depending on the orientation of magnetization with respect to the incident plane polarized light, there are three different configurations. They are named as longitudinal, transverse and polar. They will be discussed briefly in the following.

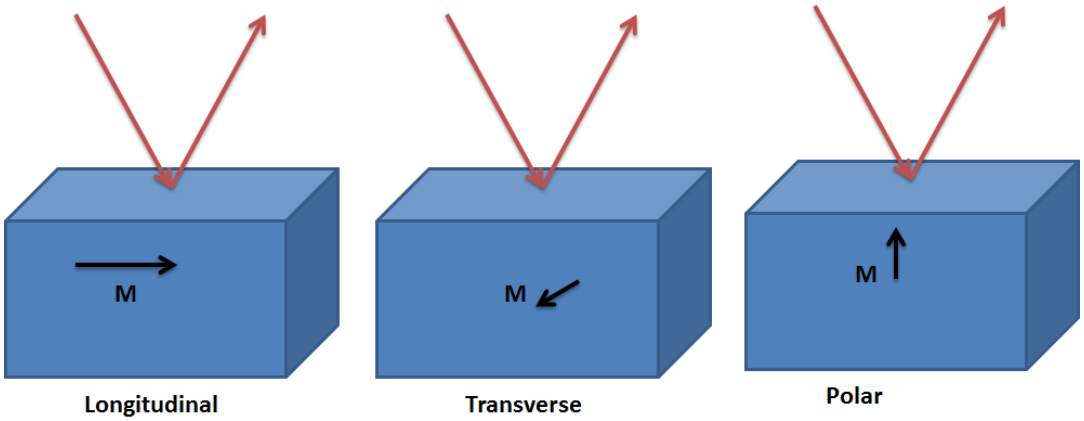

Figure2.10: orientation of plane polarized light, which is represented by red arrow, and magnetization

In Longitudinal configuration, the magnetization within sample is parallel to both reflection surface as well as plane of incident polarized light. Here, linearly polarized light incident on the surface of specimen and the elliptically polarized light is detected. The change on the polarization is proportion to the magnetization of the sample. Similarly, In case of transverse MOKE, the magnetization of sample is perpendicular to the plane of incident polarized light and magnetization is parallel to the surface. Finally,

for polar, magnetization in the specimen is perpendicular to the sample surface and in plane with the incident polarized light. The systematic for all configurations is depicted in figure 2.7.

2.3.3Magnetic Force Microscopy (MFM)

MFM is a well-established experimental technique to retrieve information about magnetic domains and switching fields. Direct observation of magnetic domains in real time, at different external magnetic field, with resolution down to nanometer scale makes this technique versatile to study magnetic materials. In addition, less effort on sample preparation and providing topography information as well makes this system further appealing.

The MFM technique basically probes the interaction force between the magnetic tip and stray magnetic field from the sample's surface. It works basically on two modes and they are static and dynamic modes. In static mode (also called dc mode), the interaction force between sample and tip has been measured by tracking the deflection of the cantilever from equilibrium position. Mathematically deflection (δ) of tip can be expressed as

$$\delta \approx \frac{F}{k}$$

Where F is the interaction force between tip and sample and k is spring constant of cantilever.

Similarly for dynamic mode (called ac mode), the cantilever is first tuned with resonance frequency. The change in amplitude, phase or frequency due to interaction between tip and sample is monitored. If A is amplitude, ω_0 is resonance frequency and ϕ is the phase of natural resonance of cantilever, the change on the amplitude, frequency and phase due to the force gradient (∂F/∂z) can be expressed as [67]

$$\Delta\varphi \approx \frac{\mathrm{Q}}{\mathrm{k}}\frac{\partial \mathrm{F}}{\partial \mathrm{z}}$$

$$\Delta A \approx \frac{2A_0 Q}{3\sqrt{3}k} \frac{\partial F}{\partial z}$$

$$\Delta\omega_0 \approx -\frac{1}{2k} \frac{\partial F}{\partial z} \omega_0$$

Here Q is the quality factor of cantilever.

Experimentally to get MFM image, the normal silicon tip is coated with the thin film of ferromagnetic material. The material is chosen depending on the nature of the sample that is going to be probed. For example, tips with variety of magnetic moment and coercivity are available to achieve high resolution

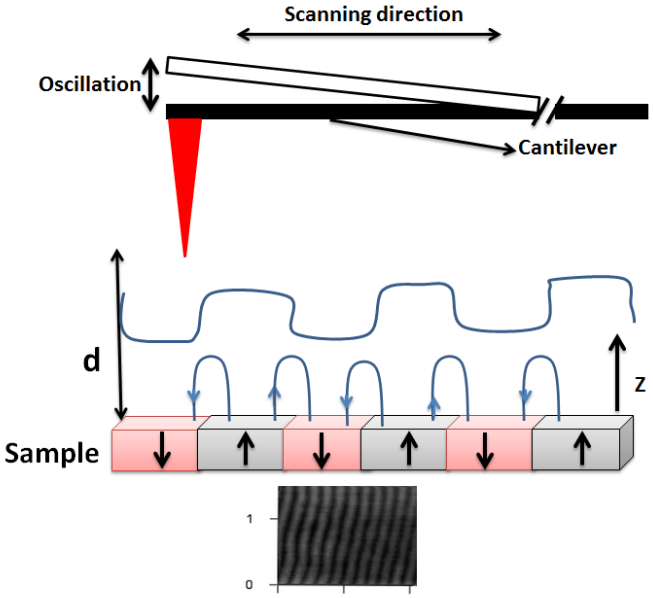

Figure 2. 7: outline of MFM components and profile of force gradient from surface.

MFM images. In regards to experimental procedure, firstly the tip is saturated by applying external magnetic field. Then, tip is tuned close to its resonance frequency. After that the tip is scanned over the sample at a fixed distance from the surface (typically 100nm to track magnetic interaction) and the deflection of the tip takes place due to the force gradient from sample. The deflection of the tip is proportional to force gradient. In addition, the spring constant of the cantilever changed due to the

interaction of the tip and sample. For example if k is a natural spring constant of cantilever, the modified spring constant due to force gradient can be expressed as,

$$k_f = k - \frac{\partial F}{\partial z}$$

For the attractive interaction, $\frac{\partial F}{\partial z} > 0$ and results cantilever spring softer. Similarly $\frac{\partial F}{\partial z} < 0$ represents the repulsive interaction. Depending on whether attractive or repulsive interaction, different contrast are observed which provides the information about the orientation of magnetization within sample. It will be worth to mention that depending on the distance between and sample and probe tip, different type of force contributes on force derivative. For example, if the gap between sample and tip is very close, it probes van der-waals force. However, the magnetic force is long range in nature thus sample is probed far away from sample surface (typically 100 nm). In figure2.7, systematic of the tip sample configuration is depicted.

Let us consider slab which has magnetic domains are oriented out of plane. Depending on the orientation of stray field, the deflection or attraction of the cantilever takes place. Then since we set the set point fix, the path of the cantilever is traced which basically provides the information about the type of stray field coming out from the sample. If the orientation of magnetization of tip and sample is same, there will be black contrast and for opposite it will be white. The black and white stripe domain on permalloy thin film is represented in the bottom of figure 2.7.

Mathematically, when the magnetic tip is brought close to the sample, the magnetic potential energy can be expressed as [67]

$$\mathrm{E} = -\mu_0 \int \mathbf{M}_{\mathrm{tip}} \,.\, \mathbf{H}_{\mathrm{sample}} \, \mathrm{dV}_{\mathrm{tip}}$$

Where $\mathbf{M}_{tip}$ is the magnetization of tip of the probe and $\mathbf{H}_{sample}$ is the stray field from the sample. Force experience by the probe can be expressed as,

$$F = -\nabla E = -\mu_0 \int \nabla(\mathbf{M}_{tip} \cdot \mathbf{H}_{sample}) dV_{tip}$$

The integration is carryout throughout the tip of probe.

2.4 Dynamic characterization techniques

2.4.1 Ferromagnetic resonance

Resonance absorption of electromagnetic radiation within the ferromagnetic materials is called ferromagnetic resonance [68]. In 1913, the first resonance spectrum was observed by Arkad'yev. The important aspect of ferromagnetic resonance technique is that low amplitude of the excitation field allows investigating the ground state properties of ferromagnetic materials without perturbation (more details on chapter 1). For example, magnetization, magnetic anisotropies, g-factor and damping constant can be determined with high precision. In addition FMR technique helps to develop microwave devices such as circulator, microwave filter, oscillator, amplifier and spintronic devices. The systematic

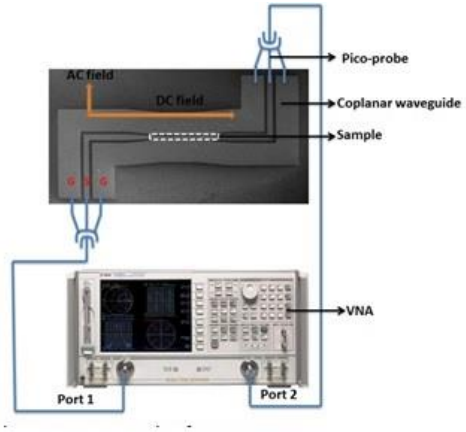

Figure 2.11 : systematic of FMR set up

diagram that was used to study the dynamic behavior of ferromagnetic materials is presented in figure

2.8. The ground- signal- ground (GSG) type coplanar waveguide was connected with non-magnetic end launch connectors followed by the coaxial cable and finally with the VNA ports. The samples were fabricated with the help of e-beam lithography, sputtering and lift-off method on the top of the signal line of CPW and process in details has been discussed in details in chapter 1.

The microwave frequency was swept at different frequency range depending on the nature of the samples. The microwave current generates uniform ac magnetic field at the signal line of CPW. External magnetic field was swept from positive saturation to negative saturation at field step of 5 Oe and the orientation of the ac field and DC field was kept perpendicular to meet the requirement for FMR. The scattering parameter (S_{21}) was recorded as a function of microwave frequency and external field. The experiments were carried out at room temperature.

Chapter 3: Exchange bias in (FeNi/IrMn)n multilayer films evaluated by static and dynamic technique.

3.1Introduction to exchange bias effect

In this chapter, we will discuss the exchange bias in multilayer systems. Exchange bias is an interfacial effect which exists at the interface between ferromagnetic [F] and antiferromagnetic [AF] specimen [69]. In antiferromagnetic system, spins in one crystal plane are parallel however orientation of spins on the adjacent plane antiparallel. For example, in case of MnO, spin on plane [111] are parallel but the adjacent plane [111] has antiparallel spins [70]. On the other hand, ferromagnetic materials have spontaneous magnetic moments. Therefore, when F and AF system are brought into contact and the system is heated in presence of a magnetic field, it generates a unique effect at the interface, which helps to pin the spins of ferromagnetic material at interface. This is called exchange bias. The first signature of the coupling is the asymmetry of MHL with respect to origin [69]. The spin configuration of

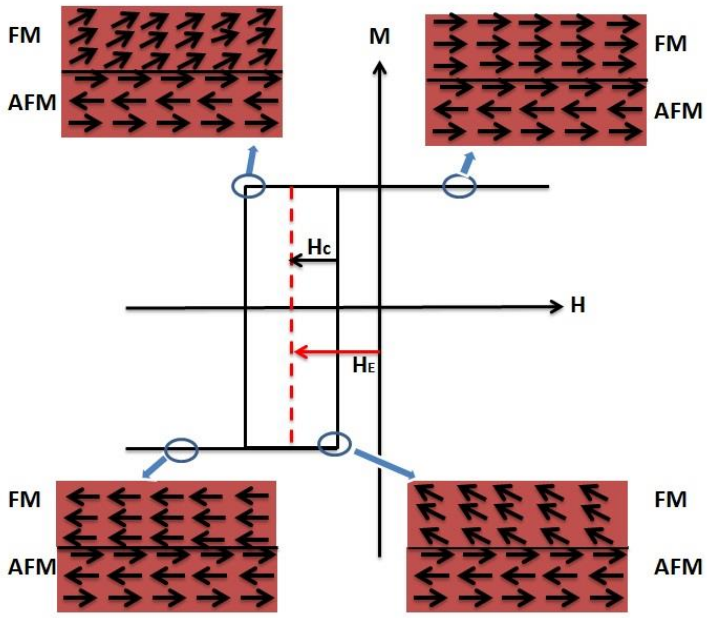

Figure 3.12: Spin configuration of FM and AF layers at different external magnetic field.

FM and AF at different external magnetic fields is represented in figure 3.1.

In figure 3.1, four different points on MHL loop are considered to explain how the spins orient at different external magnetic field. Let us consider a state where the sample is positively saturated (the spin configuration is presented on top right). The spins on FM materials are perfectly align along the applied field direction. When magnetic field value decrease (top left), the spins on FM layer are ready to flip to the opposite direction. However the switching fields are not symmetric with respect to origin. The coupling strength between FM and AF determines the shift of the center of MHL loop from the origin. It is called bias field, or, more specifically, exchange bias field. In figure 3.1 the exchange bias field is denoted by H_E. The similar process is represented on the right and left panel on the lower panel in figure 3.1 when the magnetic field is swept from negative to positive. The point to be noted here is that the magnetization on AF is hard and external magnetic field cannot flip it. The AF layer is used only to pin the FM layer.

Exchange bias effect has tremendous impact on technological applications. One of them is that this effect can be used as sensor to read and write data in magnetic memory. In the following, we will be discussing about a particular practical application in detail about uses of exchange bias effect as sensor in Giant Magnetoresistance (GMR)[71]. In GMR head, there will be four thin layers. The first one is the AFM layer and it is used to pin the spin of FM layer in specific orientation. Two F layers are separated by

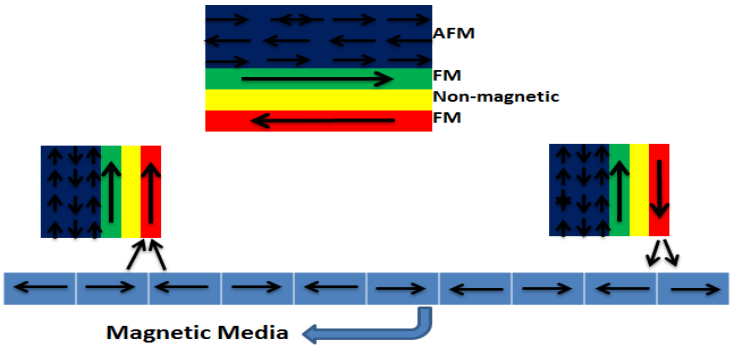

Figure3.13: systematic of GMR sensor to write and read data

non-magnetic thin layer and the schematic is presented in figure 3.2. The way GMR heads are used to read and write in the magnetic medium is following. Generally the data are stored in the magnetic domains of magnetic media. Magnetic stray field presents at the interface of magnetic domains and the orientation of magnetic moments are represented with the arrows in figure 3.2. Depending on the orientation of neighboring spins, the force between media and free layer would be attractive or repulsive. As presented in figure 3.2, when stray fields switch the orientation of free FM layer, the orientation of the spins of the pined and free layer will be parallel and the resistance across the multilayer will be small. In contrast, when the orientation of spins on pined layer and free layer are opposite, there will be maximum resistance. The change in resistance is measured electronically and the maximum and minimum resistance can be read as 0 and 1 in data storage applications.

In addition, exchange-coupled multilayer systems are also ideal candidates for spin valve sensors, microwave devices as well as in spintronic applications [72-77]. To enhance the applications of these coupled systems, understanding the coupling mechanism and consequent effect on static and dynamic properties is crucial. Extensive research in this regard has been done both theoretically as well as experimentally [78-81]. For example, in previous studies, thickness of both F and AF layer was varied to better understand thickness dependent exchange bias [82]. Temperature dependent studies on this configuration have also been considered [78]. Misalignment of anisotropies, such as uniaxial and unidirectional, because of the different thickness of the AF layer has been studied [82]. However, spin frustration, nature of the magnetic domain, domain boundaries, and imperfection coupling between F/AF layers significantly alter coupling scheme and it is hard to achieve theoretical expected exchange bias results. In addition, experimental techniques, which are used to probe exchange bias, are also important to quantify the exchange bias value.

In this study, we consider set of multilayer sample of F/AF thin layer. FeNi and IrMn were considered as FM layer and AFM layer respectively. Comprehensive study of both static and dynamic properties has been performed.

3.2 Sample preparation and characterization techniques:

A silicon substrate was coated with thermally oxidized 50nm thick SiO_2. Multilayer films of composition [FeNi(t nm)/IrMn(20 nm)]×n(t) where FeNi represent Ni(80%) and Fe(20%) were deposited on the substrate using dc-triode sputtering method with base pressure of 3.0×10^{-9} Torr and Ar pressure at the time of deposition was of 1.0×10^{-3} Torr. The deposition process was performed at room temperature. A 10 nm thick Ti layer was used as both a seed and capping layer. During the deposition process, the external magnetic of field 250 Oe was applied along the long axis of slab to induce a longitudinal magnetic anisotropy. The structural information for a set of three samples is presented in tabular form below.

Sample	FeNi t(nm)	IrMn t(nm)	Repetition number, n	Full thickness (nm)
S_1	20	20	10	400
S_2	60	20	5	400
S_3	80	20	4	400

The thickness of IrMn layers were kept constant for all samples. In-plane anisotropy and unidirectional exchange bias were induced due to specific fabrication process.

The MHL and FORC measurements were implemented to carry out the static measurements. A Princeton AGM-VSM magnetometer was used for room temperature studies. The external magnetic field was applied along the easy axis of samples. The robustness of this instrument is that it can collect

100 FORC in less than 2 hours with typical sensitivity of 0.5 μemu and 1 second average time per point [83].

In terms of dynamic characterization, X-band FMR spectra were collected using Bruker EMX-FMR spectroscopy. The FMR spectra at frequency 9.8 GHz were collected by sweeping external magnetic field from 0 to 2000 Oe. The total sweeping time for a spectrum was ∼80 sec. Angular dependent of FMR was performed with step of 3^0 up to 360^0. Angular depend resonance fields were tracked for all samples.

Broadband vector network analyzer ferromagnetic resonance (VNA-FMR) was carried at room temperature. Ground-signal-ground (G-S-G) type planer coplanar waveguide was connected VNA via co-axial cable with the help of non-magnetic connector. The samples were flipped on the top of signal line of CPW and both frequency and field-dependent resonance were tracked. The microwave field due to microwave current was kept always perpendicular to the external magnetic field to satisfy the condition for FMR. The magnetic field was swept from 3.5 KOe to -3.5 KOe with step of 10 Oe. Microwave frequency was swept from 1 GHz to 25 GHz at each magnetic field step. Transmission coefficient of scattering parameter was recorded as a function of magnetic field and microwave frequency.

3.3Static experimental results

Static measurement: MHL for samples S1, S2 and S3 is presented in figure3.3. The samples were placed in-plane parallel to external magnetic field direction and field was swept from 400 Oe to -400 Oe with field steps of 2 Oe. The MHL at orientation 0^0, 90^0 and 180^0 are represented by blue, red and black color respectively in figure 3.3. 0^0 means the applied field was applied parallel to the exchange bias orientation and so forth.

At, 0^0 orientations, the MHL loop shift from origin to the negative field axis and for 180^0 the MHL loop shifts right to the origin of MHL loop. For 90^0, the MHL loop is symmetric with respect to the origin with no bias field at all.

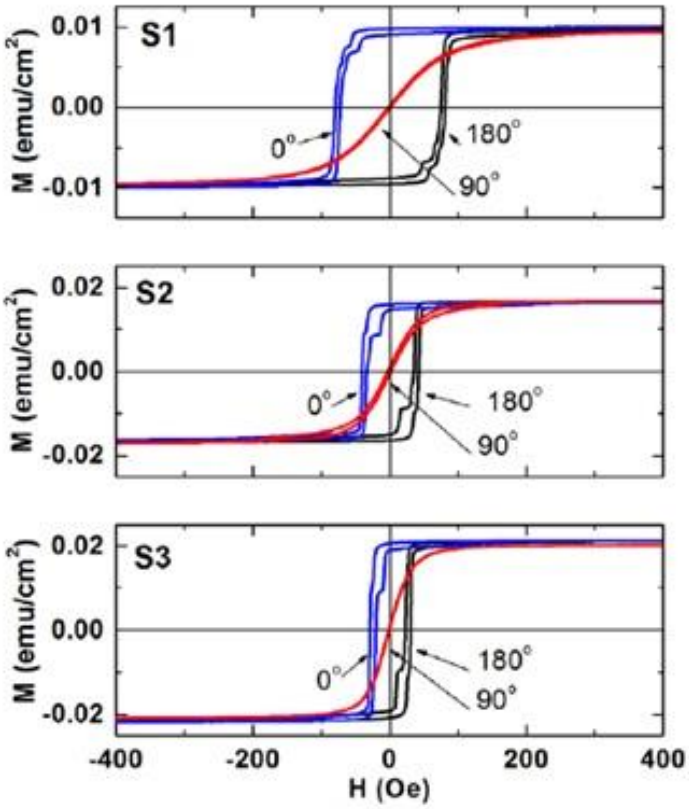

Figure 14.3: MHL at 0, 90 and 180 degree with respect to exchange bias field.

It was observed that coercivity fields (Hc) for sample S1, S2 were 3.5 Oe and 4.2 Oe for S3. However, exchange bias was significantly varied depending on the number of repetitions of FM and AFM layers. Numerically, 76.0 Oe, 37.0 Oe and 24.8 Oe exchange biases were observed for sample S1, S2 and S3 respectively. From these numbers it is elucidated that the exchange bias is significantly depends on the thickness of FM layer. The resultant coupling at the interface between FM and AFM was enhanced when the numbers of layers were increased.

If we closely look at the MHL loops, the kink at field close to the switching field has been observed for all samples. The position and the size of kinks are different for different set of samples. For sample S3, step of kink is largest and relatively smaller for S2 and S1 in a systematic way. To explain the observation of kinks, it will worthy to discuss about the sample configuration. For sample S3, there was four repetitions of (FeNi/IrMn), and the first deposited layer was FeNi. Since the exchange interaction exists at the interface of ferromagnetic and antiferromagnetic materials, the first layer of FeNi was not coupled to IrMn layer on both sides. The uncoupled surface of FeNi acts as a free layer of ferromagnetic materials and different hysteretic behavior can be observed corresponding to it. The consistency of the kink position and its shape with the number of layers substantially supports that kinks are relevant to the uncoupled region of ferromagnetic materials. Moreover, it was observed that there was one small addition kink for both S1 and S2. These additional kinks might be related to the different uniaxial anisotropy which was induced because of the microstructural defects and also roughness at the interface between F and AF layers [81, 84]. FORC study of these samples helped to explain and quantify the exchange bias as well as existed degree of inhomogeneity. In the following we will discuss about FORC study of these samples.

As we discussed in chapter 1, FORC is a well-established experimental technique to study the magnetic materials. Interaction field and switching field distribution of sample can be achieved with this technique [62, 85]. In addition, FORC technique has been using not only for magnetic systems but also for the electric and spin transition systems [86, 87].The FORC diagram represent the two dimensional contour plot in rotated coordinated system (h_c, h_u). Local coercivity (h_c) and bias field are expressed mathematically as h_c= (H-H_R)/2 and (H+H_R)/2 respectively. Irreversible switching processes as well as distribution of magnetic properties can be found using FORC method. Experimental FORC diagrams for samples S1, S2 and S3 have been presented below in figure 3.4, 3.5 and 3.6.

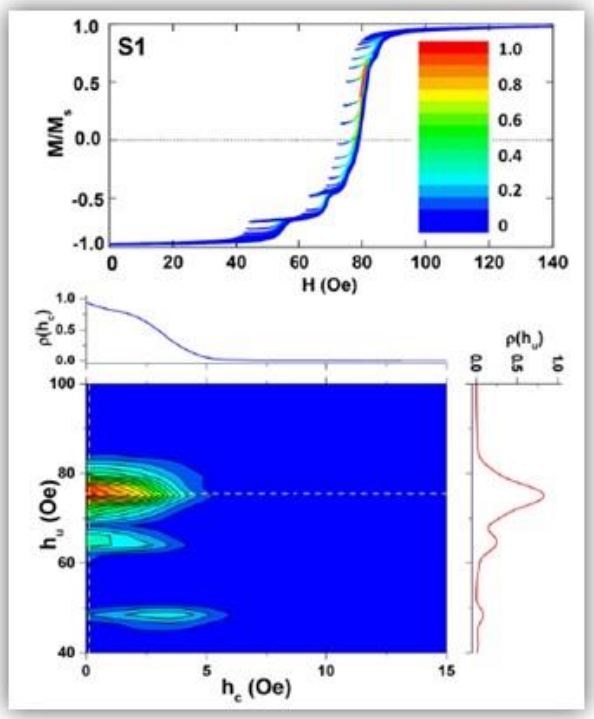

Figure3.15: FORC diagram and FORC distribution on upper and lower panel respectively for S1

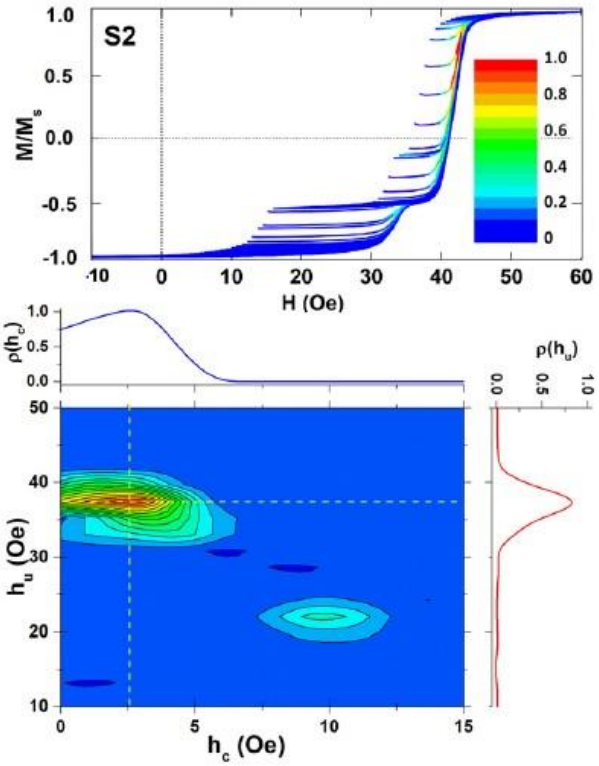

Figure3.5: FORC diagram and FORC distribution on upper and lower panel respectively for S2

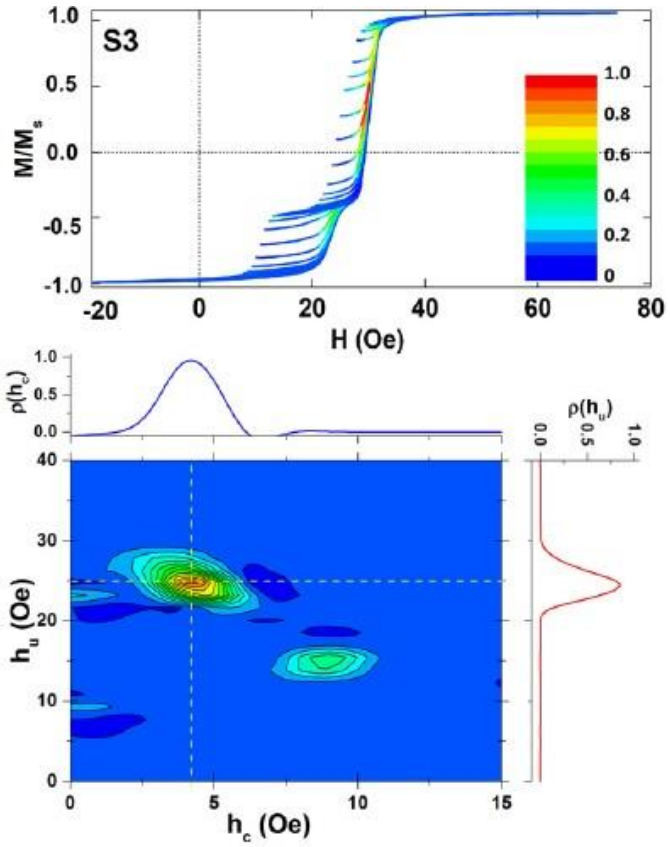

Figure3.6: FORC diagram and FORC distribution on upper and lower panel respectively for S3

In each diagram, there are two panels of figures. The top panel represents the M (H, H_R). The lower one represents the FORC distribution and has been represented by a color legend. From these figures, it has been clearly observed that in addition to the main FORC distribution there are also satellite distributions for all three samples. One possible reason for these satellite distributions might be the inhomogeneity at the interface of FM and AF layers. Pronounced distribution of additional modes for higher number of repetitions further supports this. The horizontal dotted line on center of FORC distribution represents exchange bias field and the vertical dotted line at the center of FORC distribution indicate the coercivity field. Experimentally, higher the number of repeated layers greater exchange bias has been observed.

Furthermore, in order quantify the profile of both interaction and coercivity field distributions, statistical analysis of main peaks of FORC distributions were carried out. The mean field values of $<h_c>$ and

($\langle h_u \rangle$) and corresponding standard deviation $\sigma\langle h_c \rangle$, $\sigma\langle h_u \rangle$ of both coercivity field and interaction field were obtained by using Gaussian distribution function. The extracted parameters from these distributions for all samples are presented in table below.

Table 3.1: information of sample structures

MHL			FORC			
Sample	H_{eb} (Oe)	H_C (Oe)	$H_{eb}=\langle h_u \rangle$	$\sigma(h_u)$	$H_c=\langle h_c \rangle$	$\sigma(h_c)$
S1	76.0	3.5	78.0	6.3	0.7	4.4
S2	37.0	3.5	39.0	3.4	2.8	3.0
S3	24.0	4.2	26.0	2.7	4.5	1.8

The following information can be inferred from these static experimental results. Firstly, the exchange bias value significantly depends on the number of repetition of FM and AF layers but the coercivity does not show significant change from one sample to another. Secondly, numerical bias fields evaluated from MHL and FORC methods were consistent. However, slight difference (2 Oe) on exchange bias from MHL and FORC were from the fact that the addition satellites modes were discarded to estimate the standard deviation in FORC method. Finally, FORC diagram provides more insight over MHL with additional important information such as coercivity and bias field distribution. Furthermore, increased standard deviation value of coercivity and exchange bias were consistent with the number of repetition which explicitly confirms that the increased number of FM/AFM layers results higher degree of inhomogeneity at the interface.

3.4Dynamic experimental results:

FMR is a well-established experimental technique to determine different types of anisotropies as well as to calculate damping constants of ferromagnetic system[68]. Small external perturbation energy of the

microwave allow calculating the ground state properties of the system precisely. Characterization of free energy of the system around equilibrium condition can be achieved using this technique. Since the free energy of the multilayer system is strongly dependent on the coupling between FM and AFM layer, angular variation of FMR and nature of FMR spectra provide useful information not only about the internal and demagnetization fields but also the exchange bias coupling [88-90].

There are generally two ways to get FMR spectra experimentally. First we kept the frequency of microwave constant and sweep the external magnetic field. In second method, the external magnetic field is kept constant and the microwave frequency is swept. The second method allows to get information about both field and frequency dependent FMR spectra. In this study, we use both techniques to get exchange bias values.

In-plane angular variation was carried out using Electron paramagnetic resonance (EPR) spectroscopy. X-band microwave with frequency 9.8 GHz was used and magnetic field was swept to collect the spectra. Figure 5 represents the angular variation of FMR for samples S1, S2 and S3. The unidirectional anisotropy is clearly reflected in bell-shaped angular variation. The orientation 0^0 was defined as the direction of the applied field along the direction of the exchange bias and 180^0 was antiparallel to it. Exchange bias is obtained from the angular variation by using the relation

[Hres (180^0) – Hres (0^0)] = 2 Heb.

The asymmetrical nature of angular dependence of resonance field close to 180^0 might be because of misaligning anisotropy or higher order anisotropy terms [80, 82]. In this study, the information about the anisotropy field Hk of the ferromagnetic layer is calculated by using the following equation 3.1 which provides the overall shift of the in-plane resonance field [91, 92]. So,

$$\delta H_{res} = H_{res} - H_{res,0} = H_{eb} cos\emptyset_H + H_K \, cos2\emptyset_H \qquad (3.1)$$

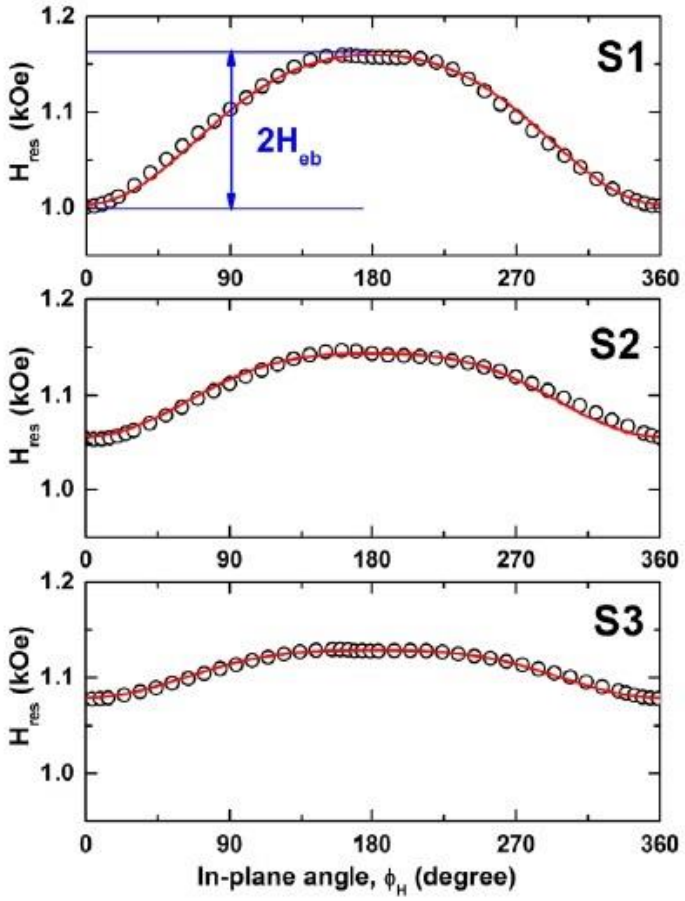

Figure 3. 7: In plane angular variation of FMR spectra with fit represented by solid line using equation (3.1)

Where the first and second term on the right side of equation (3.1) represent unidirectional and uniaxial anisotropy respectively of ferromagnetic layer. The exchange bias and anisotropy fields were extracted by fitting the X-band FMR data using equation (3.1) and presented in table below.

Table 3.2: Exchange bias values evaluated from X-band and broadband FMR

X-band FMR				Broadband FMR			
Sample	Heb (Oe)	Hk(Oe)	Hres,0(Oe)	Heb (Oe)	M(emu cm^{-1})	Hk(Oe)	Hra(Oe)
S1	78.0	10.1	1092	72.3	879	10.1	38.9
S2	43.6	8.2	1108	35.4	859	8.2	34.3
S3	24.8	5.1	1109	22.4	875	5.1	37.3

It has been clearly observed that exchange bias increased with decreasing the thickness of FM layer and the dynamic results were consistent with static results. However, the numerical exchange bias value extracted from the X-band FMR were larger than the values extracted from the static measurement such as MHL and FORC methods, especially for sample S1 and S2. These kind of discrepancies have also been observed in similar system and it was explained by considering the effect of degree of freedom in AF because of the reversal and irreversible measurement techniques [93]. We need to keep in mind that the MHL and FORC are irreversible techniques because of the switching of magnetization of FM layer is irreversible. In contrast, FMR is a reversible technique where the magnetization is perturbed with small microwave field. By comparing the date which is presented in table, it is clear that the offset on the exchange bias value measured from the MHL/FORC and from FMR are observed lower for sample S3, which means that the system with the lower number of AF layers did have little offset compared with the larger number of AF layers and it also support that the offset are somehow related to the degree of freedom of the AF layers.

To get comprehensive information in broadband frequency range, VNA-FMR was carried out at room temperature. A home designed coplanar waveguide was connected with the two port network analyzer via coaxial cables. The sample was flipped on the top of signal line of coplanar waveguide to make sure they were well contacted. The microwave frequency was scanned from 1 GHz to 25 GHz for each external magnetic field step. The magnetic field was scanned from 3.5 KOe to -3.5 KOe with field step of 5 Oe. The field and frequency dependence of the transmission scattering parameter (S_{21}) was recorded for every field and frequency scan. Three dimension contour plots of S21, frequency and field are presented in figure3.8, 3.9 and 3.10 for S1, S2 and S3 respectively.

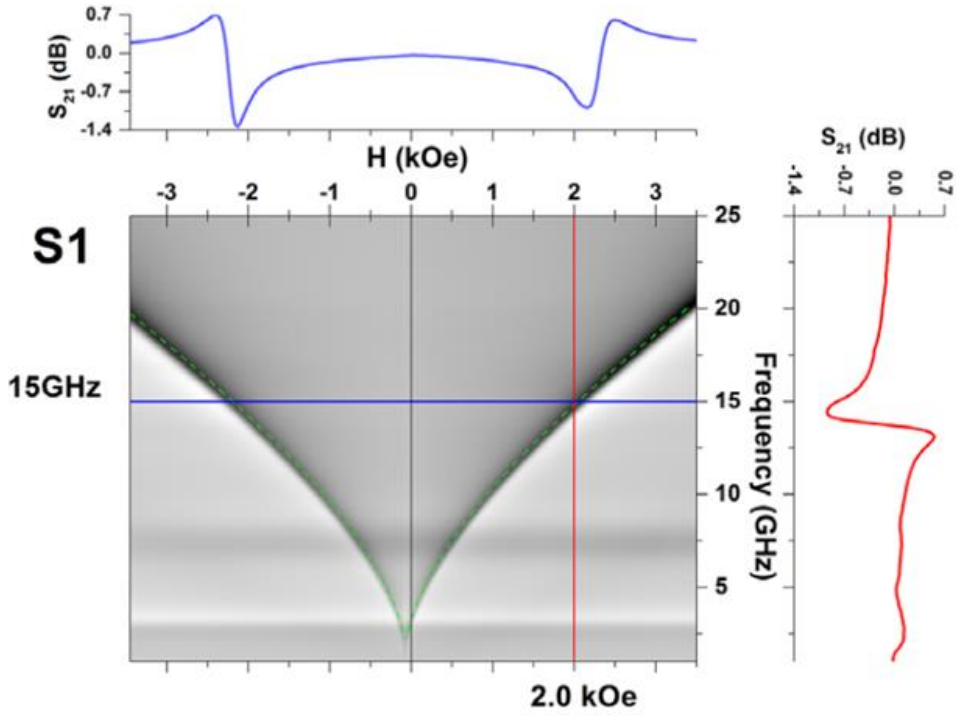

Figure 3.8: contour plot of FMR for sample S1

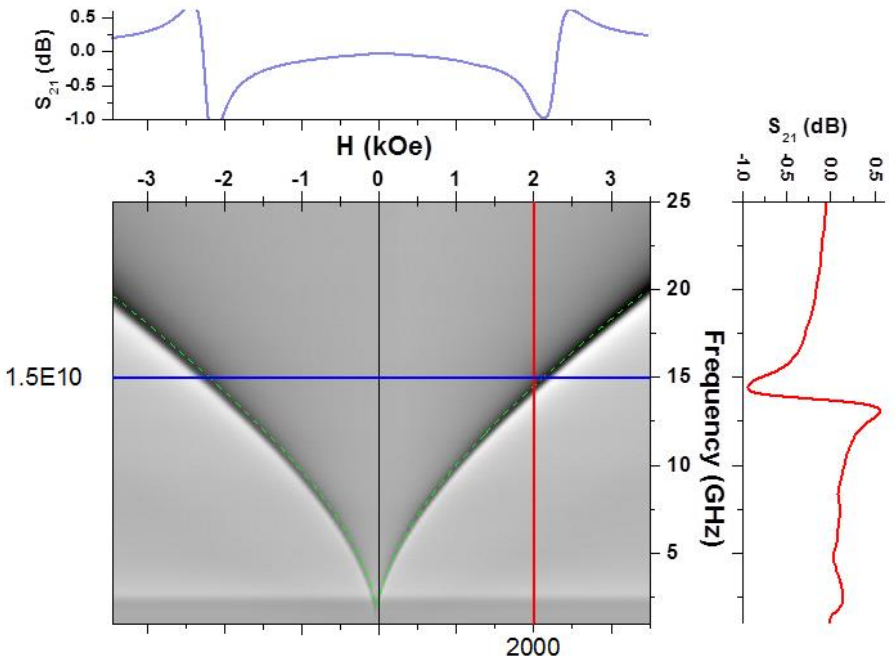

Figure3.9: contour plot of FMR for sample S2

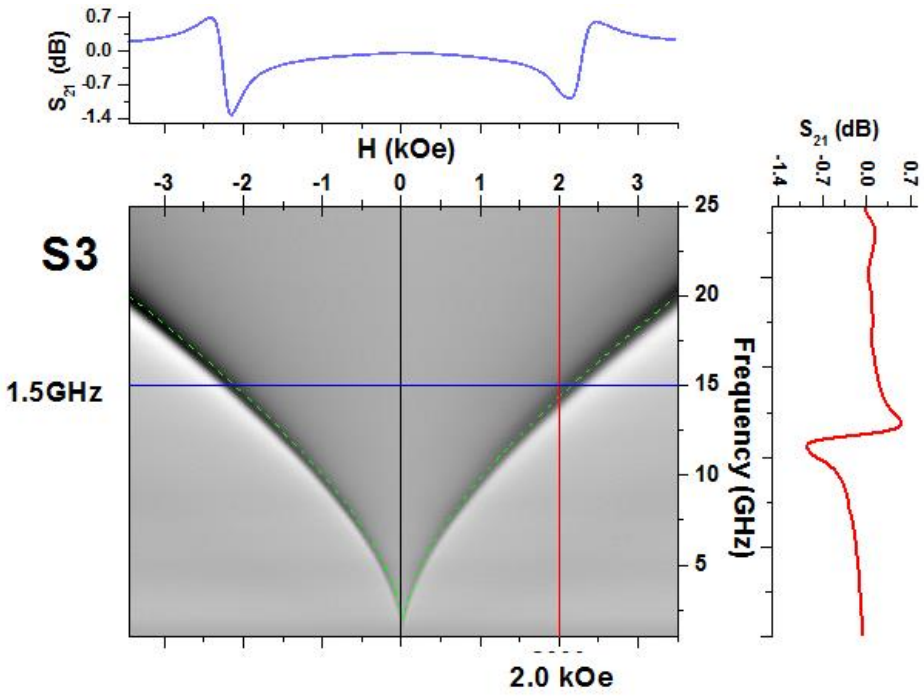

Figure 3.10: contour plot of FMR for sample S3

The top and right insets in the three dimensional contour plots represent the profile of S_{21} at magnetic field 2KOe and frequency 15 GHz respectively. The experimental results were fitted with the Kittel formula [94, 95]

$$f_{res} = \frac{\gamma}{2\pi} \times \sqrt{(H_K + H_{ra} + |H - H_{eb}|)(H_K + H_{ra} + |H - H_{eb}| + 4\pi M)} \quad (3.2)$$

Where γ is the gyromagnetic factor and H_{ra} represents the rotational anisotropy [88, 90]. The concept of including the rotational field is that it helps to explain domain wall hysteresis in AF layer that can be obtained from the perturbative methods [96]. The easy axis of the rotational anisotropy follows the macroscopic motion of magnetization direction and that minimize the free energy of system. Rotational anisotropy also helps to enhance anisotropy field of FM layer when it is coupled with the AF layer via exchange coupling. However, it is hard to detect it with static measurement techniques. The experimental results provide information about the values of H_{eb}, M and H_k+H_{ra}. The rotational anisotropy was calculated by using the value of the anisotropy field which was obtained from the in-plane angular variation of X-band FMR. The Kittel equation (3.2) was well fitted with the experimental values and fitting parameters and fitted results are presented in table above. The exchange bias values for all samples were extracted by considering the shift of FMR contour plot from origin. Basically the shift of origin of contour plot from the origin of field axes is exchange bias. Not surprisingly, the exchange bias, which was extracted from the VNA-FMR technique, was consistent with the results obtained from the other techniques. However, the additional information such as rotational anisotropy can be achieved with this technique. In addition, broadband FMR provides the insight for both field and frequency dependent results. The largest value of rotational anisotropy for the sample S1, which had largest number of F/AF interface, supports that it originates from the AF layers.

Comparing the experimental values of exchange bias which were determined from X-band and VNA-FMR, it was found that values obtained from VNA-FMR are smaller than X-band FMR. The reasons for these discrepancies might be many but most importantly the microwave field values in these techniques are crucial. The X-band FMR is a cavity based FMR and the VNA-FMR is planer FMR. The microwave field in cavity is slightly smaller than the field produced by the planer device such as CPW. The consequence is that the relaxation mechanism will be slightly different. The frequency-dependent exchange bias also indicates that the stable and unstable grain on AF at interface also results the slightly different exchange bias measured by two methods [97].

In conclusion, the static and dynamic property of coupled FM/AF multilayer system was studied to understand interfacial phenomenon for multilayer system. Different experimental techniques reveal different facets of coupled phenomenon. The regular MHL loop, when it shift from the origin, provides the simply exchange bias value. The extra kink on the MHL was because of the inhomogeneity present on the interface of FM and AF layers. The satellite distribution of the FORC in addition to main distribution further verifies the inhomogeneity produced kinks on regular MHL. In addition, the X-band and FMR results help to estimate not only the exchange bias but also the anisotropy field, saturation magnetization as well as rotational anisotropy.

In the following section, the angular variation of FMR and FORC are carried out to understand the coupling scheme in details.

3.5Angular dependent FORC and FMR of exchange-biased multilayer systems:

In addition to evaluating the exchange bias with different technique, further experimental studies have been performed to better understand the coupling between AF and FM layer using two methods: angular first order reversal curve (AFORC) and angular ferromagnetic resonance (AFMR). It is important to mention that exchange bias phenomenon have been already implemented on technology. For

example sensor to read and write data, spintronic devices, microwave devices and so on. However, since the effect exists at the interface of FM and AF magnetic layers, it is not straight forward to understand and probe it. Various theoretical as well as experimental studies have been pursued in this regards. The sample surface roughness, geometric defect and complicate nature of domain and domain wall at the interface make complicate to quantify the exchange bias [33, 73, 74, 98-101]. Previous studies showed that the inhomogeneity at the interface creates rotational anisotropy because of the magnetic moment follow the direction of applied field. To understand the contribution of all these effects, AFORC and AFMR can be helpful both in static and dynamic aspect.

In this study, AFORC distribution has been studied to evaluate the inhomogeneity at the interface of FM and AF layers and results have been correlated with the experimental AFMR results. In addition, the additional modes on FMR spectra have been considered to compare with the exchange bias evaluated via static measurement technique.

3.6 AFORC diagrams and profiles:

FORC method is a technique to quantify the interaction and coercivity field distribution. It has been explained in detail in chapter 1. FORC technique is also very sensitive regarding the data processing. Hence, it is important to process data without missing important information with meaningful results. Depending on the orientation of bias field, it is inevitable to modify the way we process data. The smoothing factors were selected very carefully. The experimental result for S1 is presented in figure 3.11. Where, angular FORC on left panel and corresponding 2D FORC diagrams on right at angles 0^0,10^0,20^0,30^0 and 40^0 in coordinates (h_c, h_u). Similarly, results for S2 and S3 are presented in figure 3.12 and 3.13 respectively. The reversal curves on the left are correlated with the 2D diagram on the right. It has been clearly observed that the FORC diagram at 0^0 has well defined coercivity and interaction

distributions. However, it is difficult to distinguish FORCs because they start to collapse after 20^0. This observation was made when the exchange bias field and the applied field do not align.

The FORC distribution merged on a single line for higher angle and results are extremely noisy with zero

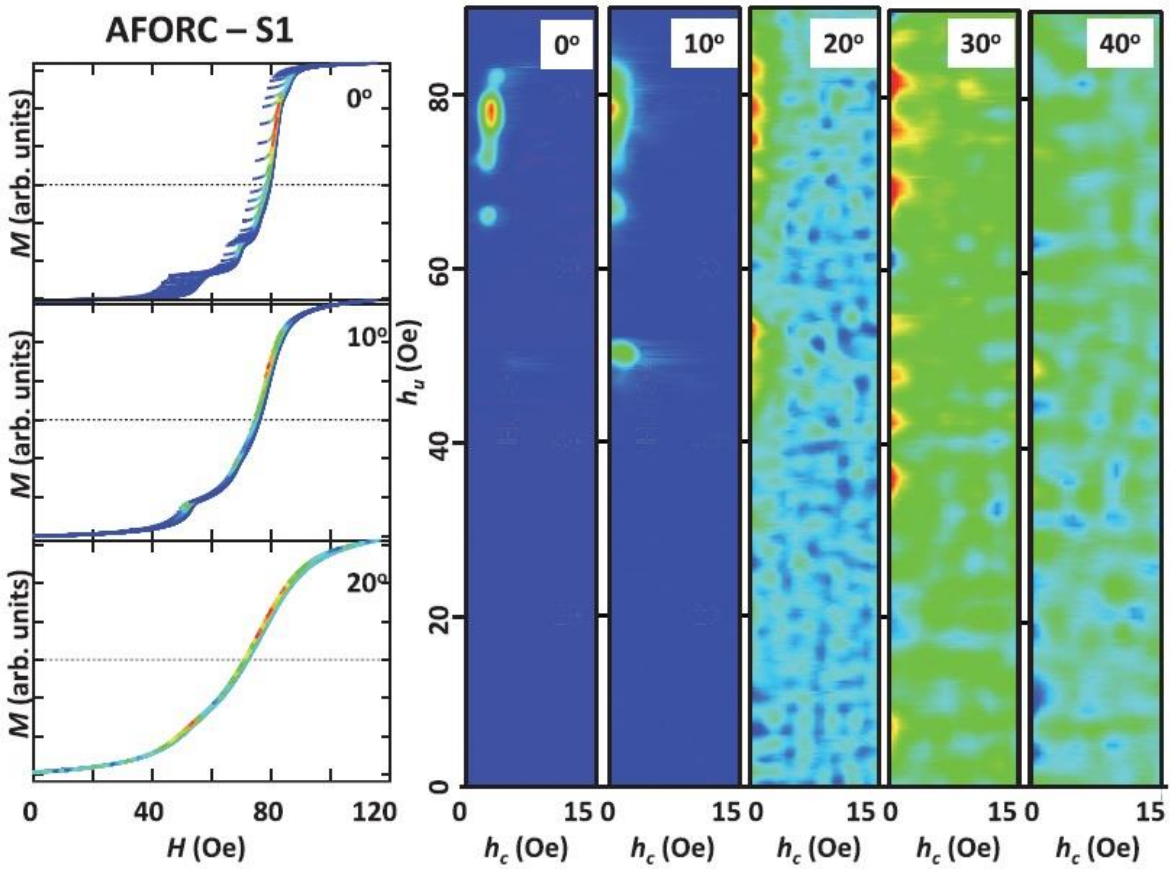

Figure3.11: AFORC diagram on left and corresponding 2D diagram at right in coordinates (hc, hu) for S1 at different angles.

coercivity and interaction. The variation on the AFORC diagram is related to the homogeneity on the axis of internal field distribution. These results also support that AFORC is an effective tool to study quantitatively about the magnetic canting, magnetic domain misalignment, variation of intrinsic interaction.

The following information has been inferred by comparing the FORC diagrams. First, it has been clearly observed that the intrinsic field distribution for all samples is cut-off quantitatively at angle 20^0. Second,

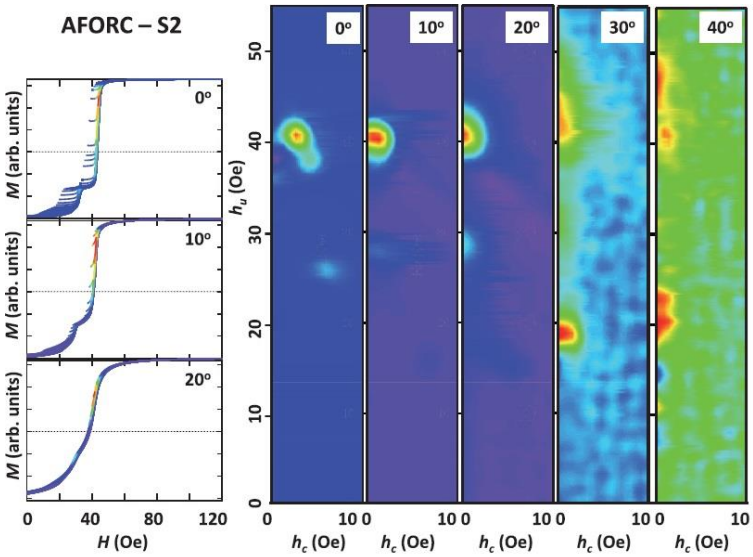

Figure3.12: AFORC diagram on left and corresponding 2D diagram at right in coordinates (hc, hu) for S2 at different angles.

AFORC diagram are symmetric at 0^0 and 180^0 for all samples. This suggests that the multiple contributions on exchange bias fields are confined mostly below 40^0. Third, different profiles of AFORC distributions for three samples are relevant to the different multilayer systems.

In addition, the sharp FORC distribution reflects the uniform strength and narrow dispersion of internal

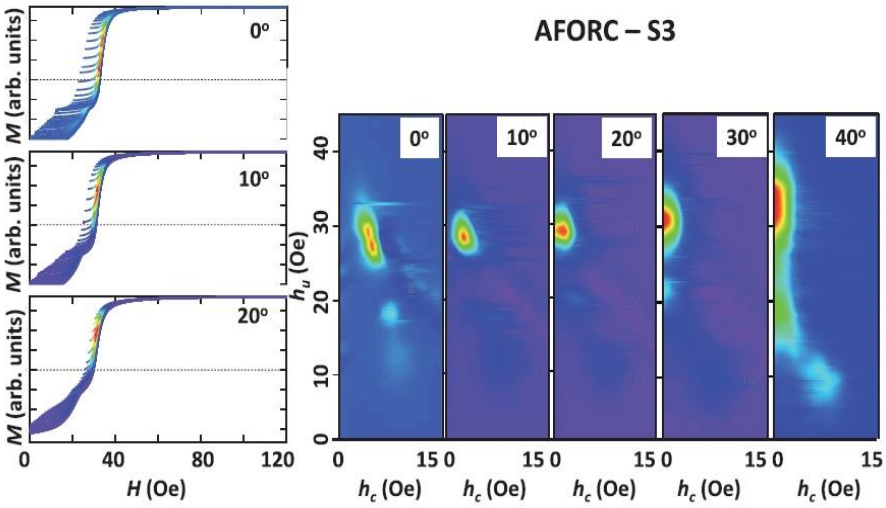

Figure3.13: AFORC diagram on left and corresponding 2D diagram at right in coordinates (hc, hu) for S3 at different angles.

field along the applied field direction. In contrast, the broad distribution of the FORC indicates the variation on the strength of internal fields with different strength along the applied field direction.

The different features of FORC distribution have been observed for different samples at different fields. In the following, the internal field value and full width at half maximum (σ_{FWHM}) of the internal field values will be discussed.

FORC diagram for sample S1 at 0^0 has main broad distribution with central field hu ~78 Oe (σ_{FWHM}= 4 Oe). Besides, weak satellite distribution at ~ 67 Oe and very weak satellites mode at ~ 49 Oe have been observed. At angle 10^0, the last two satellite distributions were reinforced to one and the main distribution was broadened σ_{FWHM} ~7 Oe. At 20^0, the main distribution was at hu ~ 78 Oe (σ_{FWHM} = 23 Oe) and additional two distributions of same strength were around the main distribution. The additional distribution with distribution strength hu ~ 49 Oe exists and the center of the main distribution (hc, hu) shifted towards the low coercivity value. At 30^0 and 40^0 the FORC distribution has multi-valley structure with different maximum and minimum values which made extremely difficult to observe the main distribution precisely.

FORC diagram for S2 at 0^0 has main distribution with central value hu~39 Oe (σ_{FWHM}= 2 Oe) in addition to a weak satellite distribution at ~ 28 Oe. Uniform distribution with σ_{FWHM}= 3 Oe was observed without vertical ridge at 10^0 and was shifted towards the lower hc value. At 20^0, the main distribution was centered at hc=0 (σ_{FWHM}= 5 Oe) with additional peak at hu~16 Oe. Multi – valley distributions, which were sharper compared to S1, were observed at 30^0 and 40^0. Vertical ridge of main distribution was extended from 40 0e to 46 Oe at 30^0. The secondary distribution shifted up to 18 Oe. At 40^0, multi-valley distribution was observed with several maximum and minimum and ridge of main distribution extended from 40 Oe up to 50 Oe.

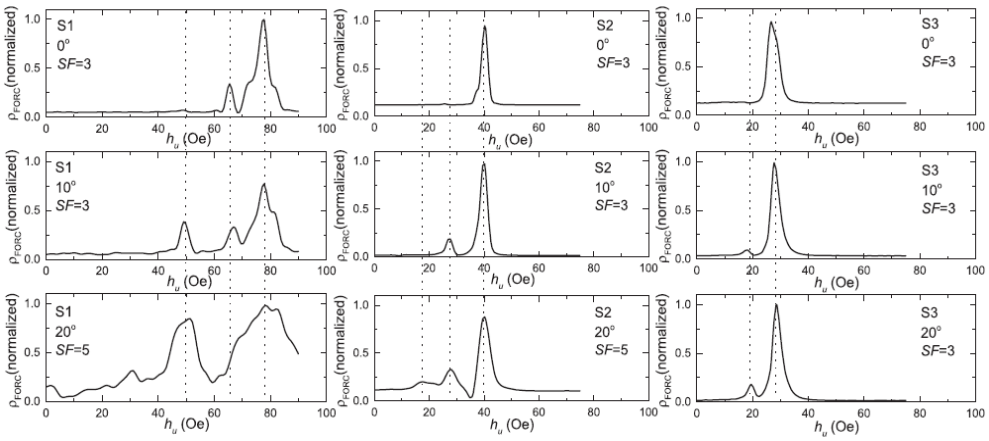

Figure 3.14: vertical cross section of 2D FORC distributions for samples S1, S2, and S3 at different angles

FORC diagrams for S3 clearly showed that two distributions were superimposed between hu ~26 Oe to 29 Oe in addition to the weak satellite distribution at 18 Oe. The σ_{FWHM}= 5 Oe was observed for the superimposed distribution. More uniform distribution with central value hu~29 Oe (σ_{FWHM}= 4 Oe) was observed at angle 10^0 and 20^0. The delocalize distribution with σ_{FWHM}= 9 Oe and vertical ridge at 15 Oe and 40 Oe were observed at 30^0 and 40^0 respectively. To sum up, it was clearly perceived that when angle increased, the center of the main distribution was shifted towards low coercivity value in (hc, hu) diagram.

AFORC diagrams of S1, S2 and S3 were considered to extract the exchange bias, Heb, for all observed distributions. Vertical cross-section of 2D AFORC distributions were used to extract the hu profile where splitting of main distribution was observed. The peak values in the distributions, which were leveled as hu^{max}, were related with the exchange bias components of samples. The hu profiles for samples S1, S2 and S3 at orientations 0^0,10^0 and 20^0 are presented in figure 3.14. The vertical dotted line corresponds to the main hu^{max} values.

The distributions at angle 30^0 and 40^0 are not presented because of the multi-valley structure which ultimately degrades the FORC distributions. The smoothing factors were optimized using FORCinel

software. It has been clearly observed that the FORC distribution and hu profiles showed complex profile of internal fields. The transition from multiple internal field components in S1 to bimodal distribution in S3 was observed. For S3, there was a single profile of hu at 0^0 however convolution of two or more distributions results the single peak distribution. The following table shows the Heb values extracted from the AFORC distribution at 0^0, 10^0, 20^0. Where, hu^{max} is the central value of each distribution in (hc, hu) diagram.

Table 3.3: Exchange bias values for different modes

Samples	hu^{max} 1st mode(0e)	hu^{max} 2nd mode (0e)	hu^{max} 3rd mode (0e)
S1	78	67	49
S2	39	28	16
S2	29	18	…

In brief, it has been clearly observed that the peak value obtained from hu distribution at 0^0, 10^0 and 20^0 AFORCs were good agreement with the results obtained from MHLs quantitatively. For example, there were multiple steps on MHL for S1 but relatively smooth steps were there for S3 compare to the S1. The detail analysis of hu^{max} peak field values and line shape profile is beyond the scope of this study. Further, computational analysis is required for the proper interpretation of the internal field in multilayer systems. In addition to the static study using AFORC distribution, angular variation study of FMR also performed to correlate the static and dynamic results and in next section we will be discussing about it.

3.7Angular ferromagnetic resonance study (AFMR) at X-band:

The regular X-band FMR study of these sample has been already done previously. However, detail study was performed considering the additional modes on FMR spectra. In plane angular variation of FMR spectra were collected with step of 5 degree. The additional mode was present at slightly higher

frequency than the main resonance mode. The X-band FMR spectra for all samples at different orientations with respect with the bias field is presented in figure 3.15. In figure 3.15, (a) represents for S1, (b) for S2 and (c) for S3.

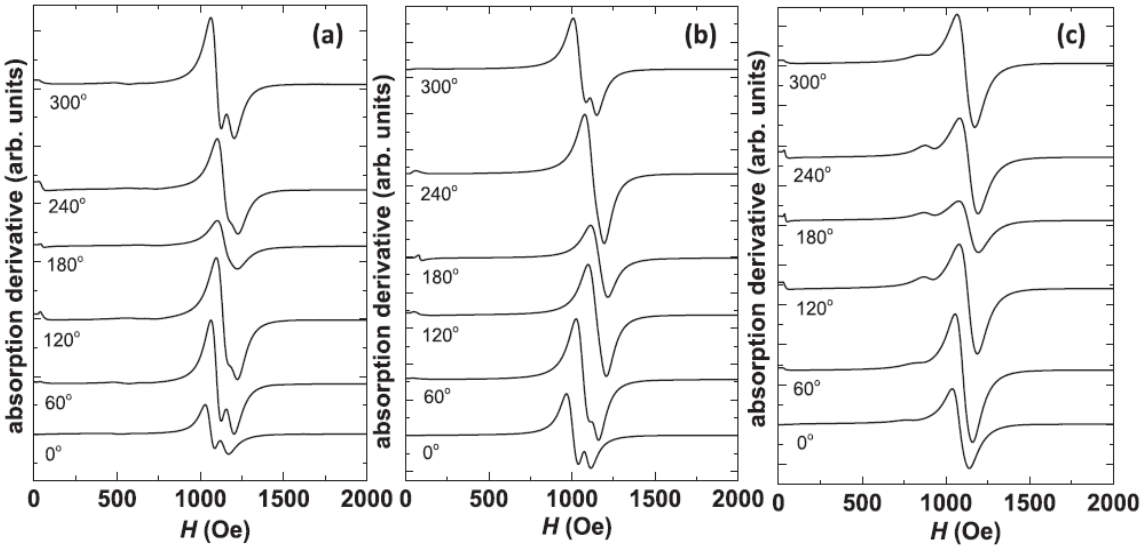

Figure 3.15: In plane angular variation of X-band FMR spectra for S1, S2 and S3.

In addition to the main mode, mode with amplitude 1/5 of main mode was observed at higher field compare to main mode especially for S1 and S2. The additional modes, which we named as satellite modes, were prominent especially at angle close to 0^0. Instead, single resonance mode was observed for S3 at angle 0^0 around the magnetic field 1100 Oe. Figure 3.16 represents the angular variation of FMR considering also those additional modes. The angular variation of first and second resonance modes are clearly defined on figure 3.16. The red solid line represents the theoretically fitted resonance modes and the dotted square and circle represents the experimental angular variation resonance modes [102]. In the following table, the numerical values of exchange bias for different modes are presented including to the rotational fields.

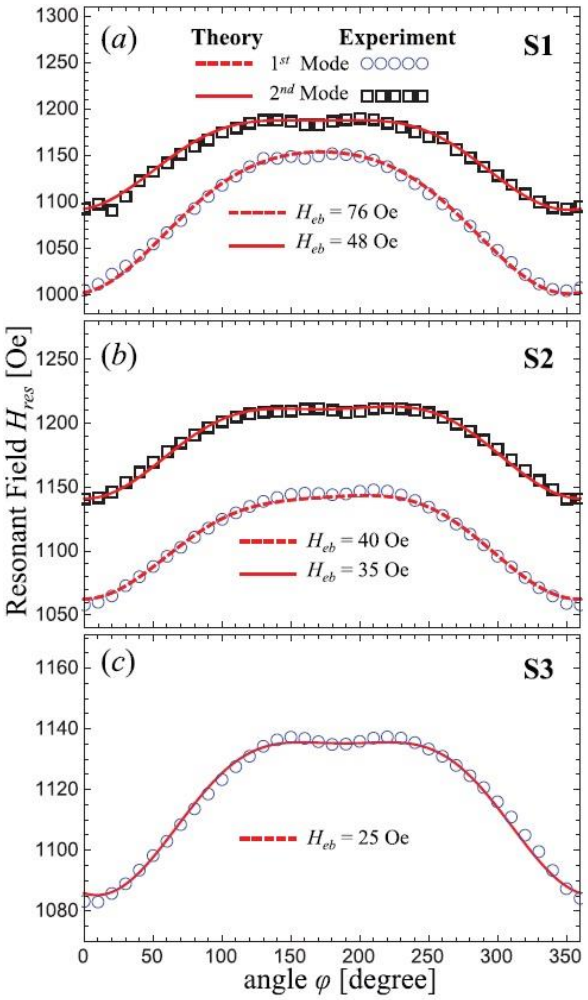

Figure 3.117: Angular variation of FMR for samples S1, S2 and S3

Table 3.4: Exchange bias values with different anisotropies

Sample	Heb (Oe)	Hra (Oe)	Hk(Oe)	φ_{AK}^0	φ_K^0	Meff(emu cm^{-3})
S1						
1st mode	76	70	16	-8	-8	878
2nd mode	48	5	16	-8	-8	878
S2						
1st mode	40	79	13	2	-3	849
2nd mode	35	3	13	2	0	849
S3						
1st mode	25	44	8	9	9	875

The domain wall effective field 1200 (Hw) was considered to make sure that M_{AF} around the z-axis is less than 4^0 during the in plane variation of the external magnetic field [102]. The decreased FMR field around 180^0 was due to the uniaxial in-plane anisotropy; which helps to reduce the FMR field when magnetization was along the easy axis.

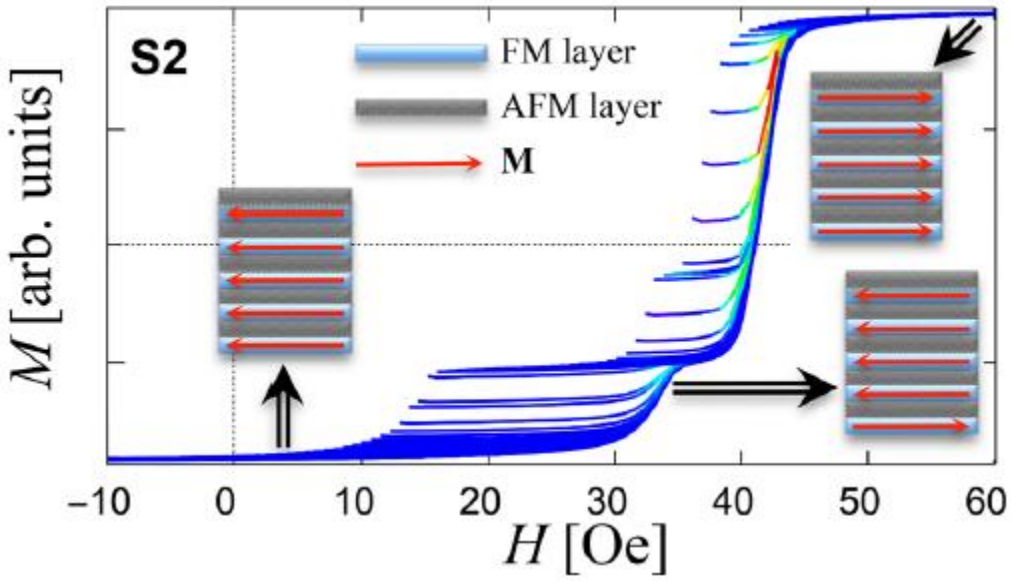

Figure 3.17: Systematic representations of magnetization switching for S2

In general, it can be inferred that the second mode was because of the one-sided couple layer (the systematic is presented in figure 3.17). The kinks on MHL reinforced that the magnetization reversal of one-sided coupled layer switch at different field compared with rest of the two-sided coupled layers. Single kink on MHL also supports that there were two nucleation fields on these system. Similar behavior with two modes also has been observed in case of S1. For S3, the resonance fields of two modes were very close and they appeared as single mode with exchange bias 25 Oe. In addition, lower rotational field was observed for second mode compare to first mode.

The reason behind this is that the first layer coupled with only one side of AFM layer and results the smaller value of rotational anisotropy. The angular dependence of exchange bias fields evaluated with AFORC and AFMR techniques for samples S1, S2 and S3 is presented in figure 3.18.

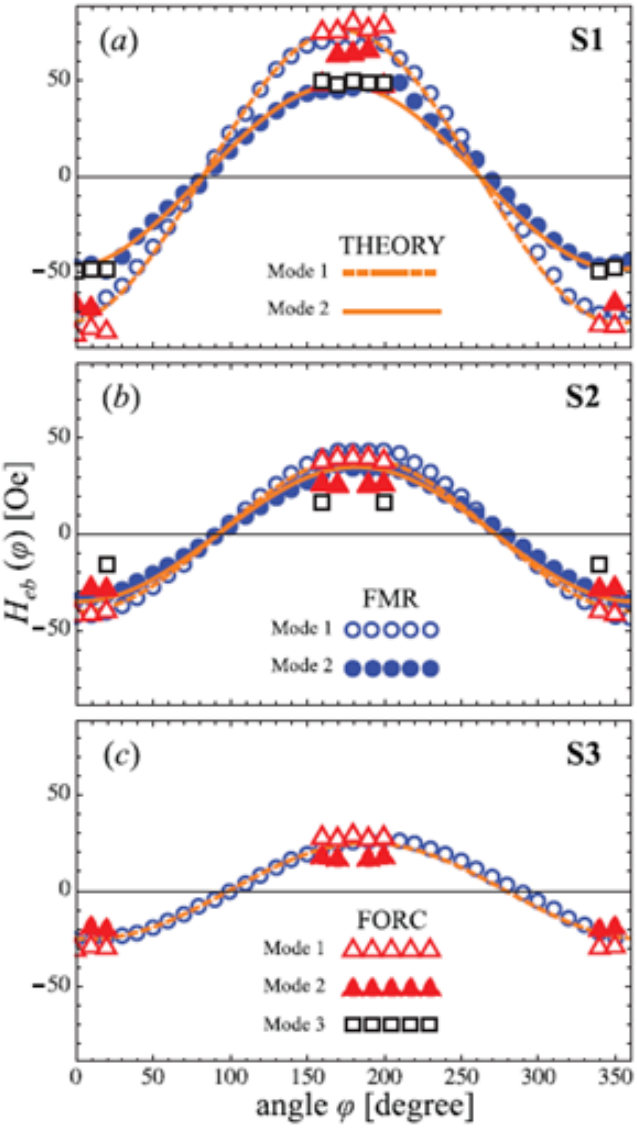

Figure 3.18: AFORC and AFMR for sample S1, S2 and S3

One additional mode appeared in case of AFORC compare to AFMR. Magnetic parameters which were evaluated from AFORC and AFMR are presented on table above. Good agreement between these two methods was observed for the exchange bias value, especially for mode 1. However some discrepancies

have been noticed in case of other modes. This discrepancy can be due to the experimental technique to probe the exchange bias field. For example, the exchange bias was determined by simply tracking resonance field at 0^0 and 180^0 and the divided the difference by two. However, in case of AFORC, exchange bias was determined by considering the physical meaning of hysterons. In addition, AFORC method strongly depends on the switching filed distribution but in case of AFMR the sample was fully saturated and experiment was done at frequency 9.8 GHz.

In case of sample S1, the exchange biases extracted for second and third mode are 67 Oe and 49 Oe respectively. However, the exchange bias corresponds to the second mode of FMR is 48 Oe and it did match with the exchange bias from third mode.

In summary, a detailed study of the angular variation of multilayer exchange bias system was performed using both static and dynamic techniques. The bottom layer, which was coupled only on one side to AF layer, was responsible for the second mode in X-band FMR. The coupling between layers was studied with FORC distribution method. The contribution of each magnetic multilayer to exchange bias values are determined by the angular variation of FORC from 0^0 to 360^0 with the step of 10^0. The multiple exchange bias values were extruded in spite of some limitations. The contribution of structural imperfection, volume of coupling regions, different switching field for different layers and inhomogeneous internal field was study with the AFORC technique. To our knowledge, this is the very first practice to study the quality of samples, frustrated magnetic domain misalignment, distribution of intrinsic interaction field with AFORC method.

Chapter 4: Static and dynamic properties surface of modulated structure

4.1 Introduction to magnonic crystals

Fundamental study and technological applications of pattern magnetic nanostructures have triggered intensive research in last few decades [103]. Magnetic memories, microwave filters, magnonic waveguide, in chip data communication are few examples where these patterned magnetic structures have already revealed enormous potential [104-107]. In addition, Spintronic, where spins behave collectively as wave, is ideal branch of physics to minimize power consumption and heat during devices operation. Strong shape anisotropy and effortlessly tune nature of ferromagnetic nanostructures can be ideal candidates for all above mentioned applications. Besides, magnonic crystals, where well defined frequency band gap can be achieved by controlling both the propagation direction of spin wave and anisotropies of specimen, draw strong attention recently [108-110]. Substantial numbers of scientific research have been reported to study the static and dynamic properties of pattern magnetic systems. Among them, nanowires, dot, antidote, multilayers, modulated wires are few examples to mention[111]. Furthermore, modulating shape, symmetry and periodicity also have significant consequence especially on magnetic properties of system[112, 113].

The periodic modulation on surface of thin film in the form of anti-dot, strips, square with different thickness has been studied especially using theory of two magnon scattering [114]. Variation on linewidth of ferromagnetic resonance [FMR] spectra also has been studied for thin film deposited on ripple substrate [115].

In this study, we consider slab of thin film and periodic modulated structure with different periodicity were fabricated. Specifically, periodic grooves structures were created by etching slab form the surface. For smooth slab, uniform ferromagnetic resonance (FMR) mode with wave vector (k=0) was observed. However, when grooves were created by removing material from the surface, multiple non-uniform

(k≠0) excitations of spin waves modes were perceived because of boundary conditions and edge effects. Moreover, when grooves come close enough, the influence of dipolar interaction becomes strong and it allows excitation of Backward Volume Magnetostatic (BVM) wave along the direction of static magnetization. Damon-Eshbach (DE) modes with smaller amplitude appears on micromagnetic simulation, however, it is extremely difficult to detect in our sample's configuration using FMR technique. Systematic angular variation was also performed to study angular dependence static and dynamic properties. Micromangetic simulation was performed to better understand experimental results and corroborate them.

4.2 Sample preparation techniques

The details photolithography process to prepare samples is well explained in chapter1. However, some specific methods and parameters which were implemented in this study will be reviewed in the following. G-S-G type coplanar waveguides (CPW) were fabricated using standard photolithography technique followed by deposition of Ti (10nm)/Cu (150 nm)/Au (10 nm) and finally liftoff process. Then, a rectangular box with size of 350 μm×10 μm was created on the top of signal line of CPW using electron beam lithography technique. Following that, Permalloy ($Ni_{80}Fe_{20}$) of thickness 40 nm was deposited at the rate of 0.2 A^0s^{-1} using sputtering method with base pressure 1×10^{-8} Torr. Eventually, lift-off technique was implemented to get a slab of Permalloy with dimensions 350 μm×10 μm× 40 nm on the top of signal line of CPW [58].

In the next step, the surface of thin film was modulated by removing materials from the surface using focus ion beam (FIB). FEI Quanta 3D FEG FIG/SEM with focus Ga ion beam was used to etch and fabricate periodic modulated structure. The systematic image of the structure and electron microscopic image is presented in figure 4.1.

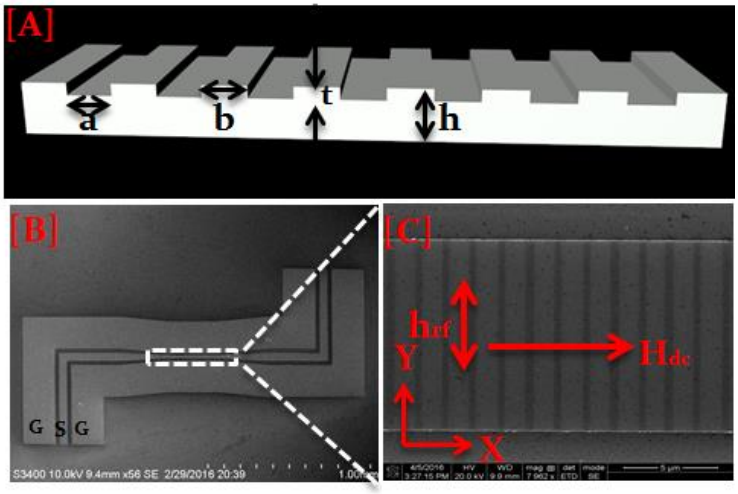

Figure 4.18 : [A] Geometry of the structure under study; [B] scanning electron microscopy image of the CPW with the groove structure on the signal line; [C] zoom-in of the CPW's signal line displaying the grooves created by the FIB.

In figure 4.1, [A] represents the sketch of the structure that was considered in this study and [B] is for the CPW with sample on the top of it. [C] the zoom in region for the center of CPW where the direction of the microwave field and the external fields are represented by arrow.

The width of grooves, width of the hill, total thickness of slab and thickness of grooves are represented by *a*, *b*, *h*, and *t* respectively as shown in figure 4.1 [A]. Two different parameters *a* and *b* were varied systematically to study the effect of periodic surface modulation on static and dynamic properties.

4.3 *a* varied systems

In this system, parameter *a* was varied keeping all other parameters constant. The following nomenclatures were used for set of samples which are considered on this study. S1 represents the slab of thin film. S2 represents sample with *a*=1000nm, S3 for *a*=500nm and S4 for *a*=200nm. All other parameters were similar for all three samples which were *b*=400 nm and *t*=4 nm.

In terms of experimental techniques, Magneto Optical Kerr Effect (MOKE) and VNA- FMR were used to study static and dynamic properties of magnetization respectively. Angular dependent MOKE was carried out by using nanoMOKE3 to study the switching of magnetization. Longitudinal configuration was implemented to probe the component of magnetization along the field direction. Angular variation of MHL from 0 degree (0 degree means applied field along the length of slab) to 90 degree was carried out with step of 10^0 for all samples.

To probe the FMR spectra, two-port network analyzer was connected to homemade CPW via coaxial cables. Non-magnetic pico-probes were used to connect planer CPW with the coaxial cables and it is well explained in chapter 1. The external magnetic field was swept from 0.5KOe to -0.5 KOe with field step of 3 Oe. The microwave frequency was swept from 1GHz to 6GHz for each magnetic field. The transmission scattering parameter (S_{21}) was recorded for each frequency scan. The contour plots of frequency, field and S_{21} are plotted. The darkest region on contour plot represents the maximum

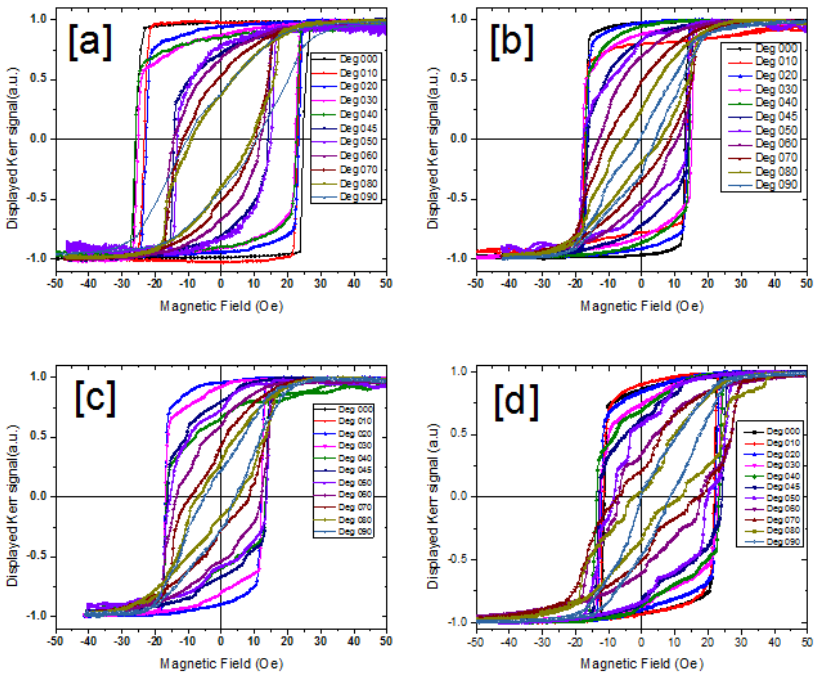

Figure4.19: Angular dependence of MHL[a] for S1, [b] for S2, [c] for S3 and [d] for S4

absorption of microwave energy within samples. The angular dependence of the MHL loop is presented in figure 4.2.For S1, the length of the slab is 35 times larger than the width thus the shape anisotropy induce the easy axis along the length of slab. The perfect square shape of MHL loop and narrow distribution of switching field at 0^0 confirms that the easy axis is along the length of slab. With increasing angle, the coercivity of the MHL loop was decreased. The abrupt change on coercivity was observed when angle increase from 40^0 to 45^0. Which supports that the magnetization reversal process was changed at angle around 45^0 .For sample S2, although the MHLs show similar nature as in S1, the coercivity did not jump quickly as in S1 for orientations close to 45^0. The angular dependence MHL was similar to the angular variation of MHL for wire. The grooves facilitate the irreversible component of magnetization which avoids the sharp switching of magnetization for higher angles. For sample S3, MHL up to 40^0 was similar in shape with S1 and S2. However, the multiple steps on MHL can be observed in angle range 40 to 60^0. The reasons for these multiple steps on MHL can be the following. The first is that the magnetization on a sample surface tends to align along the surface due to anisotropy. Thus, in our case, the magnetization on the grooves surface is perpendicular to the magnetization on the side of hills. Thus, when external magnetic field was applied, the magnetization at different regions of sample switches at different magnetic fields. In addition, the size of the sample is not infinitively large. The total volume of the sample was perfectly only on the signal line of CPW. Which means the area of sample's edge also can contribute on the switching behaviors. The interesting result we observed was that the MHL had clear multiple steps in between 30^0 to 60^0. This also supports the anisotropy nature of surface magnetic charges. Since the volume of total sample was comparatively small, it is also important to consider the magnetization at edge of the slab. Therefore the total collective effect of magnetization was present on the MHL.

Now let us consider the angular variation of MHL for S4. The width of the grooves in this sample is only 200 nm. It is well known fact that magnetic interaction is long in nature. Strong magnetic interaction can

be realized when the distance between magnetic structures is below 500 nm. In case of sample S4, despite different orientation of magnetization at different region of sample, the edge to edge distance of hill was 200 nm. Which means the magnetic charge at the edge starts to interact via dipolar interaction. This interaction made the system further complicate. The steps on MHL were significantly increased from sample S3 to S4. Up to 7 steps were clearly observed on MHL especially at 45^0. The strong dipolar interaction creates complicated configuration of magnetization. These multiple steps on MHL can be used to store different magnetic states which ultimately provide freedom to store data not only at 0 and 1 but also at the intermediate one.

The dynamic characterization was carried out using FMR technique. The detail of ac and dc magnetic field direction in CPW is explained in chapter 2. The contour plots of FMR spectra for four samples when magnetic field was applied along the length of slab are presented in figure 4.3.

For sample S1, single uniform resonance mode i.e. wave vector (k=0) was observed. And the reason we consider plain slab was to compare uniform FMR mode with multiple resonance modes on modulated structures. For sample S2, in addition to the uniform FMR mode, additional mode with smaller amplitude was observed at lower frequency region. For sample S3, the similar resonance modes as in S2 were observed with larger amplitude of absorption compare to S2. However for sample S4, the results are unique compare with rest of others. Four resonance modes, named as I, II, III and IV, are clearly observed especially at low field and frequency region.

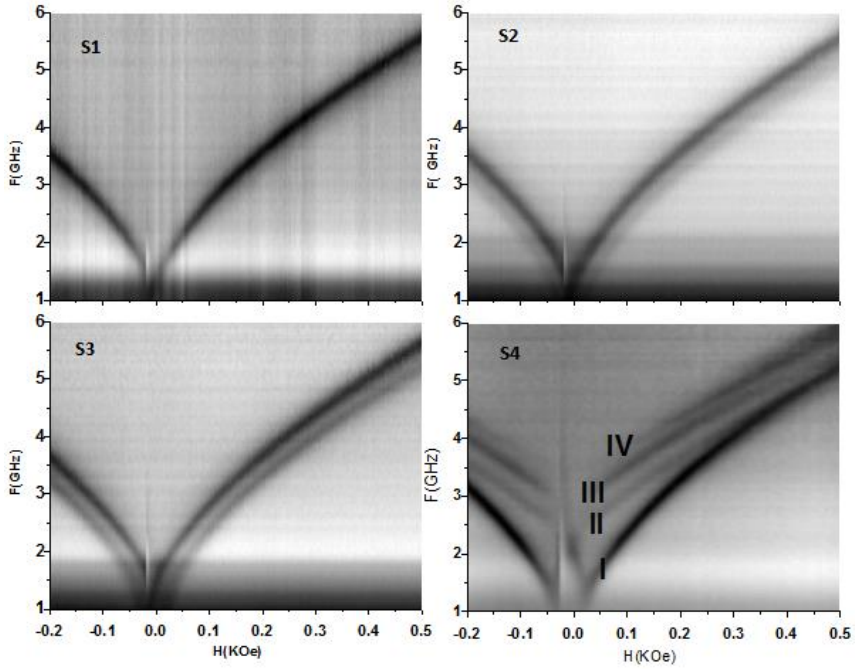

Figure4.21: contour plots of Ferromagnetic resonance spectra

To study the angular dependence of FMR, angular variation of FMR has also been studied. The external

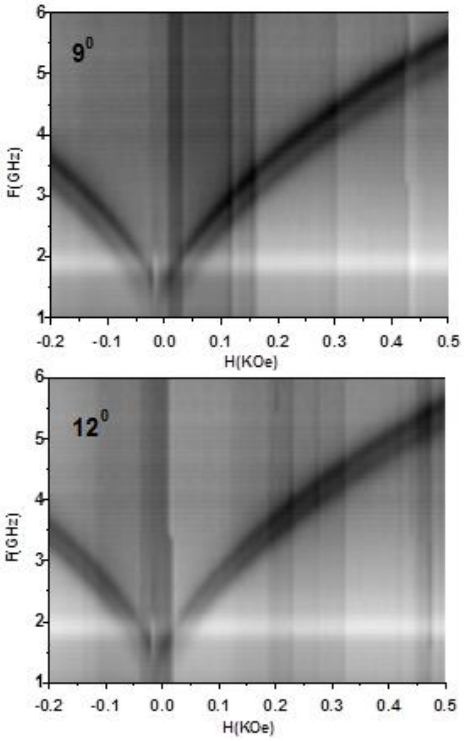

Figure 20.4: Contour plots of FMR at 9 and 1 2 degree

magnetic field was rotated keeping sample fix. It also means that the angle between ac field and dc field has been changed. For slab, not significant change on the angular variation of FMR was observed. There was always single mode even at 0^0 and 90^0 orientations. For sample S3, the two modes start to come closer and closer when angle was increased. The contour plots of FMR at angle 9^0 and 12^0 are presented in figure 4.4. The modes merge in to single mode when angle was greater than 12^0.

Results for sample S4 are quite different from sample S3. The angular variations of FMR from 0^0 to 30^0 are presented on figure 4.5.

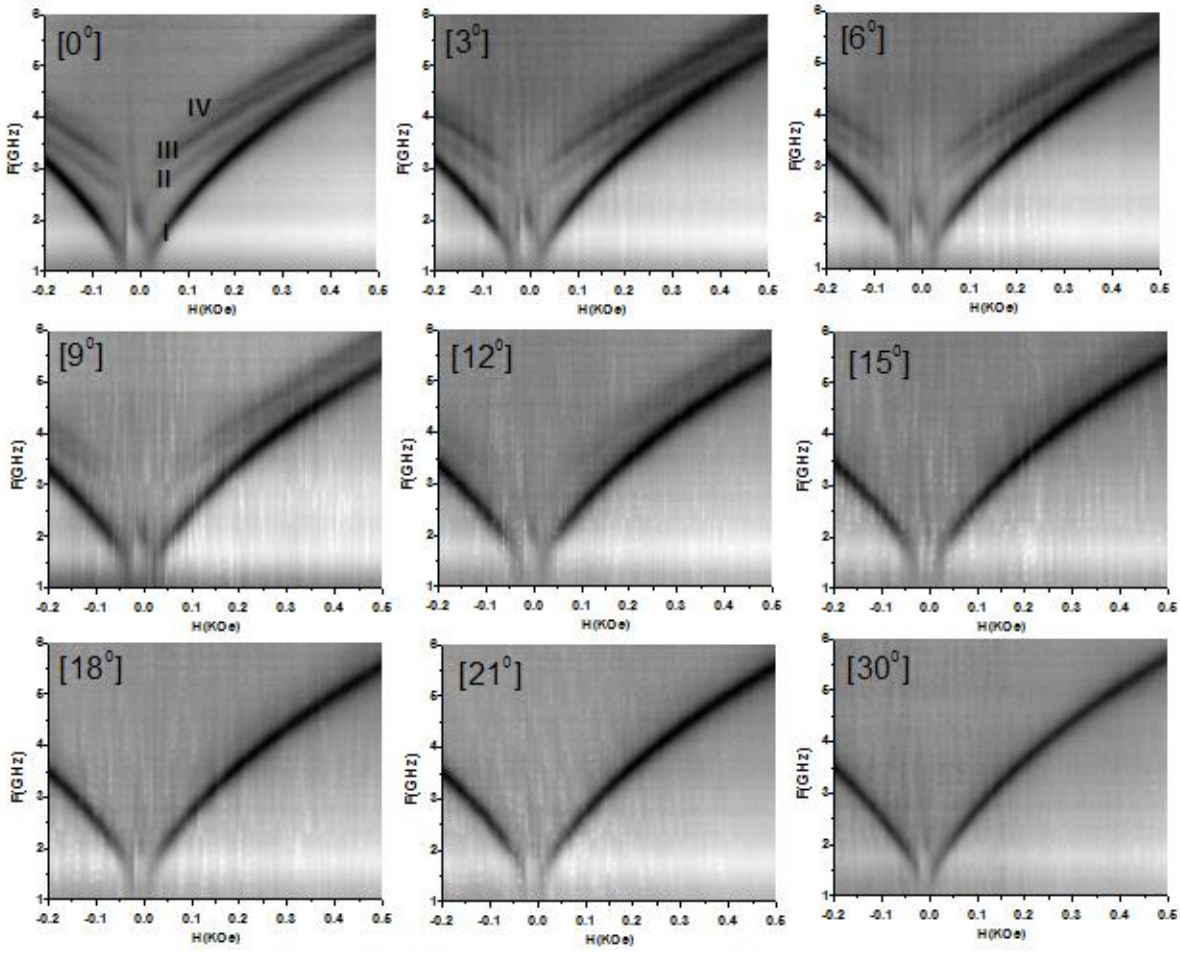

Figure 4.5: Angular dependence contour plots of FMR for S4

At 3^0 and 6^0, the result is typically similar to the 0^0 with four resonance modes. Mode IV starts to fade especially low frequency region at angle 9^0. At 12^0, most of the absorption was from the mode I with weak absorption form rest of modes. There was mainly mode I when the angle was more than 15^0. The interesting observation for S4 is that the split modes do not merge in single mode as in sample S2 and S3 rather the higher order modes are faded away for higher angles.

4.4 Micromagnetic Simulation

Micromagnetic simulation was carried out to understand and explain the experimentally observed splitting of FMR modes for the modulated structures. Systematic micromagnetic simulations was performed using a GPU (graphics processing unit)-accelerated micromagnetic simulation code, *mumax* [116]. *mumax* was ported on a 1.5 Petaflop peak performance cluster containing 504 compute nodes with 960 NVIDIA Tesla K20x GPU's and over 10,000 Intel Xeon processing cores from LONI (Louisiana Optical Network Initiative - http://www.loni.org/). The physical structure that was considered in experimental studies was large to perform micromagnetic simulation. Thus one period of the structure, which consists of a hill region with width *b* and half grooves *a*/2 on both sides of the hill (200 nm), was considered. The micromagnetic cell size was (5nm, 10 nm, 1 nm) along the (X, Y, Z) directions, where X and *Y* directions are the same as shown in Figure 4.1 and Z direction is along the film thickness. Periodic boundary condition PBC (n, 0, 0) was used along the X-axis to mimic the total experimental sample size. The material parameters used for simulation for Permalloy in S.I. (as required by *mumax*) were saturation magnetization $M_s = 8\times10^5$ A/m, exchange constant $A = 1.3\times10^{-11}$ J/m and damping parameter $\alpha=0.01$. The dynamic simulations were performed by considering a uniform exponential pulse which had excitation field perpendicular to the H_{dc}. Spatial time dependence of magnetization M(x, y, z, t) was recorded. Frequency domain susceptibility was obtained as defined by $\tilde{\chi}_{ij}(\omega) = \tilde{m}_i(\omega)/\tilde{h}_{ac,j}(\omega)$, where $\tilde{m}_i(\omega)$ is spatially averaged Fourier transform of i_{th} component of magnetization and $\tilde{h}_{ac,j}$ is the Fourier transform of the j_{th} component of dynamic magnetic field. In addition, the spatial profile modes

were calculated by considering a spatial distribution of the magnitude of $\tilde{\chi}_{yy}(x, y, z, \omega)$. Figure 4.5 summarizes the micromagnetic simulation results obtained for S-4 at different applied field directions. The main panel represents the FMR absorption spectra represented as the frequency and field dependence of the imaginary part of the susceptibility along the excitation direction. The experimental and micromagnetic results show decent agreement. The multiple resonances modes faded way and finally remain single mode when the orientation of applied field was around 21^0 and higher.

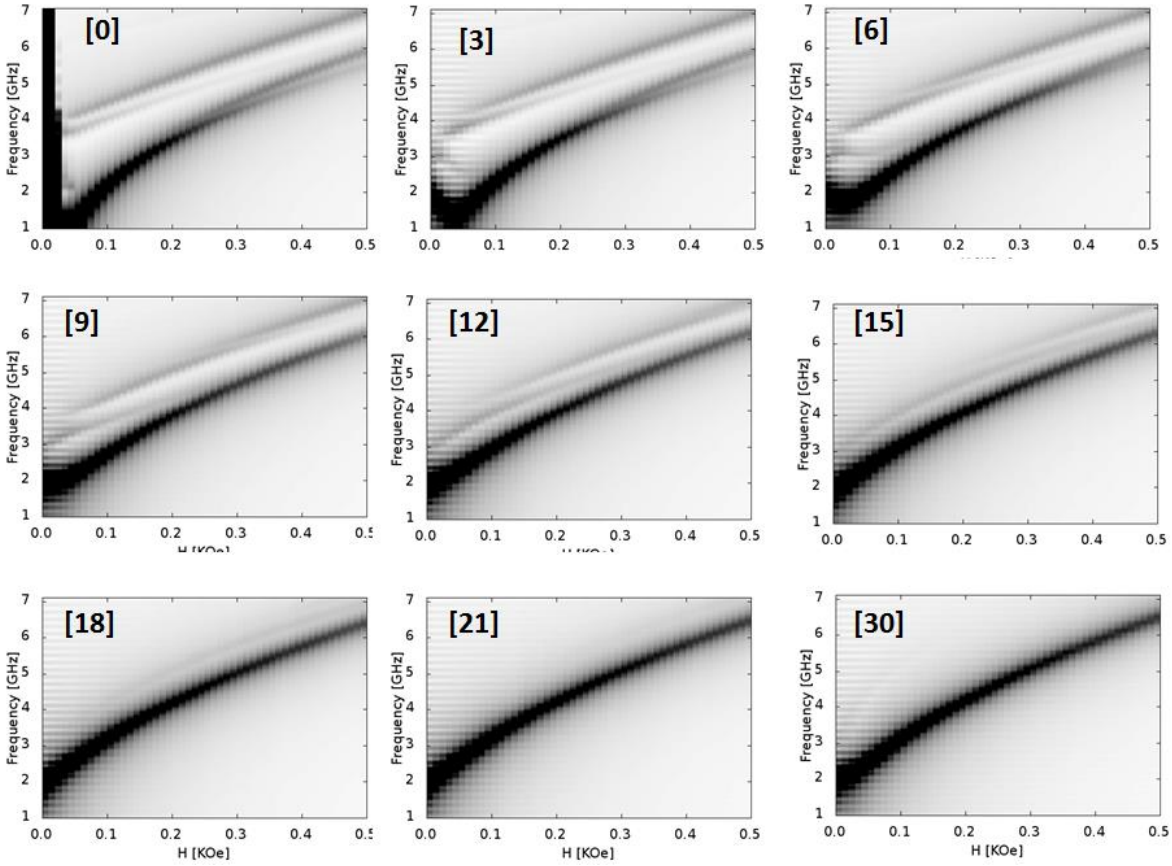

Figure 4.6: Micromagnetic simulation results of angular variation of FMR for S4

To better understand the origin of splitting of spectral line of FMR and angular variation, amplitude of magnetization was extracted from micromgnetic simulation at magnetic field 0.2KOe. The amplitude of magnetization profile along the applied dc field was considered and the spatial profile was extracted at

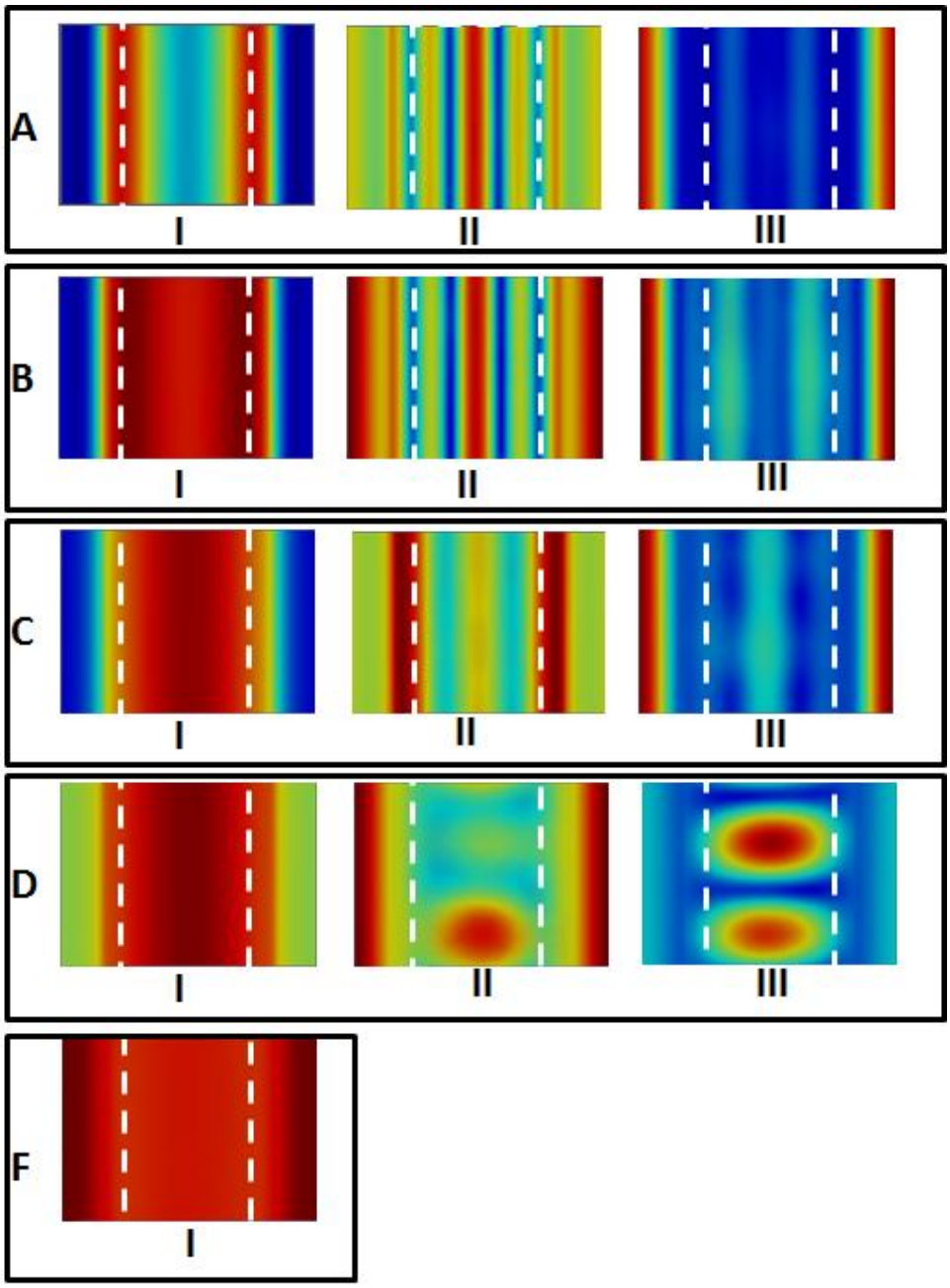

Figure 4.7: Spatial variation of magnetization amplitude at different orientation.

the resonance frequencies.

The white dotted lines in figure 4.7 represent the edges of the hill region. In terms of color coding, red color represents the highest amplitude of magnetization and blue represents the minimum. At 0^0, which is represented by A, there were main three resonance modes named as I, II and III. The first mode was excited from the region close to the edge of the hill so we called this mode as edge mode. For mode II, the wave like excitation of magnetization with different amplitude was observed. The maximum and minimum amplitude of magnetization were observed at the center of the hill and close to the edge of the hill region respectively. The mode III was contributed mainly from the edge of the grooves.

The strong angular variation on the amplitude of magnetization was observed for 6^0 which are represented by B in figure 4.7. The mode I was contributed from entire region of hill so we called it as bulk mode. Although the mode II is similar to the central region of A, the strong excitation on the grooves region was observed. Mode III was because of the strong excitation from the central region of grooves.

At 12^0 (which is represented by C in figure 4.7), the mode I was contributed from the hill region. Strong absorption for mode II was contributed from the hill and grooves edges. Mode III was mainly from the central region of grooves. For angle 18^0(represented by D in figure 4.7), the mode I was from the hill region. The mode II excited from the central region of the grooves. The third mode also observed form the central region but the standing spin wave was excited perpendicular to the grooves length. Experimentally, it was impossible to detect because of the same direction of spin wave and microwave field. Finally, for 30^0(F in figure 4.7) there was a single mode and it was solely contributed from all over the regions.

To sum up, we studied both static and dynamic properties of one dimensional modulated structure. In static study, the steps on MHL curve reveal that there are magnetic charges along the edge of the grooves especially on unsaturated condition. The strong effect of these magnetic charges appears when

field applied along the 45^0 with the grooves. In dynamic scenario, the splitting of the uniform resonance mode observed when the grooves come closer and closer. When grooves are close enough, the dipolar interaction plays vital role to split FMR spectra up to four modes. In addition, the angular variation of FMR shows that the edge modes were disappearing after angle 18^0. The excitation of the standing spin wave excited in the perpendicular direction with the applied field for higher modes especially at angle 18^0.

4.5 *b* varied systems:

In this section, the width of the hill, *b,* was varied while the other parameters were kept constant, i.e. *h*=40 nm, *t*=4 nm, and *a*=400 nm. Four samples were considered in this study, including a continuous film (with no grooves) (sample S-1), and three samples with *b* = 1000 nm (sample S-2), 500 nm (sample S-3) and 200 nm (sample S-4).

The experimentally collected spectra for all four samples are shown in figure 4.8. The transmission coefficient (S_{21}) was recorded as a function of frequency at constant applied field H_{dc}. The experiment was repeated for each static field value starting from positive saturation at 0.8 kOe and continuing to -0.8 kOe, with 5 Oe field step. The assembly of all collected data is represented as a gray scale contour plot, with highest FMR absorption shown in black. For the continuous Permalloy thin film, we have observed a well-defined single FMR mode and linewidth increases monotonically with the frequency. For all the other samples, grooves defined on top of the Permalloy thin film, splitting of the FMR spectra was observed. For each sample, the different observed modes were labelled in the order of their frequencies from the lowest (mode I) to the highest (mode IV) frequency value.

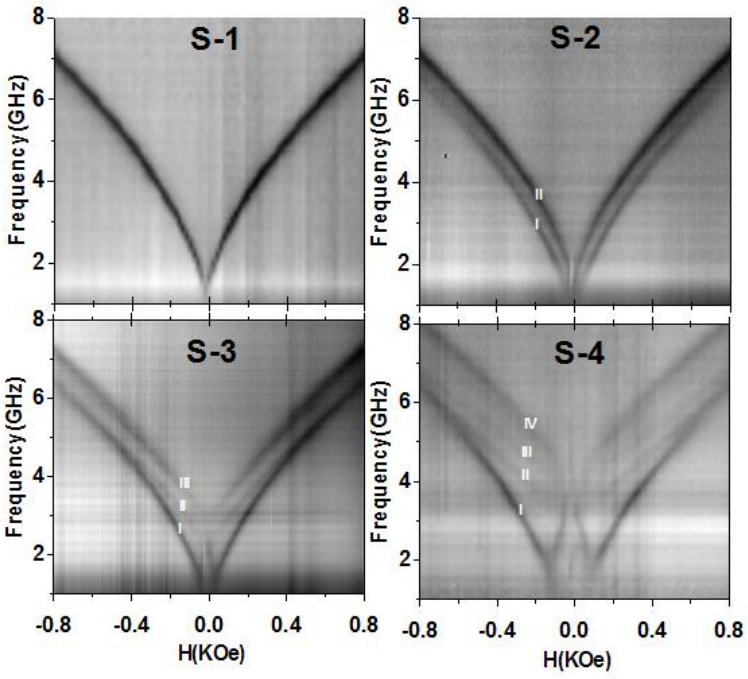

Figure 4.22: Contour plot of experimental broadband FMR spectra for sample S-1, S-2, S-3 and S-4.

4.6 Results and discussions

For the continuous thin film sample (S-1), a single uniform resonance mode (mode I) is observed. The idea to include the thin film is that it helps to compare with the non-uniform modes which were observed on the surface of modulated samples. For sample S-2, two modes of different absorption intensity were identified. These modes were labelled mode I (low frequency) and mode II (high frequency). The sample's S-2 mode II has a similar resonance frequency as the sample's S-1 uniform mode. The additional mode I observed in the case of sample S-2 is a result of the grooves presence on top of the thin film. The surface modulation creates a profile of internal demagnetization field within sample which ultimately allows the excitation of the spin wave at lower frequency compared to mode II [117]. Also, the modulation on the thin film surface helps creating magnetic charges at the edge of the grooves that will determine a non-uniform orientation of the magnetization at low applied magnetic fields. This determines different excitation frequencies for different regions of the sample. However, for

large applied fields the orientation of magnetization will become more uniform within the sample and the excitation frequencies will merge in single mode.

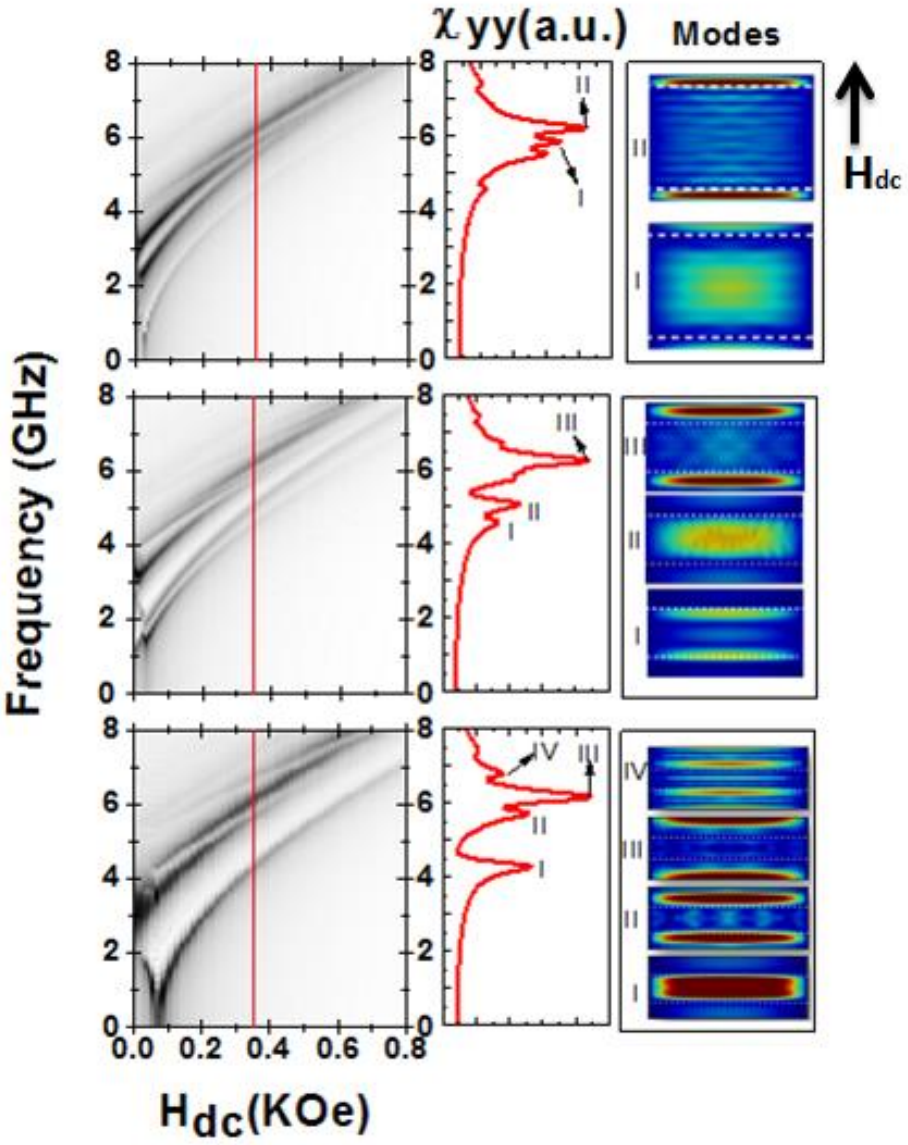

Figure 4.23: Micromagnetic simulation results for geometries similar to samples S-2, S-3 and S-4. The spectra at external field 0.35 kOe are shown in middle column and the corresponding spectra in the right column

Micromagnetic simulation for sample S-2 supports that there are two main modes. Moreover, additional low amplitude spin waves were observed in the micromagnetic simulations, that they would be hard to be detected experimentally. The spectral analysis for S-2 at the bias field 0.35 kOe shows that mode I is due to the excitation of spin waves from the hill region while mode II is coming from grooves part of the sample. For sample S-3, in addition to the modes I and III as in sample S-2, one additional satellite mode was observed due to the splitting of the mode I in magnetic field range $0 \leq H \leq 0.5$ kOe, and it is represented as mode II. For sample S-4, mode I splits in two different satellite modes at magnetic field $0 \leq H \leq 0.5$ kOe and $0 \leq H \leq 0.8$ kOe and these modes were represented as mode II and III respectively. The systematic representation of resonance modes observed for all samples is presented in table below.

Table I: Systematic representation of modes from micromagnetic simulation results

Sample	**H_{DC} (kOe)**	**Mode I**	**Mode II**	**Mode III**	**Mode IV**
S-2	0.35	Hill	Grooves		
S-3	0.35	Edge of hill	Hill	Grooves	
S-4	0.35	Hill	Edge of grooves	Grooves	Edge of groove + hill

The observed negative slope of the resonance curves (for mode IV) at lower applied fields for samples S-3 and S-4 is consistent with an applied field perpendicular to the easy axis, i.e along the grooves. As the grooves become closer to each other (*b* decreasing, from sample S-2 to S-4) the "hill" parts of the structure behave more like nanowires with shape anisotropy along the grooves, and perpendicular to applied field. The induced shape anisotropy is enhanced with decreasing the distance between the grooves *b* The FMR for thin films on a ripple substrate has shown similar induced anisotropy when they come closer [118]. Interestingly, the systematic splitting of the uniform mode which was observed in this study has not been observed in the study reported in [118].

In conclusion, the periodicity of the modulation was varied to comprehend their effect on the magnetization dynamics. The uniform mode was observed for the continuous thin film dominated by the exchange interaction. The splitting of the uniform mode is due to the periodic inhomogeneity of internal magnetic field within the sample. When the distance between grooves (the hill) decreases, more localized modes appear with different excitation frequencies on different regimes of samples. Experimentally, splitting of uniform mode to second, third and even fourth spectra were achieved, especially at low magnetic field and frequency region. The experimental results are also corroborated with micromagnetic simulation to identify and understand the nature of the observed resonance modes.

Chapter 5: Static and dynamic study of shape modulated structures

5.1 Introduction

Artificially engineered structures to achieve unique properties which do not exist in nature are called metamaterials. Magnonic crystals (MCs), where spin waves are the transmission waves, are analogous to well-known photonic crystal. Metamaterials design in one, two and three dimensional form could offer the potential applications especially to tune both static and dynamic properties of materials. Low propagating speed, compared to the electromagnetic wave, and frequency in giga-hertz range brand MCs ideal candidate for many technological applications. Information transformation, signal processing, spintronic devices, high density data storage and sensors [119-122] are few examples where MC have shown the promising great applications. In addition, MCs are also a perfect candidate for on chip data communication, phase shifters, splitters, and non-linear networks as well as magnonic logic devices [123-127]. The unique non-reciprocal properties of spin waves have possible application in microwave devices such as isolators, circulators and microwave filters [116, 128].

The beauty of MC is that we can tune the static and dynamic properties by simply the changing the shape, size, spacing and symmetry of structure. Moreover, controlling these parameters in a systematic manner to achieve distinctive properties is equally important from technological perspective. Saturation magnetization, anisotropy constant, exchange stiffness, and damping constant are no longer only intrinsic properties of the magnetic structure because of different boundary condition for diverse structures. At the same time, this complicated phenomenon opens up new possibility to make artificial structures with wide range of applications. Extensive studies on nanowires, dots, rings, grooves, couple dots, modulated wires and many more structures have been performed. Periodic modulations on one or both sides of nanowires to study the effect on static and dynamic properties was studied in

reference[129]. In this chapter, we have studied two types of samples. The first type was dumbbells with different sizes and the second was repeated multilayers of magnetic and non-magnetic layers.

5.2 Static and dynamic study of dumbbell structure

Joining the planer symmetric structure dot to the non-planer symmetric wire is interesting system to study how static and dynamic properties can be modulated from individual to combined form. Magnetic nanowires where magnetization reversal (MR) generally takes place by nucleation and propagation of domain walls are different from the dot structure where MR takes place depending on the aspect ratio as well as size[130]. Understanding MR on these combined structures and effect on the both static and dynamic properties is main drive of this section. Magneto-Optic Kerr Effect (MOKE) and vector network analyzer- ferromagnetic resonance (VNA-FMR) were used to study the static and dynamic properties respectively. Experimental results are supported by the micromagnetic simulation.

5.3 Sample preparation

Ground-signal-ground (G-S-G) type coplanar waveguides (CPW) were prepared by the combine method of photolithography, DC sputtering and liftoff process .Again the details about fabrication of CPW is well explained in chapter2. Periodic $Ni_{80}Fe_{20}$ (Permalloy) arrays of dumbbell were fabricated on the top of signal line of CPW with the help of electron beam lithography, sputtering and liftoff process. Scanning electron microscopy image is presented in figure 5.1. In figure 5.1, [a] is SEM image of CPW, [b] Center line of CPW with dumbbell and [c] zoom in of the central region of [b]. The dimensions and naming of samples are as follows. Six sets of samples were prepared on top of a CPW, three parallel and three perpendicular to the signal line (since the dot is symmetric, parallel and perpendicular refer to the orientation of the wire axis with respect to the signal line). The samples parallel to the signal line are named D-1-PA, D-2-PA, D-4-PA, which means the diameter of the dots are 1, 2, and 4 micrometer, respectively. D-1-PE, D-2-PE, D-4-PE refers to samples with dot diameter 1 , 2 and 4 micrometer

respectively and oriented perpendicular to the signal line. In all samples, the wire has a length of 4 micrometers and width of 1 micrometer. Thickness of all samples was 50 nm and the gap between individual dumbbells was kept more than 1 micrometer to ensure the structures did not interact with each other.

MOKE technique was used to study static properties, such as collective magnetization reversal, sweeping the external magnetic field. VNA-FMR method was used to study the dynamic properties at room temperature. The microwave frequency was swept from 1 to 8 GHz while keeping the dc magnetic

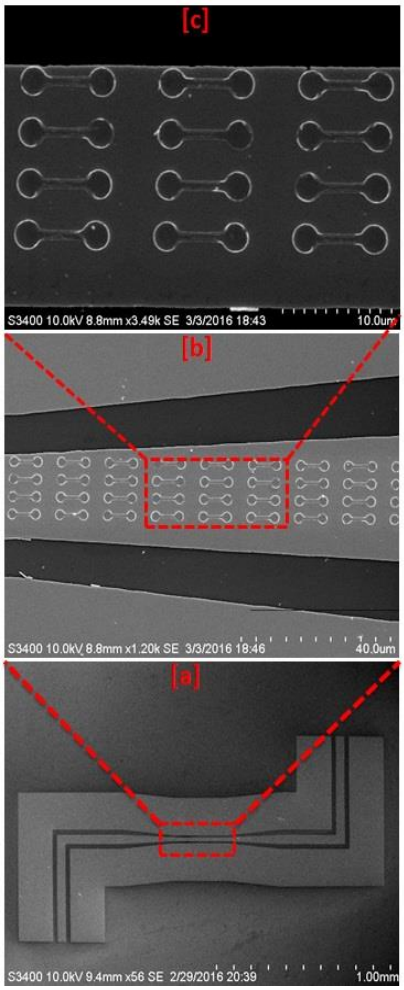

Figure 5.1: [a] SEM image of CPW [b] dumbbells on central line of CPW [c] zoom in on figure [b]

field constant. The dc field was swept from 1500 to -1500 Oe with field step of 10 Oe. The transmission coefficient (S_{21}) was collected as a function of frequency and field. Micromagnetic simulations were carried out to understand the static and dynamic experimental results. Graphics processing unit (GPU) accelerated micromagnetic simulation was performed using MuMax3 and details of it has been presented in chapter 4.

5.4 Experimental and static micromangetic results

The experimental MHLs, which were collected with the MOKE technique, is presented in figure 5.2.

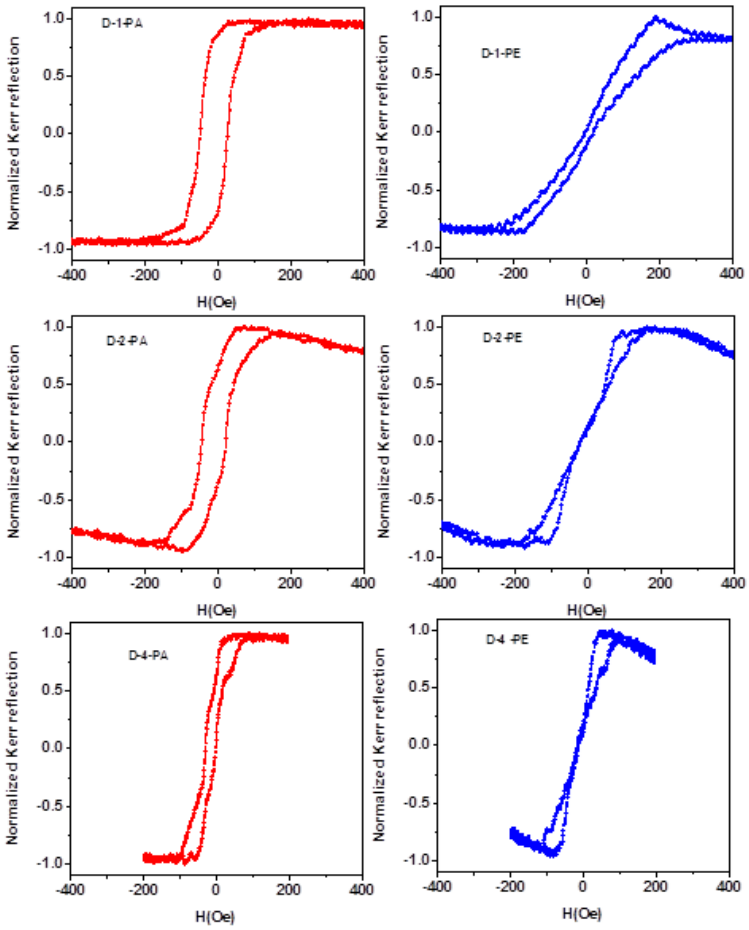

Figure 5.2: Experimental MHL for set of samples

Sample D-1-PA is set of wires with round ends. The MHL loop is similar to the MHL loop for wires with coercivity 38 Oe. The coercivity 12 Oe was observed when external magnetic field was applied perpendicular to the wire. The lower coercivity and higher saturation field was because of the shape anisotropy of wire. The reversal nature of MHL also confirms the hard axis was in perpendicular direction with wire axis. For D-2-PA, two kinks on MHL at unsaturated state have been clearly observed. However, MHL was significantly contributed from the wire region with total coercivity 33 Oe. For D-2-PE, the zero coercivity close to the origin suggests the vortex was evolved during the magnetization reversal

process. In case of D-4-PA, at the region of kinks, the MHL loop has small coercivity and modulated MHL was clearly observed with coercivity 15 Oe. In case of D-4-PE, the nature of the MHL also shows the strong signature of vortex evolution during the magnetization reversal process. In addition, extra steps also observed close to the annihilation field.

To better understand these experimental MHLs, micromagnetic simulations were performed using Mumax code. The MHL for nanowires are well understood both theoretically as well as experimentally [38]. The specific attention was paid to understand the MHLs of dumbbell structure. In the following, we will be presenting the micromanetic simulation results to explain the magnetization reversal process in this regards.

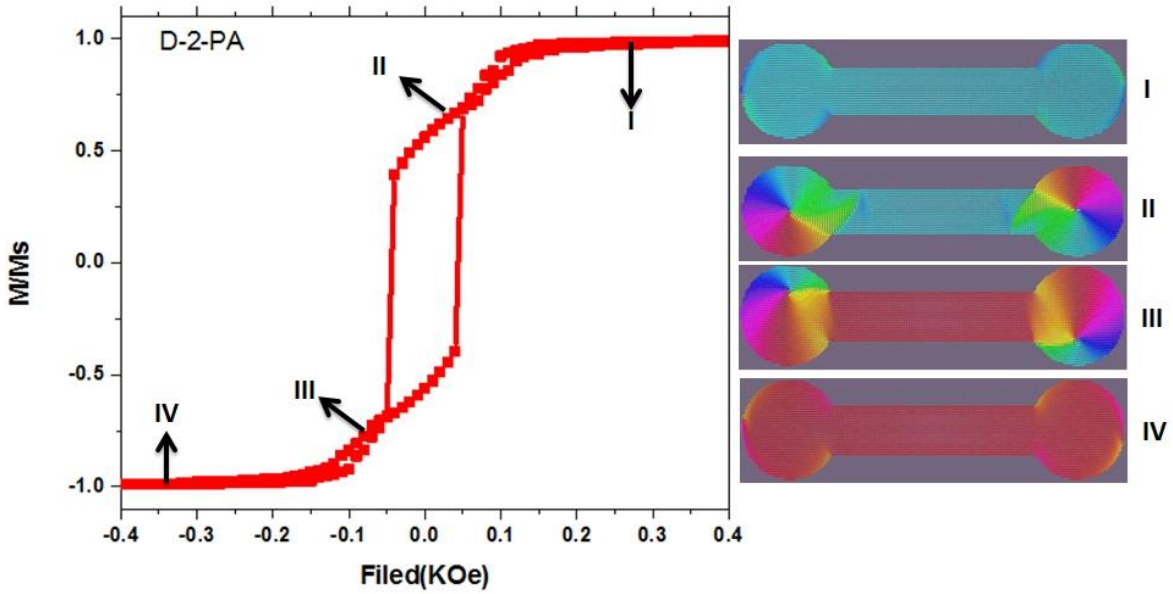

5.3: MHL loop for D-2-PA and snapshot of magnetization at different location of MHL

When magnetic field was decreasing from positive saturation, the excitation was started from the dot or wire depending on the direction of applied field. For D-1-PA, at saturation field, the magnetic moments aligned along the field direction as in figure 5.3 I. When external field was started to decrease, the vortexes with opposite chirality started to evolve from the edge of dot. Further decreasing the magnetic field, the vortexes started to move towards the center of dot as in II of figure 5.3. Right after

that the switching of the wire took place. The vortex could not pass via the constriction region at the joining of wire and dot. The vortexes again started move along the edge of the dot when decreasing field and shown III of figure 5.3. Finally, when external magnetic field was strong enough, the orientation of the magnetization aligned along the field direction as in IV of figure 5.3. The effective contribution of vortexes was cancelled due to the opposite chirality and finally dominated contribution on MHL from the wire was observed.

The micromagnetic results for D-2-PE show the different and complicated magnetization reversal

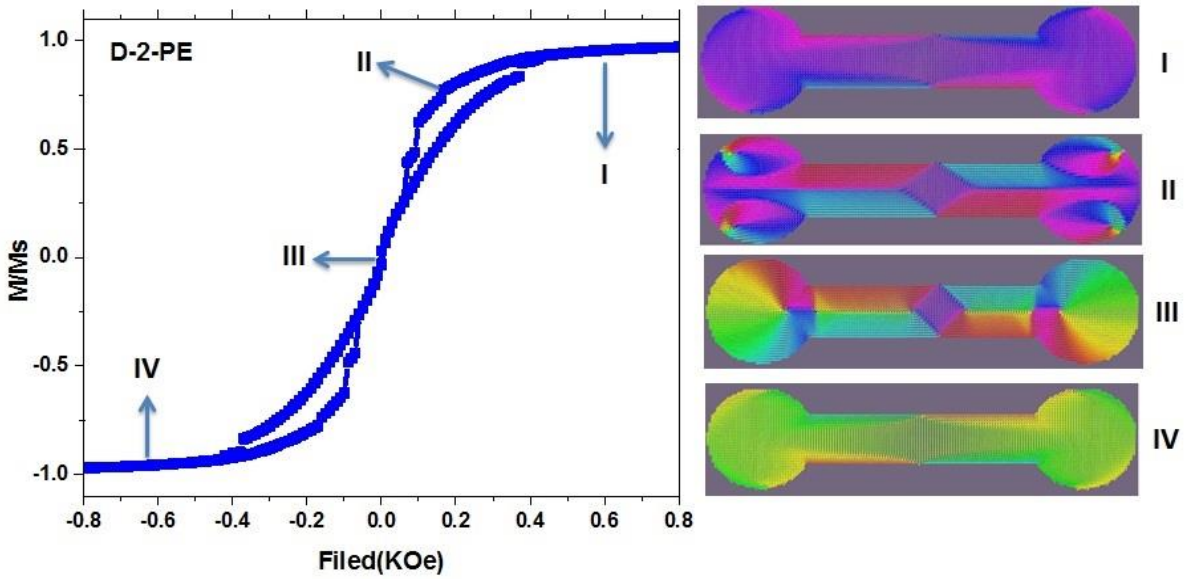

Figure 5.4: MHL loop for D-2-PE and snapshot of magnetization at different location of MHL

process compare with D-2-PA. The MHL and snapshot of magnetization at different point of MHL is presented in figure 5.4. When external magnetic field applied, the changes on magnetization starts form the edge of the wires which is opposite compare with D-2-PA. At II region, the diamond shape of magnetization was observed at the center of wire and two vortexes with opposite chirality was observed on each dot. The two vortexes merge on a single vortex on each dot and finally two dots with opposite vortex chirality observed.

The interesting observation in this case was that the vortexes moves towards each other and meets at the center of wire. When two vortexes meet, the transverse type domain wall was observed at the center of wire. The micromagnetic simulated results for D-4-PA is presented in figure 5.5. Similar to D-2-PA, the excitation of the magnetization starts from dots. The bigger size of dot allows the nucleation of two vortexes on each dot. The vortexes did not move along the wire instead the two vortexes merge in single and move the perpendicular direction with respect to the applied field. The notch, at the joining of the wire and dot, did not allow the propagation of the vortex along wire. Again, the overall effect was

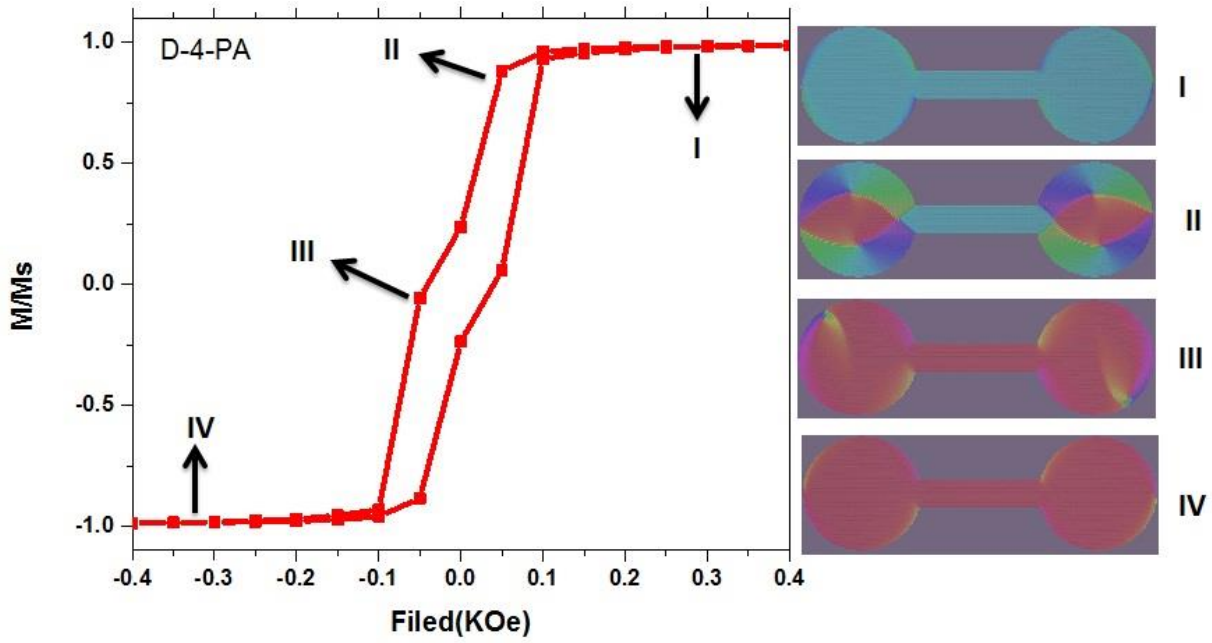

Figure 5.5: MHL loop for D-4-PA and snapshot of magnetization at different location of MHL

dominated from the wire and it was clearly observed in results. Comparing with the experimental results, there are also two modulations on MHL. Although the position of modulations on MHL on experimental results were slight offset compare with the micromagnetic MHLs, the overall results were comparable.

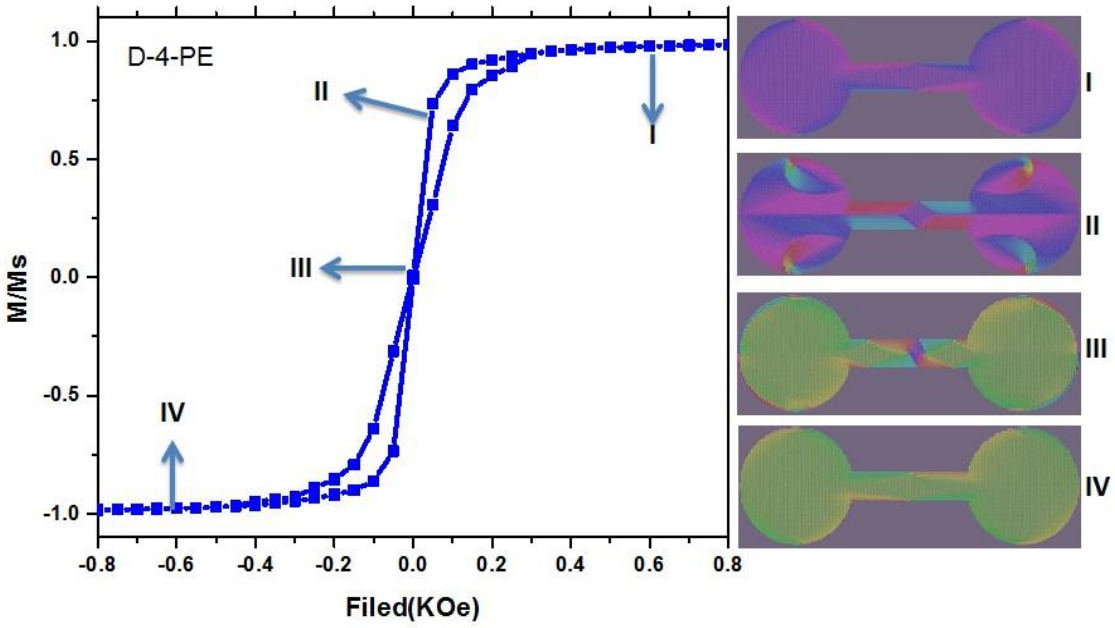

Figure 5.6: MHL loop for D-4-PA and snapshot of magnetization at different location of MHL

Figure 5.6 represents the micromagnetic results of MHL and snapshot of magnetization for D-4-PE at different applied fields. The evolution and dynamic of vortexes was very similar to the D-2-PE. However the vortexes were existed on the narrow field range. The transverse magnetic domain wall at the perpendicular direction with the applied field also observed.

5.5 Experimental dynamic results:

The ferromgnetic resonance spectroscopy was used to probe the microwave characterization of the samples. The three dimensional contour plots for six set of samples have been presented in figure 5.7. The corresponding naming has also been indicated on contour plots. For sample D-1-PA, broad line width of ferromagnetic resonance spectra was observed. However, the intensity of absorption was not smooth. The weak absorption of microwave signal within sample was because of the shape of the wires at the end (round end). The round ends of wire allows to excite the edge mode very close to the main

mode so untimately single resonance at lower frequency was observed. For D-1-PE, there was single

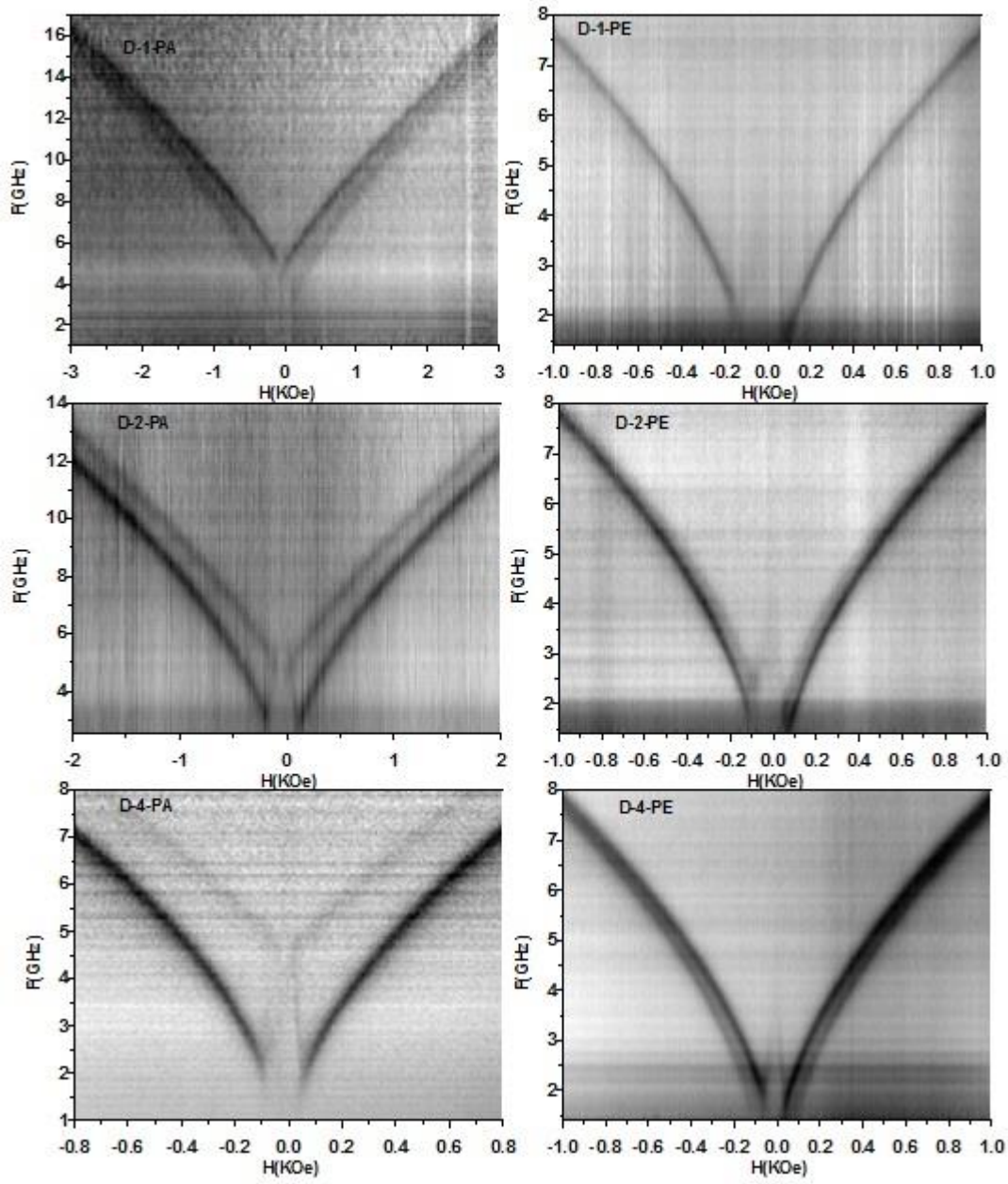

Figure 5.7: Experimental 3D plot of FMR for different samples

uniform mode with linewidth smaller than for D-1-PA.

Well defined two resonance modes were observed for samples D-2-PA. The resonace frequencies gap between two modes decrease with increasing external magnetic fields. The different shape anisotropy of wire and dot allows to excite FMR at different frequency range.In case of D-2-PE, there was a well defined single mode. In addition, comparatively absorption with lower intensity observed on higher frequency region. However, the modes are close enough so they come out as a single mode. Two distict resonance modes were present for sample D-4-PA. Well definded frequency gap was presents between them. The frequency gap of 1.8 GHz was observed at external magnetic field 0.8KOe. The negative slope was observed at the low field and frequency region. Simular contour like as D-2-PE was for D-4-PE however the intensities was switched. The higher absorpion intensity was observed for the higher frequency region. In the following, the micromagnetic simulated results will be presented to better explain the experimentally observed results.

5.4 Micromagnetic simulated results for ferromagnetic resonance spectra.

The micromagnetic simulated results for all six set of sample is presented in figure 5.7. The experimental

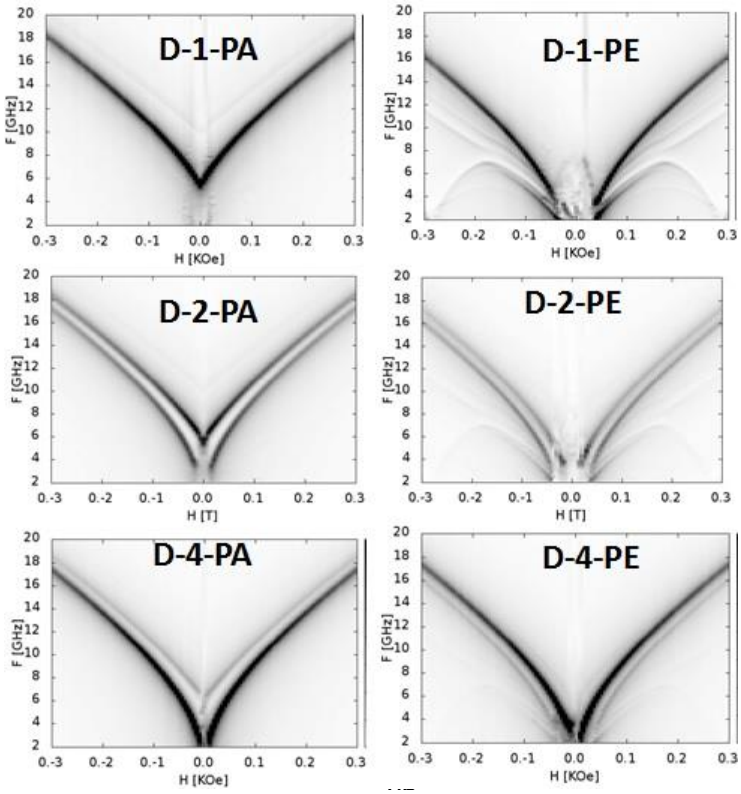

Figure 5.8: Micromagnetic results for set of samples

results were reproduced. The micromagnetic simulation was performed using software mumax. The details of the technique as well as cell size for micromagnetic simulation have been presented in chapter 3. The orientation of the applied pulse and magnetic field were kept always perpendicular. For D-1-PA, the excitation of the magnetization was studied by sweeping the microwave frequency at external magnetic field 1KOe. The magnetization starts to excite from the edge at lower frequency. When microwave frequency was swept, spatial variation of susceptibility was observed. Wave like variation of susceptibility was there close to the resonance frequency. This mode has been represented as mode I in figure 5.9. At main resonance, bulk mode was observed and represented by mode II. When microwave frequency was swept further, wave like variation on susceptibility on perpendicular direction to the external magnetic field was observed and it is donated by mode III in figure 5.9.

For D-1-PE, the spatial variation of dynamic susceptibility was quite complicated compare to D-1-PA and has been presented in figure 5.10. The excitations of susceptibility with smaller amplitude were observed at low frequency region however it was not prominently observed on experimental results. For main resonance (mode III), the excitation was from the bulk region. Spatially wave like behavior of susceptibility was observed right before and after the bulk mode along the applied field direction. In addition, variation on susceptibility along the wire also observed after the main mode.

For sample D-2-PA, two main resonance modes with equal absorption intensity were observed. The mode I was clearly bulk mode and it was from the dots. It was more localized close to the joining of wire and dots as shown in figure 5.11. The mode II was contributed from the wire region. The different shape anisotropy for wire and dot allows the excitation of susceptibility at two different frequencies.

The profile of susceptibility, on the frequency scan at field 1KOe for sample D-2-PE, has been presented in figure 5.12. Experimentally, double modes of FMR with equal amplitude of absorption were observed.

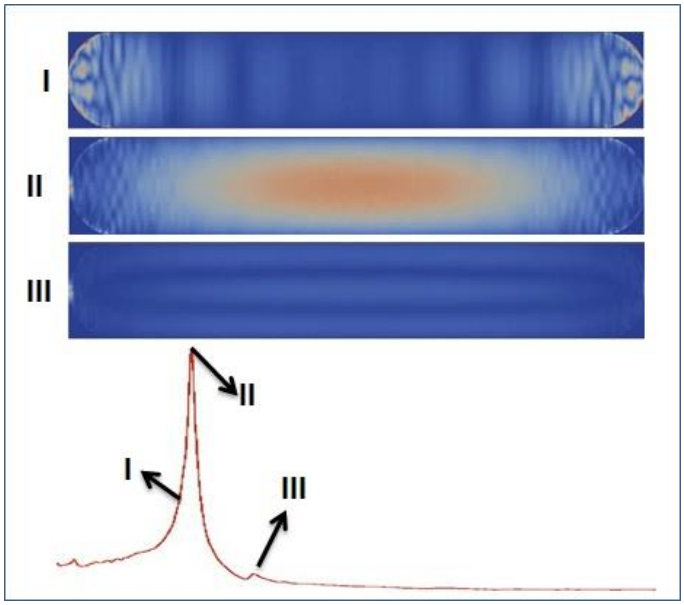

Figure 5.9: Spatial variation of susceptibility for D-1-PA

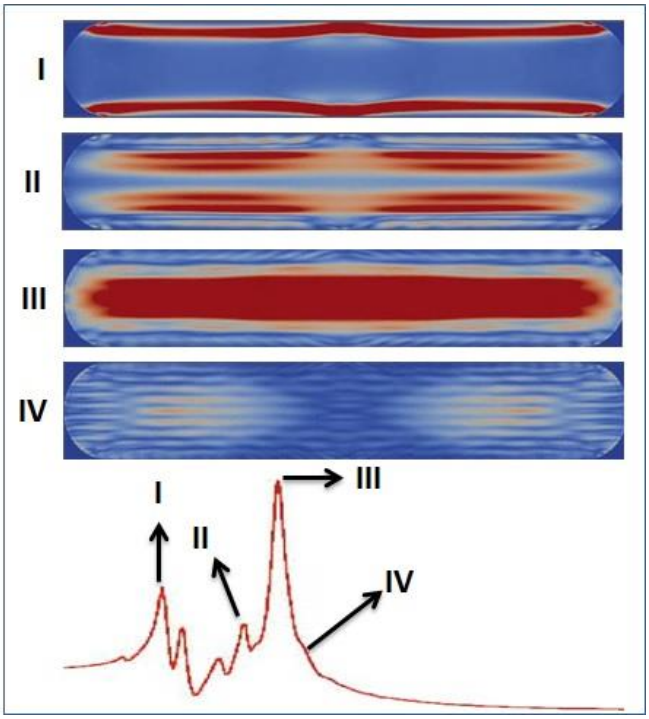

Figure 5.10: Spatial variation of susceptibility for D-1-PE

In addition, lower amplitudes of the susceptibility were there but they were not able to detect experimentally. Three modes were considered in this case. The mode I was from the edge of the wire

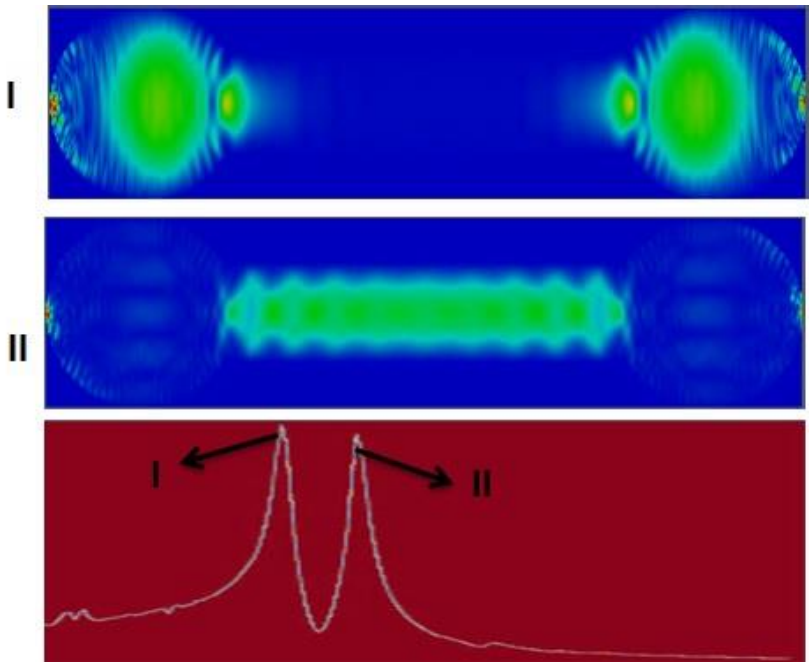

Figure 5.11: Spatial variation of susceptibility for D-2-PA

and the II was from the middle of the wire as bulk mode. Interesting, the excitation on the dot region was not so pronounced in this case. Which means, there was not anymore bulk mode in dot rather wave like variation of susceptibility was all over sample especially in case of mode III.

Sample D-4-PA has also two distinct resonance modes i.e. first from the dot and second from the wire. In addition, interesting distribution of susceptibility was observed after the main resonance modes. For example, mode I and III were from the dot and wire respectively. The systematic dotted type distribution of susceptibility was observed on wire for mode II. Similarly the modes perpendicular to the applied field was there for mode IV.

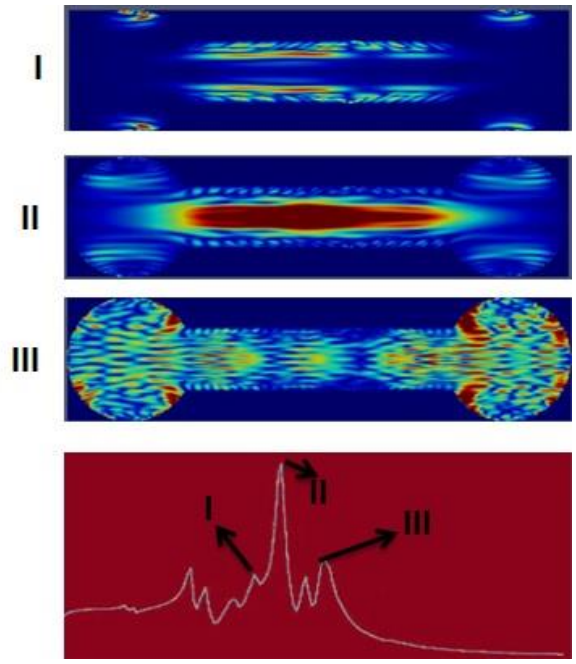

5.12: Spatial variation of susceptibility for D-2-PA

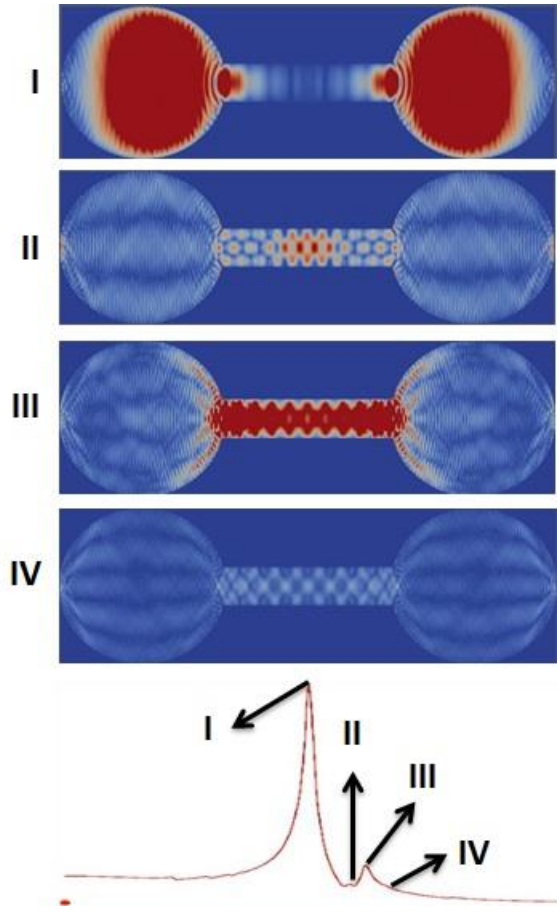

Figure 5.12: Spatial variation of susceptibility for D-4-PA

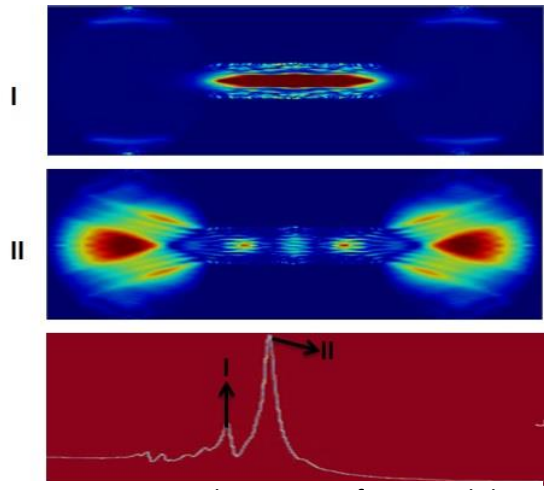

Figure 5.13: Spatial variation of susceptibility for D-4-PE

The systematic variation of susceptibility for sample D-4-PE is presented in figure 5.13. Mainly, there were two modes which were represented by I and II. The additional modes at lower frequency were not able to detect experimentally because of low amplitude. The first mode was (mode I) contributed from the wire. The bulk mode at the center of the wire extended up to close to the notch of wire and dots Mode II, which was mainly contributed from the disc, has showed the unique features. That means the bulk type mode was there at disc but wave like variation on the amplitude of susceptibility was extended throughout the disc. In addition, alternative high and low on susceptibility values was observed along the length of wire.

Conclusion and future work

Magnetic structures shows interesting properties when the their dimensions go down to nanoscale. They could be one, two or even three dimensional structures. For example, they can be thin film, wire, dot or even three dimensional structures. Understanding of high frequency properties of magnetic materials open up new route for the devices which work in nanosecond time scale. Different magnetic structures have been considered in this thesis to expore and explain both static and dynamic properties. The multilayer systems of ferromagnetic and antiferromagnetic were prepared to study the exchange bias phenomenon. Set of samples where the thickness of ferromgnetic layer was varied keeping the thickness of the antiferromagnetic layer constant to explain the thickness dependence exchange bias. Different experimental techniques were implemented to evaluate the both static and dynamic properties. The slight discrepancies on the exchange bias values that were evaluated using different techniques have been explained considering roughness of the surface, domain wall behaviour as well the reversible and irreversible process in magnetization switching. To better understand experimental results, the angular variation of both FORC and FMR were performed. The modified theroritical model of domain wall formation was used to explain the experimental results and good aggreement was achieved between experimental results and theoretical results.

Tremendous research efforts have been growing to understanding the spin wave in magnetic confined nanostructures. Anisotriopic nature of spin dispersion relation at different magnetic states is crucial to better understand the spin wave in such structures. The tuneability of magnetic nanostrucure by simply changing the physical shape and size open many options especially on data processing technology using spin wave. Tailoring of magnetic properties with the help of reconfiguration magnonic device is equally important. Multifuntional microwave and logic devices could be realized by especially on the broad and high frequency regime. To better understand these effects, we considered the sufrace modulated thin

flim structures. The uniform excitation of microwave field was realized in sample by fabrication the sample on the top of signal line of CPW. Uniform resonance mode was observed for unpattern films. When periodic grooves were introduced, the splitting of resonance mode was observed. Periodicity of two parameters, for example, period of grooves and hill were varied to understand the effect of periodic modulation on static and dynamic response. Upto four modes were observed when the grooves comes close. Which means, the dipolar type interaction played important role for the splitting of the main resonance mode. The localize modes were excited at different frequency at same magnetic fields. The spatial and temporal distribution of spin wave were identified with the help of micromagnetic simulations. Good agreement between experimental and micromagnetic simulation results were obtained. These types of excitaion will be very useful to design the broadband microwave filtes as well as understanding the nature of spin waves in periodic modulated structures.

We also considered the dumbell shaped structures, which is bacially the hybrid structure of arrays of wires and dots in planer form, to better understand the static and dynamic properties. Dots with different diameters were connected with the wire. In case of static properties, the motion of domains along the notch showed unique behaviour. In addition, the vortex were formed on dots and the propagation of these vortex was perpendicular to the external magnetic field. Different shape anisotropy for wire and dot was responsible to switch magnetization differently at two different structures. The overall shape of the MHL loop was dominated from the wire with modulation effect especially unsaturated case when external magnetic field was parallel to the wire. However, when magnetic field was applied perpendular to the wire, wire get saturated first and then dot at higher fields. The MHL loop clearly showed the dominant contribution was from the dot with zero coercivity. In dyanamic case, the dot and wire were excitaed at two different frequencies. The excitation of the spin wave do not propagate through the notch which cause two different resonance fields. Depending on the

orientaion of the applied field with respect to the shape of sample and with the size of the dots, they were tuned with different frequencies. Moreover, the gap between the two resonance modes was changed by simply chaning the size of the dots.

From few years back, realization of tuned bandgap especially in three dimenional magnetic structure is mounting. Potential uses of spin wave for data processing demands the better understanding of spin wave in confined magnetic nanostructure . In addition to the dipolar interaction on plane, the three dimenisonal structures could have additional interaction along the height and that can be one more additional parameter to tune the band gap for magnonic crystals. In addition, the the magnetic and non magnetic multipayers has great application sepecially for the sensor to read and write data. In this study we considered the multilayres of the magnetic and non magnetic layer to understands the coupling along the z-direction. Both static and dynamic properties showed the unique behaviour especially in non saturated regime. The ring type multilayer with different inner diameter also considered to better understand the dynamic of vortex and also the excitation of the spin wave in confined geometry.

Fabrication of three dimensonal magnetic nanostructures and tune the physical parameters to achieved the desired properties would be the most promising route especially for data processing technology.

References

[1] N. A. Spaldin, *Magnetic Materials: Fundamentals and Applications*: Cambridge University Press, 2010.

[2] T. R. Albrecht, H. Arora, V. Ayanoor-Vitikkate, J. M. Beaujour, D. Bedau, D. Berman*, et al.*, "Bit-Patterned Magnetic Recording: Theory, Media Fabrication, and Recording Performance," *Ieee Transactions on Magnetics,* vol. 51, May 2015.

[3] C. Murapaka, P. Sethi, S. Goolaup, and W. S. Lew, "Reconfigurable logic via gate controlled domain wall trajectory in magnetic network structure," *Scientific Reports,* vol. 6, Feb 3 2016.

[4] K. M. Krishnan, *Fundamentals and applications of magnetic materials*: Oxford University Press, 2016.

[5] R. White and T. E. Downs, *How Computers Work*: Que, 2006.

[6] R. Kergoat, M. Labrune, J. Miltat, T. Valet, and J. C. Jacquet, "Magnetization Reversal in Ni80fe20/Cu/Co Spin-Valves," *Journal of Magnetism and Magnetic Materials,* vol. 121, pp. 339-343, Mar 1993.

[7] D. Lottis, A. Fert, R. Morel, L. G. Pereira, J. C. Jacquet, P. Galtier*, et al.*, "Magnetoresistance in Rf-Sputtered (Nife/Cu/Co/Cu) Spin-Valve Multilayers," *Journal of Applied Physics,* vol. 73, pp. 5515-5517, May 15 1993.

[8] T. Valet and A. Fert, "Theory of the Perpendicular Magnetoresistance in Magnetic Multilayers," *Physical Review B,* vol. 48, pp. 7099-7113, Sep 1 1993.

[9] M. Julliere, "Tunneling between Ferromagnetic-Films," *Physics Letters A,* vol. 54, pp. 225-226, 1975.

[10] J. Mathon and A. Umerski, "Theory of tunneling magnetoresistance of an epitaxial Fe/MgO/Fe(001) junction," *Physical Review B,* vol. 63, Jun 1 2001.

[11] K. Mahmoudi and C. G. Hadjipanayis, "The application of magnetic nanoparticles for the treatment of brain tumors," *Frontiers in Chemistry,* vol. 2, 2014.

[12] A. Ito, M. Shinkai, H. Honda, and T. Kobayashi, "Medical application of functionalized magnetic nanoparticles," *Journal of Bioscience and Bioengineering,* vol. 100, pp. 1-11, Jul 2005.

[13] V. Sharma, J. Saha, S. Patnaik, and B. K. Kuanr, "YIG based broad band microwave absorber: A perspective on synthesis methods," *Journal of Magnetism and Magnetic Materials,* vol. 439, pp. 277-286, Oct 1 2017.

[14] R. E. Camley, Z. Celinski, T. Fal, A. V. Glushchenko, A. J. Hutchison, Y. Khivintsev*, et al.*, "High-frequency signal processing using magnetic layered structures," *Journal of Magnetism and Magnetic Materials,* vol. 321, pp. 2048-2054, Jul 2009.

[15] B. K. Kuanr, N. R. Anderson, Z. J. Celinski, and R. E. Camley, "Monolithic Microwave Nonlinear Phase Shifter," *Ieee Magnetics Letters,* vol. 6, 2015.

[16] B. K. Kuanr, T. J. Fal, Z. Celinski, and R. E. Camley, "Iron based microstrip phase shifter; optimization of phase shift," *Journal of Applied Physics,* vol. 111, Apr 1 2012.

[17] B. K. Kuanr, V. Veerakumar, R. Marson, S. R. Mishra, R. E. Camley, and Z. Celinski, "Nonreciprocal microwave devices based on magnetic nanowires," *Applied Physics Letters,* vol. 94, May 18 2009.

[18] B. Kuanr, Z. Celinski, and R. E. Camley, "Tunable high-frequency band-stop magnetic filters," *Applied Physics Letters,* vol. 83, pp. 3969-3971, Nov 10 2003.

[19] P. Gruszecki, M. Kasprzak, A. E. Serebryannikov, M. Krawczyk, and W. Smigaj, "Microwave excitation of spin wave beams in thin ferromagnetic films," *Scientific Reports,* vol. 6, Mar 14 2016.

[20] K. Y. Guslienko and A. N. Slavin, "Boundary conditions for magnetization in magnetic nanoelements," *Physical Review B,* vol. 72, Jul 2005.

[21] J. Jorzick, C. Kramer, S. O. Demokritov, B. Hillebrands, B. Bartenlian, C. Chappert*, et al.*, "Spin wave quantization in laterally confined magnetic structures (invited)," *Journal of Applied Physics,* vol. 89, pp. 7091-7095, Jun 1 2001.

[22] J. Bass and W. P. Pratt, "Spin-diffusion lengths in metals and alloys, and spin-flipping at metal/metal interfaces: an experimentalist's critical review," *Journal of Physics-Condensed Matter,* vol. 19, May 9 2007.

[23] M. Abes, C. T. Koops, S. B. Hrkac, J. McCord, N. O. Urs, N. Wolff*, et al.*, "Domain structure and reorientation in CoFe2O4," *Physical Review B,* vol. 93, May 18 2016.

[24] J. Trutzschler, K. Sentosun, B. Mozooni, R. Mattheis, and J. McCord, "Magnetic domain wall gratings for magnetization reversal tuning and confined dynamic mode localization," *Scientific Reports,* vol. 6, Aug 4 2016.

[25] V. Patsula, M. Moskvin, S. Dutz, and D. Horák, "Size-dependent magnetic properties of iron oxide nanoparticles," *Journal of Physics and Chemistry of Solids,* vol. 88, pp. 24-30, 2016/01/01/ 2016.

[26] C. Bran, Y. P. Ivanov, D. Trabada, J. Tomkowicz, R. del Real, O. Chubykalo-Fesenko*, et al.*, "Structural dependence of magnetic properties in Co-based nanowires: Experiments and micromagnetic simulations," *IEEE Transactions on Magnetics,* vol. 49, pp. 4491-4497, 2013.

[27] O. Fesenko and L. Yatsenko, *Nanophysics, Nanophotonics, Surface Studies, and Applications: Selected Proceedings of the 3rd International Conference Nanotechnology and Nanomaterials (NANO2015), August 26-30, 2015, Lviv, Ukraine*: Springer International Publishing, 2016.

[28] A. Fernandez-Pacheco, R. Streubel, O. Fruchart, R. Hertel, P. Fischer, and R. P. Cowburn, "Three-dimensional nanomagnetism," *Nature Communications,* vol. 8, Jun 2017.

[29] S. S. Parkin, M. Hayashi, and L. Thomas, "Magnetic domain-wall racetrack memory," *Science,* vol. 320, pp. 190-194, 2008.

[30] S. Pan, J. W. Klos, S. Mieszczak, A. Barman, and M. Krawczyk, "Spin waves in periodic antidot waveguide of complex base," *Journal of Physics D-Applied Physics,* vol. 50, Jul 2017.

[31] A. V. Chumak, A. A. Serga, and B. Hillebrands, "Magnonic crystals for data processing," *Journal of Physics D-Applied Physics,* vol. 50, Jun 2017.

[32] L. L. Xiong, M. Kostylev, and A. O. Adeyeye, "Magnetization dynamics of Ni80Fe20 nanowires with continuous width modulation," *Physical Review B,* vol. 95, Jun 2017.

[33] M. Kiwi, "Exchange bias theory," *Journal of Magnetism and Magnetic Materials,* vol. 234, pp. 584-595, 2001.

[34] J. Nogués and I. K. Schuller, "Exchange bias," *Journal of Magnetism and Magnetic Materials,* vol. 192, pp. 203-232, 1999.

[35] S. Parkin, K. Roche, M. Samant, P. Rice, R. Beyers, R. Scheuerlein*, et al.*, "Exchange-biased magnetic tunnel junctions and application to nonvolatile magnetic random access memory," *Journal of Applied Physics,* vol. 85, pp. 5828-5833, 1999.

[36] B. Sambandam, N. Rajendran, M. Kanagaraj, S. Arumugam, and P. T. Manoharan, "Switching on Antiferromagnetic Coupled Superparamagnetism by Annealing Ferromagnetic Mn/CdS Nanoparticles," *Journal of Physical Chemistry C,* vol. 115, pp. 11413-11419, Jun 2011.

[37] J. D. Jackson, *Classical electrodynamics*: Wiley, 1975.

[38] B. D. Cullity, *Introduction to magnetic materials*. Reading, Mass.: Addison-Wesley Pub. Co., 1972.

[39] R. Szewczyk, "Modelling of the magnetic and magnetostrictive properties of high permeability Mn-Zn ferrites," *Pramana,* vol. 67, pp. 1165-1171, 2006.

[40] D. C. Jiles, *Introduction to Magnetism and Magnetic Materials, Second Edition*: Taylor & Francis, 1998.

[41] E. C. Stoner and E. P. Wohlfarth, "A Mechanism of Magnetic Hysteresis in Heterogeneous Alloys," *Philosophical Transactions of the Royal Society of London. Series A, Mathematical and Physical Sciences,* vol. 240, pp. 599-642, 1948.
[42] A. G. Gurevich and G. A. Melkov, *Magnetization Oscillations and Waves*: Taylor & Francis, 1996.
[43] S. Khanal, A. Diaconu, J. M. Vargas, D. R. Lenormand, C. Garcia, C. A. Ross*, et al.*, "Exchange bias in (FeNi/IrMn)n multilayer films evaluated by static and dynamic techniques," *Journal of Physics D-Applied Physics,* vol. 47, Jun 25 2014.
[44] J. Lindner, R. Meckenstock, and M. Farle, "Applications of ferromagnetic resonance," *Characterization of Materials,* 2012.
[45] C. Herring and C. Kittel, "On the Theory of Spin Waves in Ferromagnetic Media," *Physical Review,* vol. 81, pp. 869-880, 03/01/ 1951.
[46] A. V. Kimel, A. Kirilyuk, P. A. Usachev, R. V. Pisarev, A. M. Balbashov, and T. Rasing, "Ultrafast non-thermal control of magnetization by instantaneous photomagnetic pulses," *Nature,* vol. 435, pp. 655-657, 06/02/print 2005.
[47] M. J. Klein and R. S. Smith, "A Note on the Classical Spin-Wave Theory of Heller and Kramers," *Physical Review,* vol. 80, p. 1111, 1950.
[48] J. Van Vleck, "The dipolar broadening of magnetic resonance lines in crystals," *Physical Review,* vol. 74, p. 1168, 1948.
[49] B. Kalinikos and A. Slavin, "Theory of dipole-exchange spin wave spectrum for ferromagnetic films with mixed exchange boundary conditions," *Journal of Physics C: Solid State Physics,* vol. 19, p. 7013, 1986.
[50] D. D. Stancil, *Theory of magnetostatic waves*. New York :: Springer-Verlag, 1993.
[51] D. M. Pozar, *Microwave Engineering*: Wiley, 2004.
[52] R. N. Simons, *Coplanar waveguide circuits, components, and systems* vol. 165: John Wiley & Sons, 2004.
[53] R. Handa and L. Gu, "Electron Beam Lithography Process Optimization," 2011.
[54] S. Reyntjens and R. Puers, "A review of focused ion beam applications in microsystem technology," *Journal of Micromechanics and Microengineering,* vol. 11, p. 287, 2001.
[55] R. Watkins, P. Rockett, S. Thoms, R. Clampitt, and R. Syms, "Focused ion beam milling," *Vacuum,* vol. 36, pp. 961-967, 1986.
[56] L. A. Giannuzzi, *Introduction to focused ion beams: instrumentation, theory, techniques and practice*: Springer Science & Business Media, 2006.
[57] M. Marko, C. Hsieh, R. Schalek, J. Frank, and C. Mannella, "Focused-ion-beam thinning of frozen-hydrated biological specimens for cryo-electron microscopy," *Nature methods,* vol. 4, p. 215, 2007.
[58] S. Khanal, P. Sherpa, and L. Spinu, "Splitting Of Ferromagnetic Resonance Spectra In Periodically Modulated One Dimensional Magnonic Crystal," *IEEE Transactions on Magnetics,* 2017.
[59] S. Foner, "Versatile and sensitive vibrating-sample magnetometer," *Review of Scientific Instruments,* vol. 30, pp. 548-557, 1959.
[60] A. P. Roberts, C. R. Pike, and K. L. Verosub, "First-order reversal curve diagrams: A new tool for characterizing the magnetic properties of natural samples," *Journal of Geophysical Research: Solid Earth,* vol. 105, pp. 28461-28475, 2000.
[61] R. J. Harrison and J. M. Feinberg, "FORCinel: An improved algorithm for calculating first-order reversal curve distributions using locally weighted regression smoothing," *Geochemistry, Geophysics, Geosystems,* vol. 9, 2008.
[62] C. R. Pike, A. P. Roberts, and K. L. Verosub, "Characterizing interactions in fine magnetic particle systems using first order reversal curves," *Journal of Applied Physics,* vol. 85, pp. 6660-6667, May 1 1999.

[63] A. P. R. A. R. Muxworthy, First-Order-Reversal-Curve (FORC) Diagrams, Encyclopedia and S. of Geomagnetism and Paleomagnetism, 2007.
[64] C. L. Z. Y. Fang, S. Bonetti, J. Akerman, FORC Studies of Exchange Biased NiFe in and J. o. P. C. S. L10 (111) FePt-based Spin Valves, 200, 2010.
[65] C. Pike, C. Ross, R. Scalettar, and G. Zimanyi, "First-order reversal curve diagram analysis of a perpendicular nickel nanopillar array," *Physical Review B,* vol. 71, p. 134407, 2005.
[66] A. Rotaru, J.-H. Lim, D. Lenormand, A. Diaconu, J. B. Wiley, P. Postolache*, et al.*, "Interactions and reversal-field memory in complex magnetic nanowire arrays," *Physical Review B,* vol. 84, p. 134431, 2011.
[67] H. S. Nalwa, *Magnetic Nanostructures*: American Scientific Publishers, 2002.
[68] S. V. Vonsovski, *Ferromagnetic Resonance*: Israel Program for Scientific Translations, 1964.
[69] W. H. Meiklejohn and C. P. Bean, "New Magnetic Anisotropy," *Physical Review,* vol. 105, pp. 904-913, 02/01/ 1957.
[70] C. Kittel, *Introduction to Solid State Physics*: Wiley, 2004.
[71] C. Reig, S. Cardoso, and S. Mukhopadhyay, *Giant Magnetoresistance (GMR) Sensors: From Basis to State-of-the-Art Applications*: Springer Berlin Heidelberg, 2013.
[72] R. B. da Silva, A. D. C. Viegas, V. P. Nascimento, M. A. Correa, L. F. Schelp, E. Baggio-Saitovitch*, et al.*, "High frequency magnetoimpedance in Ni81Fe19/Fe50Mn50 exchange biased multilayer," *Applied Physics Letters,* vol. 94, Jan 26 2009.
[73] J. Dubowik, F. Stobiecki, I. Goscianska, Y. P. Lee, A. Paetzold, and K. Roll, "Temperature dependence of ferromagnetic resonance in permalloy/NiO exchange-biased films," *European Physical Journal B,* vol. 45, pp. 283-288, May 2005.
[74] M. Gloanec, S. Rioual, B. Lescop, R. Zuberek, R. Szymczak, P. Aleshkevych*, et al.*, "Dynamical effect in measurement of the exchange-bias field: A consequence of the slow-relaxer mechanism," *Physical Review B,* vol. 80, Dec 2009.
[75] E. Jimenez, J. Camarero, P. Perna, N. Mikuszeit, F. J. Teran, J. Sort*, et al.*, "Role of anisotropy configuration in exchange-biased systems," *Journal of Applied Physics,* vol. 109, Apr 1 2011.
[76] J. Sort, B. Dieny, and J. Nogues, "Exchange bias in antiferromagnetic-ferromagnetic-antiferromagnetic structures with out-of-plane magnetization," *Physical Review B,* vol. 72, Sep 2005.
[77] J. Sort, G. Salazar-Alvarez, M. D. Baro, B. Dieny, A. Hoffmann, V. Novosad*, et al.*, "Controlling magnetic vortices through exchange bias," *Applied Physics Letters,* vol. 88, Jan 23 2006.
[78] K. M. Chui, D. Tripathy, and A. O. Adeyeye, "Temperature dependence of magnetotransport properties of Ni80Fe20/Fe50Mn50/Ni80Fe20 trilayers," *Journal of Applied Physics,* vol. 101, May 1 2007.
[79] C. Garcia, J. M. Florez, P. Vargas, and C. A. Ross, "Asymmetrical giant magnetoimpedance in exchange-biased NiFe," *Applied Physics Letters,* vol. 96, Jun 7 2010.
[80] C. Garcia, J. M. Florez, P. Vargas, and C. A. Ross, "Effect of the exchange bias coupling strength on the magnetoimpedance of IrMn/NiFe films," *Journal of Applied Physics,* vol. 109, Apr 1 2011.
[81] N. N. Phuoc, F. Xu, Y. Ma, and C. K. Ong, "Permalloy-FeMn exchange-biased multilayers grown on flexible substrates for microwave applications," *Journal of Magnetism and Magnetic Materials,* vol. 321, pp. 2685-2690, Sep 2009.
[82] H.-C. Choi, C.-Y. You, K.-Y. Kim, J.-S. Lee, J.-H. Shim, and D.-H. Kim, "Antiferromagnetic layer thickness dependence of noncollinear uniaxial and unidirectional anisotropies in NiFe/FeMn/CoFe trilayers," *Physical Review B,* vol. 81, Jun 4 2010.
[83] Diaconu A. Khanal S, Vargas J M, Lenormand D R, Garcia C, and Ross C A. a. Spinu L. J. P. D. A. P. 255002.

[84] N. N. Phuoc and C. K. Ong, "Diluted antiferromagnet effect on magnetic and microwave characteristics of exchange-biased multilayered thin films," *Journal of Applied Physics,* vol. 111, May 1 2012.

[85] I. D. Mayergoyz, "MATHEMATICAL-MODELS OF HYSTERESIS," *Ieee Transactions on Magnetics,* vol. 22, pp. 603-608, Sep 1986.

[86] A. Stancu, D. Ricinschi, L. Mitoseriu, P. Postolache, and M. Okuyama, "First-order reversal curves diagrams for the characterization of ferroelectric switching," *Applied Physics Letters,* vol. 83, pp. 3767-3769, Nov 3 2003.

[87] R. Tanasa, C. Enachescu, A. Stancu, J. Linares, E. Codjovi, F. Varret*, et al.*, "First-order reversal curve analysis of spin-transition thermal hysteresis in terms of physical-parameter distributions and their correlations," *Physical Review B,* vol. 71, Jan 2005.

[88] B. K. Kuanr, S. Maat, S. Chandrashekariaih, V. Veerakumar, R. E. Camley, and Z. Celinski, "Determination of exchange and rotational anisotropies in IrMn/Fe(t)/IrMn exchange coupled structures using dynamic and static techniques: Application to microwave devices," *Journal of Applied Physics,* vol. 103, Apr 1 2008.

[89] J. McCord, R. Mattheis, and D. Elefant, "Dynamic magnetic anisotropy at the onset of exchange bias: The NiFe/IrMn ferromagnet/antiferromagnet system," *Physical Review B,* vol. 70, Sep 2004.

[90] W. Stoecklein, S. S. P. Parkin, and J. C. Scott, "FERROMAGNETIC-RESONANCE STUDIES OF EXCHANGE-BIASED PERMALLOY THIN-FILMS," *Physical Review B,* vol. 38, pp. 6847-6855, Oct 1 1988.

[91] A. Layadi, W. C. Cain, J. W. Lee, and J. O. Artman, "INVESTIGATION OF ANISOTROPY BY FERROMAGNETIC-RESONANCE (FMR) IN EXCHANGE-COUPLED BILAYER FILMS," *Ieee Transactions on Magnetics,* vol. 23, pp. 2993-2995, Sep 1987.

[92] J. C. Scott, "FERROMAGNETIC-RESONANCE STUDIES IN THE BILAYER SYSTEM NI0.80FE0.20/MN0.50FE0.50 - EXCHANGE-ANISOTROPY," *Journal of Applied Physics,* vol. 57, pp. 3681-3683, 1985 1985.

[93] H. W. Xi, R. M. White, and S. M. Rezende, "Irreversible and reversible measurements off exchange anisotropy," *Physical Review B,* vol. 60, pp. 14837-14840, Dec 1 1999.

[94] C. Bilzer, T. Devolder, J.-V. Kim, C. Chappert, M. Ruehrig, and L. Baer, "Dynamics of the exchange field supplied by MnIr layers studied by network analyzer ferromagnetic resonance," *Journal of Applied Physics,* vol. 106, Sep 15 2009.

[95] H. Glowinski, K. Zaleski, J. Sprada, and J. Dubowik, "Exchange Coupled NiFe/NiMn Bilayer Studied by a Vector Network Analyzer Ferromagnetic Resonance," *Acta Physica Polonica A,* vol. 121, pp. 1145-1147, May-Jun 2012.

[96] M. D. Stiles and R. D. McMichael, "Model for exchange bias in polycrystalline ferromagnet-antiferromagnet bilayers," *Physical Review B,* vol. 59, pp. 3722-3733, Feb 1 1999.

[97] J. Geshev, L. G. Pereira, J. E. Schmidt, L. C. C. M. Nagamine, E. B. Saitovitch, and F. Pelegrini, "Frequency-dependent exchange bias in NiFe/NiO films," *Physical Review B,* vol. 67, p. 132401, 2003.

[98] J. E. Davies, O. Hellwig, E. E. Fullerton, G. Denbeaux, J. B. Kortright, and K. Liu, "Magnetization reversal of Co/Pt multilayers: Microscopic origin of high-field magnetic irreversibility," *Physical Review B,* vol. 70, Dec 2004.

[99] J. Nogues and I. K. Schuller, "Exchange bias," *Journal of Magnetism and Magnetic Materials,* vol. 192, pp. 203-232, Feb 1999.

[100] S. Parkin, X. Jiang, C. Kaiser, A. Panchula, K. Roche, and M. Samant, "Magnetically engineered spintronic sensors and memory," *Proceedings of the Ieee,* vol. 91, pp. 661-680, May 2003.

[101] F. Radu and H. Zabel, "Exchange bias effect of ferro-/antiferromagnetic heterostructures," in *Magnetic Heterostructures*. vol. 227, H. Zabel and S. D. Bader, Eds., ed, 2008, pp. 97-184.

[102] R. A. Gallardo, S. Khanal, J. M. Vargas, L. Spinu, C. A. Ross, and C. Garcia, "Angular dependent FORC and FMR of exchange-biased NiFe multilayer films," *Journal of Physics D-Applied Physics,* vol. 50, Feb 22 2017.
[103] V. V. Kruglyak, S. O. Demokritov, and D. Grundler, "Magnonics," *Journal of Physics D: Applied Physics,* vol. 43, p. 264001, 2010.
[104] A. V. Chumak, V. I. Vasyuchka, A. A. Serga, M. P. Kostylev, V. S. Tiberkevich, and B. Hillebrands, "Storage-recovery phenomenon in magnonic crystal," *Phys Rev Lett,* vol. 108, p. 257207, Jun 22 2012.
[105] F. Garcia-Sanchez, P. Borys, R. Soucaille, J. P. Adam, R. L. Stamps, and J. V. Kim, "Narrow Magnonic Waveguides Based on Domain Walls," *Phys Rev Lett,* vol. 114, p. 247206, Jun 19 2015.
[106] A. A. Serga, A. V. Chumak, and B. Hillebrands, "YIG magnonics," *Journal of Physics D: Applied Physics,* vol. 43, p. 264002, 2010.
[107] A. Khitun, M. Bao, and K. L. Wang, "Magnonic logic circuits," *Journal of Physics D: Applied Physics,* vol. 43, p. 264005, 2010.
[108] Z. Wang, V. Zhang, H. Lim, S. Ng, M. Kuok, S. Jain*, et al.*, "Observation of frequency band gaps in a one-dimensional nanostructured magnonic crystal," *Applied Physics Letters,* vol. 94, p. 083112, 2009.
[109] S. Nikitov, P. Tailhades, and C. Tsai, "Spin waves in periodic magnetic structures—magnonic crystals," *Journal of Magnetism and Magnetic Materials,* vol. 236, pp. 320-330, 2001.
[110] K.-S. Lee, D.-S. Han, and S.-K. Kim, "Physical origin and generic control of magnonic band gaps of dipole-exchange spin waves in width-modulated nanostrip waveguides," *Physical review letters,* vol. 102, p. 127202, 2009.
[111] F. Capolino, *Theory and Phenomena of Metamaterials*: CRC Press, 2009.
[112] R. Cowburn, "Property variation with shape in magnetic nanoelements," *Journal of Physics D: Applied Physics,* vol. 33, p. R1, 2000.
[113] R. Skomski, "Nanomagnetics," *Journal of Physics: Condensed Matter,* vol. 15, p. R841, 2003.
[114] R. Gallardo, A. Banholzer, K. Wagner, M. Körner, K. Lenz, M. Farle*, et al.*, "Splitting of spin-wave modes in thin films with arrays of periodic perturbations: theory and experiment," *New Journal of Physics,* vol. 16, p. 023015, 2014.
[115] M. Körner, K. Lenz, R. Gallardo, M. Fritzsche, A. Mücklich, S. Facsko*, et al.*, "Two-magnon scattering in permalloy thin films due to rippled substrates," *Physical Review B,* vol. 88, p. 054405, 2013.
[116] F. Garcia-Sanchez, P. Borys, A. Vansteenkiste, J.-V. Kim, and R. L. Stamps, "Nonreciprocal spin-wave channeling along textures driven by the Dzyaloshinskii-Moriya interaction," *Physical Review B,* vol. 89, 2014.
[117] P. Landeros, R. A. Gallardo, O. Posth, J. Lindner, and D. L. Mills, "Role of the spin transfer in the ferromagnetic resonance response of thin films," *Physical Review B,* vol. 81, Jun 23 2010.
[118] J. Fassbender, T. Strache, M. O. Liedke, D. Markó, S. Wintz, K. Lenz*, et al.*, "Introducing artificial length scales to tailor magnetic properties," *New Journal of Physics,* vol. 11, p. 125002, 2009.
[119] A. Haldar and A. O. Adeyeye, "Deterministic Control of Magnetization Dynamics in Reconfigurable Nanomagnetic Networks for Logic Applications," *ACS Nano,* vol. 10, pp. 1690-8, Jan 26 2016.
[120] "<Spinwave logic circuits UCLA.pdf>."
[121] K. Vogt, F. Y. Fradin, J. E. Pearson, T. Sebastian, S. D. Bader, B. Hillebrands*, et al.*, "Realization of a spin-wave multiplexer," *Nat Commun,* vol. 5, p. 3727, 2014.
[122] L. E. Hueso, J. M. Pruneda, V. Ferrari, G. Burnell, J. P. Valdes-Herrera, B. D. Simons*, et al.*, "Transformation of spin information into large electrical signals using carbon nanotubes," *Nature,* vol. 445, pp. 410-3, Jan 25 2007.

[123] V. V. Kruglyak, A. Barman, R. J. Hicken, J. R. Childress, and J. A. Katine, "Picosecond magnetization dynamics in nanomagnets: Crossover to nonuniform precession," *Physical Review B,* vol. 71, 2005.
[124] Y. Au, M. Dvornik, O. Dmytriiev, and V. V. Kruglyak, "Nanoscale spin wave valve and phase shifter," *Applied Physics Letters,* vol. 100, p. 172408, 2012.
[125] S.-K. Kim, K.-S. Lee, and D.-S. Han, "A gigahertz-range spin-wave filter composed of width-modulated nanostrip magnonic-crystal waveguides," *Applied Physics Letters,* vol. 95, p. 082507, 2009.
[126] S. Kaka, M. R. Pufall, W. H. Rippard, T. J. Silva, S. E. Russek, and J. A. Katine, "Mutual phase-locking of microwave spin torque nano-oscillators," *Nature,* vol. 437, pp. 389-92, Sep 15 2005.
[127] J. Ding, M. Kostylev, and A. O. Adeyeye, "Realization of a mesoscopic reprogrammable magnetic logic based on a nanoscale reconfigurable magnonic crystal," *Applied Physics Letters,* vol. 100, Feb 13 2012.
[128] K. Di, S. X. Feng, S. N. Piramanayagam, V. L. Zhang, H. S. Lim, S. C. Ng*, et al.*, "Enhancement of spin-wave nonreciprocity in magnonic crystals via synthetic antiferromagnetic coupling," *Scientific Reports,* vol. 5, p. 6, May 2015.
[129] L. L. Xiong and A. O. Adeyeye, "Dynamic behavior of Ni80Fe20 nanowires with controlled periodic width modulation," *Applied Physics Letters,* vol. 108, p. 262401, 2016.
[130] C. A. Ross, M. Hwang, M. Shima, J. Y. Cheng, M. Farhoud, T. A. Savas*, et al.*, "Micromagnetic behavior of electrodeposited cylinder arrays," *Physical Review B,* vol. 65, 2002.

Vita

The author of this thesis was born in Yeladi-8, Syangja, Nepal. He completed master in Physics from Tribhuwan University in 2008. He joined university of New Orleans in August 2011. He received master in applied physics in 2014 and PhD in engineering and applied science (major physics) in summer of 2017 under the supervision of Prof. Leonard Spinu.